

# Bioelectricity Generation in Sludge Microbial Fuel Cells (MFCs) Coupled with Iron-based Nanoparticles

カウラ, ベンサイダ

<https://hdl.handle.net/2324/4496097>

---

出版情報 : Kyushu University, 2021, 博士 (学術), 課程博士  
バージョン :  
権利関係 :



KYUSHU UNIVERSITY

DOCTORAL THESIS

---

**Bioelectricity Generation  
in Sludge Microbial Fuel Cells (MFCs)  
Coupled with Iron-based Nanoparticles**

---

*By:*  
Khaoula BENSAIDA

*Supervisor:*  
Dr. Osama ELJAMAL

*Presented in Fulfillment of the Requirements  
for the Degree of Doctor of Philosophy*

*in the*

Water and Environmental Engineering Laboratory  
Department of Advanced Environmental Science and Engineering  
Interdisciplinary Graduate School of Engineering Sciences IGSES



July, 2021

© Copyright by  
Khaoula BENSAIDA  
2021

*“Great things are not done by one person. They are done by a team of people.”*

Steve Jobs



KYUSHU UNIVERSITY

## *Abstract*

Interdisciplinary Graduate School of Engineering Sciences IGSES  
Department of Advanced Environmental Science and Engineering

Doctor of Philosophy

**Bioelectricity Generation  
in Sludge Microbial Fuel Cells (MFCs)  
Coupled with Iron-based Nanoparticles**

by Khaoula BENSAIDA

Microbial fuel cells (MFCs) are a versatile technology for power generation from biodegradable solid wastes. This study aimed to investigate  $\text{Fe}^0$  nanoparticles' effects on MFC's performance in power generation and wastewater treatment.  $\text{Fe}$ ,  $\text{Cu}/\text{Fe}^0$ ,  $\text{Ag}/\text{Fe}^0$ , and  $\text{Ni}/\text{Fe}^0$  nanoparticles have been adopted as additives to bacterial's mixed culture. The experimental procedure went through MFCs construction, collection and characterization of waste sludge samples, synthesis and characterization of iron-based nanoparticles, and estimating bacterial growth improvement. All MFCs were operated in a batch mode and incubated at a constant temperature ( $40\text{ }^{\circ}\text{C}$ ) for 45 days of operation. TEM characterizations showed that  $\text{Fe}^0$  morphology had crystalline and pure structure whereas the introduction of Cu particles led to a larger surface area and more ductile chain. The living microorganisms were less sensitive to  $\text{Fe}^0$  treatment under an optimum concentration of  $50\text{ mg/L}$ , and bacterial growth increased significantly by  $50\%$ .  $\text{Ag}/\text{Fe}^0$  addition reduced the bacterial growth by  $46.15\%$ , whereas it increased by  $15.38\%$ ,  $53.85\%$ , and  $84.61\%$  for  $\text{Ni}/\text{Fe}^0$ ,  $\text{Fe}^0$ , and  $\text{Cu}/\text{Fe}^0$ , respectively. Moreover, two different samples of sludge were used and the maximum daily voltage obtained in the control MFC filled with S2 ( $\text{COD} = 37802\text{ mg/L}$ ) increased by  $182\%$  compared to the MFC filled with S1 ( $\text{COD} = 5561\text{ mg/L}$ ). The addition of Fe nanoparticles reduced the daily voltage by  $31\%$  and  $9\%$  for the MFCs filled with S1 and S2, respectively. These results highlight the effect of organic matter content on the MFC response. In addition, the use of copper / $\text{Fe}^0$  bimetallic nanoparticles enhanced the maximum voltage value by  $43.33\%$  and the power density by  $65.57\%$ . Furthermore,  $\text{Fe}^{3+}$  addition exhibited a higher power output by  $295\%$  and a shorter start-up time. The microbial growth increased by  $92.18\%$  and the anolyte's resistivity decreased with an increase in the organic matter digestion by  $52.78\%$ . The addition of various types of coated  $\text{Fe}^0$  nanoparticles enhanced the MFC performance.  $\text{Mg}/\text{Fe}:0.2$  had the most remarkable voltage generation improvement of the suggested coating ratios by over 4 times. After 45 days of operation,  $\text{Mg}/\text{Fe}$  nanoparticles' addition increased the anolyte conductivity and enhanced bacterial growth by  $122\%$ . Microbial fuel cell response still low, and the use of real waste sludge is challenging. MFC technology could be used to generate power with biodegradable waste and sewage. At the same time, it could provide help with wastewater treatment and bioremediation. Future work should be developed to understand how the sludge composition affects the MFCs response, particularly the anolyte's conductivity and the nutrient's availability.

**Keywords:** Anaerobic digestion,  
Bacterial growth,  
COD removal,  
Iron-based nanoparticles,  
Microbial fuel cells,  
Organic matter degradation,  
Total volatile solids.



# Acknowledgements

*I thank GOD. He guided me by the skillfulness of his hands.*

*The research activities presented in this thesis have been developed and financially supported by the Water and Environmental Engineering Laboratory (WEEL), Department of Advanced Environmental Science and Engineering, Interdisciplinary Graduate School of Engineering Sciences, Kyushu University (KU), Japan.*

*I sincerely appreciate the financing received from the scholarship granted by the Ministry of Education, Culture, Sports, Science and Technology, Japan (MEXT).*

*My sincere gratitude goes to my supervisor Professor Osama ELJAMAL, who kindly agreed to supervise me during my thesis works. I am grateful for his warm welcome, friendly working atmosphere, and for the unwavering enthusiasm that he kindly reserved for me in his laboratory.*

*A special word of gratitude goes to Professor Yuji SUGIHARA and Professor Hooman FARZANEH for their precious time, review, and consideration.*

*I am grateful to Professor Ali ELKAMEL from the University of Waterloo for the guidance he offered me at the start of the project.*

*I am also grateful to all of those I have had the pleasure to work with during these works.*

*Last but not least, these works would not have been possible without the unwavering support and encouragement of my friends and beloved family. I would like to express my love and gratitude, in particular, to my beloved mother for her unconditional love and for motivating me for higher achievements in whatever I pursue. Special thanks also go to my dear friend Amr ISMAEIL for listening, offering me advice, and supporting me through this entire process. I look forward to being friends forever.*

*Khaoula Bensaida*

*July, 2021*



# Contents

<b>Abstract</b>	<b>v</b>
<b>Acknowledgements</b>	<b>vii</b>
<b>List of Figures</b>	<b>xv</b>
<b>List of Tables</b>	<b>xv</b>
<b>List of Abbreviations</b>	<b>xv</b>
<b>1 Electricity Generation in Microbial Fuel Cells using Iron-based Nanoparticles</b>	<b>1</b>
1.1 Introduction	1
1.2 MFC as a Source of Renewable Energy	2
1.2.1 Principle working of MFC	3
Anode chamber	3
Cathode chamber	4
Proton exchange membrane (PEM)	4
Microorganisms	5
Extracellular electron transfer (EET) mechanisms	6
MFC Losses	7
1.2.2 Factors affecting the MFC performance	8
Waste sludge	8
Electrochemically active bacteria	9
MFC reactor configuration	9
MFC operating conditions	10
1.3 Fe <sup>0</sup> Nanoparticles and Microbial Fuel Cell System	11
1.3.1 Nanoparticles	11
1.3.2 Literature review	13
1.4 Research interests	16
1.5 Conclusion	18
<b>2 Materials and Methodology</b>	<b>21</b>
2.1 Introduction	21
2.2 Microbial Fuel Cells Set-up	22
2.2.1 Waste Sludge Collection and Characterization	26
2.2.2 Data Measurements and Analysis	29
2.3 Nanoparticles Synthesis and Characterization	30
2.3.1 Reagents	30
2.3.2 Synthesis	30
2.3.3 Characterization	33
2.4 Culture and Analysis of Bacterial Growth	34
2.5 Conclusion	36

<b>3</b>	<b>Investigation on The Effect of Iron-based Nanoparticles on Bacterial Growth</b>	<b>37</b>
3.1	Introduction	37
3.2	Characterization of Fe <sup>0</sup> and Cu/Fe <sup>0</sup> Nanoparticles	38
3.3	Bacterial Growth Response to Fe <sup>0</sup> -bimetallic Nanoparticles Treatment	39
3.3.1	Effect of Fe <sup>0</sup> on bacterial cells at different concentrations	39
3.3.2	Effect of Cu/Fe <sup>0</sup> , Ag/Fe <sup>0</sup> , and Ni/Fe <sup>0</sup> on bacterial cells	42
3.4	Effect of Fe <sup>0</sup> -bimetallic Nanoparticles at Different System Conditions	46
3.4.1	Effect of pH variation on COD Removal	47
3.4.2	Effect of temperature variation on COD Removal	49
3.4.3	Aerobic/anaerobic digestion and COD Removal	52
3.5	Conclusion	55
	Effect of Fe on the anaerobic digestion at high concentrations	55
	Effect of Fe on the anaerobic digestion at low concentrations	56
<b>4</b>	<b>Application of Iron-based Nanoparticles on Bioelectricity Generation Using MFCs</b>	<b>57</b>
4.1	Introduction	57
4.2	Evaluation of Double-chamber MFCs Response to Fe <sup>0</sup> treatment	59
4.3	Application of Fe <sup>0</sup> and Cu/Fe <sup>0</sup> for Power Generation in MFCs	63
4.3.1	MFCs performance in time	63
4.3.2	Iron concentration analysis	65
4.3.3	Wastewater treatment and organic matter removal	65
4.4	Effect of Fe <sup>2+</sup> , Fe <sup>3+</sup> , and Fe <sup>2+</sup> /Fe <sup>3+</sup> for Electricity Generation in MFCs	68
4.4.1	MFCs performance in time	68
4.4.2	Iron concentration analysis	71
4.4.3	Analysis of internal resistances	73
4.4.4	Wastewater treatment and organic matter removal	73
4.5	Power Generation Enhancement Using Fe <sup>0</sup> Coated with Mg(OH) <sub>2</sub>	79
4.5.1	Characterization of bare and coated Fe <sup>0</sup> nanoparticles	79
4.5.2	Iron concentration analysis	81
4.5.3	MFCs performance in time using bare and coated Fe <sup>0</sup> nanoparticles	83
4.5.4	Effect of system conditions variation on MFCs performance	88
	MFC's response to pH variations	89
	MFC's response to anoxic/aerobic conditions	92
4.6	Conclusion	94
<b>5</b>	<b>Conclusions and Future work</b>	<b>95</b>
5.1	Conclusions	95
5.2	Future work	99
	<b>Bibliography</b>	<b>101</b>

# List of Figures

1.1	General principle working of a double-chamber microbial fuel cell (MFC). . . . .	3
1.2	General principle of a double-chamber microbial fuel cell (MFC). Electrons can be carried by protein carriers, nanowires or mediators. . . . .	6
1.3	Bare Fe <sup>0</sup> nanoparticles. . . . .	12
1.4	Fe <sup>0</sup> -based nanoparticles introduced to a double-chamber MFC. . . . .	18
1.5	Schematic drawing of Fe <sup>0</sup> -based nanoparticles. . . . .	19
2.1	Schematic design of the lab-scale H-type microbial fuel cell (MFC). . . . .	22
2.2	Mechanical drawing of the lab-scale H-type microbial fuel cell (MFC). . . . .	23
2.3	Construction of the rectangular double-chamber MFC. . . . .	24
2.4	Schematic design of the lab-scale H-type microbial fuel cell (MFC). . . . .	24
2.5	Real illustration of the lab-scale H-type MFCs. . . . .	25
2.6	Photo of Mikasagawa wastewater treatment plant in Fukuoka city, Japan. . . . .	26
2.7	(A) UV spectrophotometer (Hach DR 3900, USA, (B) Various vials testing the COD values in different waste sludge samples. The vials change the color from orange to green based on the amount of oxidation. (C) Drying the mixed samples of waste sludge in the oven at 105 °C for 24 hours. . . . .	27
2.8	Schematic design of Fe <sup>0</sup> -based nanoparticles synthesis procedure. (A) Fe <sup>0</sup> nanoparticles synthesis, (B) freshly synthesized Fe <sup>0</sup> . . . . .	31
2.9	Synthesis of the Fe <sup>0</sup> -based nanoparticles in the laboratory. . . . .	31
2.10	Ultrasonication (38 kHz, 100 W) and nitrogen gas purging for the preparation of coated iron nanoparticles. . . . .	32
2.11	(A) Transmission Electron Microscope, (B) X-Ray Diffraction. . . . .	33
2.12	Pour plate method for bacterial growth measurements. . . . .	34
2.13	(A) Prepared standard plate count agar (APHA) CM0463 (OXOID LTD., England). (B) Bacterial colonies in a Petri dish after 24 hours. . . . .	35
2.14	The bacterial growth cycle. . . . .	36
3.1	TEM characterization of the synthesized bimetallic nanoparticles . . . . .	38
3.2	XRD characterization of the synthesized bimetallic nanoparticles . . . . .	39
3.3	Activation of bacterial growth when exposed to Fe <sup>0</sup> nanoparticles with different concentrations under anaerobic conditions . . . . .	40
3.4	Effect of Fe <sup>0</sup> , Cu/Fe <sup>0</sup> , Ag/Fe <sup>0</sup> , and Ni/Fe <sup>0</sup> on the bacterial growth . . . . .	42
3.5	COD removal efficiencies under Fe <sup>0</sup> nanoparticles treatment . . . . .	43
3.6	pH values after 13 days of the exposure of wastewater 1 to the bimetallic nanoparticle's treatment with a concentration of 50 mg/L at 37 °C and under anaerobic conditions with an initial pH: 7,74 . . . . .	44
3.7	ORP levels after 13 days of the exposure of wastewater 1 to the bimetallic nanoparticles' treatment with a concentration of 50 mg/L at 37°C, pH=7 under anaerobic conditions with an initial ORP value -106 mV. . . . .	44
3.8	Fe <sup>2+</sup> after 13 days of the exposure of wastewater 1 to the bimetallic nanoparticles' treatment with a concentration of 50 mg/L at 37 °C, pH=7 under anaerobic conditions with an initial Fe <sup>2+</sup> value: 1,87 mg/L. . . . .	45

3.9	Fe concentration after 13 days of the exposure of wastewater 1 to the bimetallic nanoparticles' treatment with a concentration of 50 mg/L at 37 °C, pH=7 under anaerobic conditions with an initial $\text{Fe}^{2+}$ value: 9.37 mg/L. . . . .	45
3.10	COD removal efficiencies of the mixed culture samples of wastewater 2 when exposed to bimetallic nanoparticles with respect to the pH variation . . . . .	48
3.11	Iron concentrations after 20 days of operation using wastewater 2 under the bimetallic nanoparticles' treatment with a concentration of 50 mg/L at 37 °C, under anaerobic conditions. . . . .	48
3.12	pH variations after 20 days of operation using wastewater 2 under the bimetallic nanoparticles' treatment with a concentration of 50 mg/L at 37 °C, under anaerobic conditions. . . . .	49
3.13	COD removal efficiencies of the mixed culture samples of wastewater 2 when exposed to bimetallic nanoparticles with respect to temperature variation . . . . .	50
3.14	pH variations with respect to temperature variations after 20 days of operation using wastewater 2 under the bimetallic nanoparticles' treatment with a concentration of 50 mg/L. . . . .	51
3.15	Iron concentrations after 20 days of operation using wastewater 2 under the bimetallic nanoparticles' treatment with a concentration of 50 mg/L, under anaerobic conditions. . . . .	51
3.16	COD removal efficiencies when exposed to bimetallic nanoparticles under aerobic/anaerobic conditions . . . . .	52
3.17	pH variations when exposed to bimetallic nanoparticles under aerobic and anaerobic conditions. . . . .	53
3.18	ORP variations when exposed to bimetallic nanoparticles under aerobic and anaerobic conditions. . . . .	53
3.19	Iron concentrations analysis when exposed to bimetallic nanoparticles under aerobic and anaerobic conditions. . . . .	54
3.20	$\text{Fe}^0$ nanoparticles can be adsorbed on cell membranes of bacteria, or penetrate through them, which often leads to disturbances in the functioning of the cell. . . . .	56
4.1	Daily voltage variation in MFCs using Fe nanoparticles. . . . .	59
4.2	Daily voltage variation in MFCs using Fe nanoparticles. . . . .	60
4.3	Resistivity variation throughout the days of operation. . . . .	61
4.4	pH variations throughout the days of operation with an initial pH values 6.77 and 5.94 for S1 and S2, respectively. . . . .	62
4.5	ORP variations throughout the days of operation with an initial ORP values -14 mV and 32 mV for S1 and S2, respectively. . . . .	62
4.6	Daily voltage variation in MFCs using Fe and Cu/Fe nanoparticles throughout the operation period throughout the operation period. . . . .	64
4.7	Voltage cell in MFCs using Fe and Cu/Fe nanoparticles throughout the operation period throughout the operation period. . . . .	64
4.8	Power density in MFCs using Fe and Cu/Fe nanoparticles throughout the operation period . . . . .	65
4.9	Iron concentration in the anode chamber throughout the operation period. . . . .	66
4.10	Bacterial growth in the anode chamber under anaerobic conditions during the operation period when exposed to: (a) the control MFC, (b) Fe MFC, and (c) Cu/Fe MFC. . . . .	67
4.11	COD removal efficiencies in the anode chamber throughout the operation period. . . . .	68
4.12	Daily voltage generation in MFCs using $\text{Fe}^{2+}$ , $\text{Fe}^{3+}$ , and $\text{Fe}^{3+}/\text{Fe}^{2+}$ iron ions with 10 mg/L at the anode throughout the operation period. . . . .	69
4.13	Accumulative voltage generation in MFCs with time using $\text{Fe}^{2+}$ , $\text{Fe}^{3+}$ , and $\text{Fe}^{2+}/\text{Fe}^{3+}$ iron ions with 10 mg/L at the anode. . . . .	70
4.14	Power density variations of MFCs using $\text{Fe}^{2+}$ , $\text{Fe}^{3+}$ , and $\text{Fe}^{3+}/\text{Fe}^{2+}$ iron ions with 10 mg/L at the anode throughout the operation period. . . . .	70

4.15	Iron concentration in the anolyte for control and iron ions-supplemented MFCs throughout the days of operation. . . . .	72
4.16	Resistance of the anode chamber of MFCs using $\text{Fe}^{2+}$ , $\text{Fe}^{3+}$ , and $\text{Fe}^{3+}/\text{Fe}^{2+}$ iron salts with 10 mg/L throughout the operation period. . . . .	74
4.17	Bacterial growth with time using $\text{Fe}^{2+}$ , $\text{Fe}^{3+}$ , and $\text{Fe}^{3+}/\text{Fe}^{2+}$ iron ions with 10 mg/L at the anode. The addition of iron ions was favorable for the enrichment of bacteria. . . . .	74
4.18	COD removal using $\text{Fe}^{2+}$ , $\text{Fe}^{3+}$ , and $\text{Fe}^{3+}/\text{Fe}^{2+}$ iron salts with 10 mg/L in the anode chamber throughout the operation period. . . . .	75
4.19	ORP variations for MFCs supplemented with $\text{Fe}^{2+}$ , $\text{Fe}^{3+}$ , and $\text{Fe}^{3+}/\text{Fe}^{2+}$ iron salts throughout the operation period. . . . .	76
4.20	pH variations for MFCs supplemented with $\text{Fe}^{2+}$ , $\text{Fe}^{3+}$ , and $\text{Fe}^{3+}/\text{Fe}^{2+}$ iron salts throughout the operation period. . . . .	76
4.21	Total dissolved solids variations for MFCs supplemented with $\text{Fe}^{2+}$ , $\text{Fe}^{3+}$ , and $\text{Fe}^{3+}/\text{Fe}^{2+}$ iron salts throughout the operation period. . . . .	77
4.22	TEM characterization of the synthesized bare and coated $\text{Fe}^0$ . . . . .	79
4.23	(A) XRD characterization of the synthesized bare and coated $\text{Fe}^0$ , (B) FTIR characterization of the synthesized bare and coated $\text{Fe}^0$ . . . . .	80
4.24	$\text{Fe}^0$ analysis in the anolyte . . . . .	82
4.25	The representative accumulative cell voltage-time of MFCs equipped with bare and coated Fe nanoparticles. . . . .	84
4.26	Power density-time curves plotted in Log scale of MFCs equipped with bare and coated Fe nanoparticles. . . . .	84
4.27	The daily cell voltage-time plots for MFCs equipped with bare $\text{Fe}^0$ and coated Fe nanoparticles. . . . .	85
4.28	Bacterial growth response in the anode chamber of MFCs supplemented with bare and coated $\text{Fe}^0$ nanoparticles (Mg/Fe:0.1, Mg/Fe:0.2, Mg/Fe:0.5, and Mg/Fe:1.0). . . . .	87
4.29	Current generated (red) by the MFCs when fed with different waste sludges whose COD is shown in red. . . . .	88
4.30	Variations of the cell voltage of MFCs when treated under acidic, neutral, and alkaline conditions. Curves are plotted in Log scale. MFCs were supplemented with Mg/Fe:0.5 for 45 days of operation. . . . .	89
4.31	Power density of MFCs when treated under acidic, neutral, and alkaline conditions. Curves are plotted in Log scale. MFCs were supplemented with Mg/Fe:0.5 for 45 days of operation. . . . .	90
4.32	pH variations during the 45 days of operation. Curves are plotted in Log scale. MFCs were supplemented with Mg/Fe:0.5 for 45 days of operation. . . . .	91
4.33	MFCs response to aerobic/anoxic conditions plotted in Log scale. . . . .	92
5.1	The response of mixed culture bacteria to $\text{Fe}^0$ -based nanoparticles treatment. . . . .	96
5.2	The response of microbial fuel cells to $\text{Fe}^0$ -coated nanoparticles treatment. . . . .	97
5.3	Current generated (red) by the MFCs when fed with different waste sludges whose conductivity is shown in red. . . . .	98



# List of Tables

2.1	Initial waste sludges characteristics. . . . .	26
2.2	MFC reactor constant parameters. . . . .	29
3.1	Wastewater 1 properties. . . . .	40
3.2	Properties of wastewaters used in this study. . . . .	47
3.3	Ferrous ions concentrations $[\text{Fe}^{2+}]$ for control, $\text{Fe}^0$ , $\text{Cu}/\text{Fe}^0$ , $\text{Ag}/\text{Fe}^0$ , and $\text{Ni}/\text{Fe}^0$ with respect to temperature variations. . . . .	50
4.1	Measurements values recorded and calculated from the experiments. . . . .	60
4.2	Anolyte characteristics when exposed to Fe and Cu/Fe addition after 45 days of operation. . . . .	67
4.3	Measurements values recorded and calculated from the experiments. . . . .	71
4.4	TVS concentrations using $\text{Fe}^{2+}$ , $\text{Fe}^{3+}$ , and $\text{Fe}^{3+}/\text{Fe}^{2+}$ iron ions with 10 mg/L in the anode chamber throughout the operation period. . . . .	75
4.5	Maximum power density, maximum current, TVS removal, conductivity, and coulombic efficiency (CE) from different MFCs using (S1) after 45 days. $P_{\text{max}}$ : maximal power. I at $P_{\text{max}}$ : current value obtained at $P_{\text{max}}$ . N: negative due to the increase of TVS. . . . .	86
4.6	Waste sludge characteristics in the anode chambers fed with (S2) after 45 days. Initial waste sludge characteristics (S2) are described in chapter 2, Table 2.1. . . . .	91
4.7	Waste sludge characteristics in the anode chambers fed with (S2) after 45 days. Initial waste sludge characteristics (S2) are described in chapter 2, Table 2.1. . . . .	93



# List of Abbreviations

<b>BOD</b>	<b>B</b> iochemical <b>O</b> xygen <b>D</b> emand
<b>COD</b>	<b>C</b> hemical <b>O</b> xygen <b>D</b> emand
<b>CE</b>	<b>C</b> oulombic <b>E</b> fficiency
<b>CFU</b>	<b>C</b> olony <b>F</b> orming <b>U</b> nit
<b>DDIW</b>	<b>D</b> eoxygenated <b>D</b> eionized <b>W</b> ater
<b>DET</b>	<b>D</b> irect <b>E</b> lectron <b>T</b> ransfer
<b>EET</b>	<b>E</b> xtracellular <b>E</b> lectron <b>T</b> ransfer
<b>EMF</b>	<b>E</b> lectro <b>M</b> otive <b>F</b> orce
<b>EPS</b>	<b>E</b> xtracellular <b>P</b> olymer <b>S</b> ubstances
<b>MET</b>	<b>M</b> ediated <b>E</b> lectron <b>T</b> ransfer
<b>MFC</b>	<b>M</b> icrobial <b>F</b> uel <b>C</b> ell
<b>OCV</b>	<b>O</b> pen <b>C</b> ircuit <b>V</b> oltage
<b>PEM</b>	<b>P</b> roton <b>E</b> xchange <b>M</b> embrane
<b>ROS</b>	<b>O</b> xidative <b>S</b> tress <b>R</b> esponse
<b>S</b>	<b>S</b> ludge
<b>TDS</b>	<b>T</b> otal <b>D</b> issolved <b>S</b> olids
<b>TFS</b>	<b>T</b> otal <b>F</b> ixed <b>S</b> olids
<b>TS</b>	<b>T</b> otal <b>S</b> olids
<b>TSS</b>	<b>T</b> otal <b>S</b> uspended <b>S</b> olids
<b>TVS</b>	<b>T</b> otal <b>V</b> olatile <b>S</b> olids
<b>VFT</b>	<b>V</b> olatile <b>F</b> atty <b>A</b> cids



*To my beloved Family...*



# General Introduction

The energy demand has been increasing worldwide, and the scarcity of fossil fuels has urged the necessity for environmental and eco-friendly energy sources. The search for novel energy solutions has grown tremendously. The urge to limit the consumption of carbon-based energy resources has been raised to restrain greenhouse gas emissions and environmental pollution. Moreover, water depletion is emerging as a vital issue, and it becomes crucial to define sustainable water conservation and wastewater treatment techniques in the present situation. In this context, microbial fuel cell (MFC) technology has been gaining popularity over the past decades.

Biofuel cells are at an early stage of development compared to other fuel cell technology. Significant research studies are still needed to approach technology integration and commercialization. In a typical fuel cell, expensive fuel and catalysts are needed. A catalyst is what gets a chemical reaction going, and therefore an electrical current is generated as a result of these chemical reactions. In contrast, in microbial fuel cells, catalysis is done by living bacteria, which break down the waste and release electricity in the process. An MFC is an anaerobic container of concentrated bacteria that feed biodegradable material. It operates via biochemistry, meaning that the energy used to run the cell is generated from electron transfer from bacteria to electrodes with no outside energy source is needed. Such a process would simultaneously reduce the waste treatment costs, unlike conventional fuel cells. Microbial fuel cell systems are recognized as energy production systems with great potentials.

MFCs have the advantage of running off widely available sources of energy. Substantial improvements will be required for the uses of microbial fuel cells, such as the large-scale conversion of organic wastes and biomass to electricity or powering vehicles, mobile electronic devices, or households with suitably scaled microbial fuel cells will be possible. A primary developing application of MFCs is its use in sustainable bioenergy, organic wastewater treatment coupled with electricity, although further technical developments are necessary for its practical use. The limitation to widespread the MFC's utilization is that the power densities are too low for envisioned applications. Broad application of MFCs will require substantial increase in current density. A better understanding of the microbiology may help.

Therefore, essential questions should be addressed:

- ★ What microorganisms are capable of effectively interacting with the electrode surface.
- ★ What factors influence the growth and metabolism of the microbes.
- ★ What are the mechanisms of electronic communication between microorganisms and electrodes.

This research's overall objective was to study the effects of iron-based nanoparticles on the performance of a lab-scale microbial fuel cell (MFC). The specific objectives are as follows:

- Improve the bacterial growth owing to their critical role in microbial fuel cell technology,
- Implement the iron nanoparticles technology in the anode chamber as it represents the powerhouse of MFCs, and
- Improve the iron performance and understand the factors that affect the MFC response,

In contributing to the enhancement of bioenergy generation, we have been involved in the design and study of microbial fuel cell technology. Developed in Kyushu University, our works are synthesized in the present dissertation, which is structured in five chapters:

- The first chapter is devoted to state of the art regarding microbial fuel cell technology. A background related to the principle of operation of MFCs is recalled. The chapter aims to review nanoparticles technology, and their advantages and challenges are analyzed.
- The second chapter aims to discuss material and experimental methods used in this study. Special attention is paid to the MFC construction procedure, the nanoparticles synthesis, and the bacterial growth analysis,
- The third chapter investigates the response of bacterial growth under iron-based nanoparticles treatment. Such an improvement is essential for microbial fuel cell applications,
- The fourth chapter considers the most promising material among those proposed in chapter 3. An experimental study is carried out aiming at the improvement of the system performance. A new proposed approach leads to selecting a set of parameters making the MFC reach the required arrangements, and
- In chapter five, significant findings of this dissertation are summarized with some recommendations for future work.

## Chapter 1

# Electricity Generation in Microbial Fuel Cells using Iron-based Nanoparticles

### 1.1 Introduction

According to the shortage of global energy, the energy consumption of excess sludge treatment is too high. Abundant organics can not be utilized effectively in sludge, causing waste of resources. Anaerobic digestion is a process in which anaerobic bacteria utilize organics to produce methane under anaerobic conditions. It is a traditional method for sludge decrement and stabilization. However, the methane production will consume about 30 % of the total produced energy, whereas microbial fuel cell (MFC) utilizes sludge as fuel and generate electrical currents via oxidizing organics in sludge directly, achieving the same sludge time's stabilization and decrement. Wastewater treatment plants consume electrical power, and we can imagine a time when these treatment plants are transformed into what we hope would be power plants. In this context, microbial fuel cells (MFCs) have drawn attention as a versatile technique for eco-friendly energy production and bioremediation (Franks and Nevin, 2010; Kong et al., 2017; Munoz-Cupa et al., 2021a; Zhao, Slade, and Varcoe, 2009). Wastewater treatment and bioremediation are considered among the critical fields of research in environmental engineering. Researchers have been developing practical solutions for wastewater treatment, and many techniques have been exploited in waste management and bioremediation. Metallic nanoparticles have received much attention over the past decade due to their high chemical activities and specificities of interaction. Metal nanoparticles are effective catalysts for chemical transformations due to their large surface area and a unique combination of reactivity, stability, and selectivity (Eljamal et al., 2018; Bensaida et al., 2020).  $\text{Fe}^0$  is considered a source of electrons used to transform many common contaminants present in wastewater. Its reducing power ( $E_0 = -0.44 \text{ V}$ ) and its ability to transform significant contaminants led to widespread use in environmental engineering.

## 1.2 MFC as a Source of Renewable Energy

Evidence that electrons from microbial metabolism can be harvested with electrodes had existed for nearly 100 years. The research on MFCs technology began in 1911 when Michael Potter discovered that bacteria could generate electricity when a platinum electrode was inserted into a liquid suspension of yeast and *Escherichiacoli* (Hu et al., 2018; Mathuriya and Yakhmi, 2016). The discovery of bacteria capable of complete oxidation of organic compounds and efficient electron transfer to electrodes via direct contact has a landmark in this research field. However, early progress was plodding due to technical difficulties.

Since the 1980s, the bio-electricity generation has evolved, and further investigations into MFC technology's practical uses are expected (Alan, 1992). MFC systems can be applied as biosensors in trial applications for power production, treatment, and sensing (Gajda, Greenman, and Ieropoulos, 2018; Munoz-Cupa et al., 2021b). MFCs are constructed in an ever-increasing diversity of topologies. The MFCs performances are closely related to their design, the type of electrodes, the inoculum pretreatment (Wei, Elektorowicz, and Oleszkiewicz, 2011), and microorganisms' activity (Hamdan and Salam, 2020; Vicari et al., 2018). MFCs are operated under different system conditions (Marks, Makinia, and Fernandez-Morales, 2019; Obata et al., 2020) that include temperature and pH variation (Chen et al., 2020), electron acceptor (Ter Heijne et al., 2011), electrode surface areas, reactor size, and operation time. MFCs are considered environmentally friendly technology, and their operation depends on microbial metabolism. MFCs can harvest electrical energy from wastewater and remove organic matter through microbial metabolism. When microbes decompose organic matter, electrons, hydrogen ions, and carbon dioxide are produced. MFCs could monitor the amount of material left and provide help with wastewater treatment and bioremediation. However, the efficiency of organics utilization and electricity generation in MFCs is low.

Many challenges have been facing the MFC technology. The electron transfer mechanisms (Santoro et al., 2017), the low system performance, high resistivity, and low Coulombic efficiency (Devasahayam and Masih, 2012) are the main weaknesses of this technology, and many studies have highlighted the main advancements to improve MFC technology's performance (Li et al., 2018; Myung, Saikaly, and Logan, 2018). MFC reactor size, operating mode, electrode material, external resistance, inoculum culture source, proton exchange membrane (PEM), and substrate type are crucial to define the MFC's output.

### 1.2.1 Principle working of MFC

MFCs create a sustainable way to produce energy and power. In other words, if MFC delivers on its promise, wastewater would be waste no longer. An MFC represents an electrochemical device for the direct conversion of chemical compounds into electrical energy. In the anode chamber, the digestion of organic matter results in low redox potential. In contrast, in the cathode chamber, the reduction of oxygen ions results in high redox potential. The high difference in redox potentials drives the electrons to flow, and therefore, bioelectricity is generated. The most important part of an MFC is microbes. The microbes grow on an electrode that is oxygen-free. So that, they send off their electrons to the electrode rather than to oxygen. Electrons flow through a circuit, so we extract that electrical current. The electrons end up on the other side of the MFC and combine with oxygen. The theory is simple but putting it into practice is challenging. Figure 1.1 illustrates the MFC principle functioning of a typical double-chamber MFC.

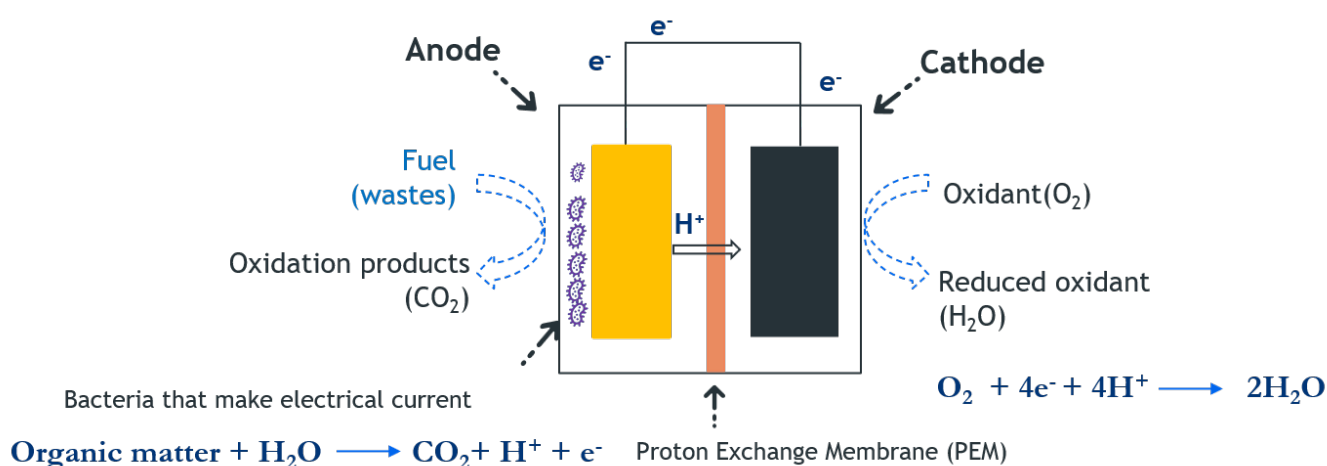
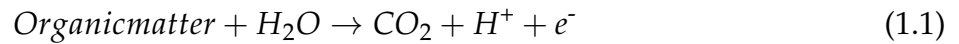


FIGURE 1.1: General principle working of a double-chamber microbial fuel cell (MFC).

#### Anode chamber

The anode chamber, which contains an electrode, microorganisms, and an anolyte, is maintained under anaerobic conditions for the oxidation of organic matter. Bacteria oxidize the organic compounds under anaerobic conditions and thereby free protons H<sup>+</sup> and electrons e<sup>-</sup>. Electrons are withdrawn from an electron-rich fuel and conducting over an external load, producing electricity.

The anaerobic reduction process always proceeds with a low rate and requires along period for microbial growth.



The anode material is essential for power performance in MFC's application. It is considered to be the surface for colonization. The anode surface is expected to serve as the sole electron acceptor from electrode-reducing bacteria during the organic matter oxidation. The material's characteristics influence biofilm formation, bacterial attachment, electron transfer, and substrate oxidation. The electrode material should have high biocompatibility, large surface area, low electric resistance, good corrosion resistance, and chemical stability. Besides, the operating temperature has a significant impact on biofilm formation and development. It provides an effective method to reduce the MFC losses and improve its output.

#### **Cathode chamber**

During electron production, protons are also produced in excess. These protons migrate through the PEM into the cathode chamber. The electrons flow from the anode through an external resistance (or load) to the cathode where they react with the final electron acceptor and protons. The loop is closed by a proton exchange membrane connection between the sludge in the anode chamber and the cathode chamber. The  $\text{e}^-$  from the cathode combine with dissolved oxygen and the  $\text{H}^+$  ions to form pure water, as described in the following equation:



Usually, the electron acceptors that exhibit high redox potential, faster kinetics, low cost, and easy availability are significant and interesting in MFC's applications. Oxygen is one of the most promising and widely used electron acceptors.

#### **Proton exchange membrane (PEM)**

The type of proton exchange membrane can affect the system's internal resistance. The primary role of PEM is to separate the two reactants, transport protons, and prevent the diffusion of oxygen while blocking a direct electronic pathway. PEMs can be made from pure polymer membranes or composites membrane.

Nafion<sup>TM</sup> is the most intensively studied fuel cell membrane as it provides high ionic conductivity. However, the main limitations of Nafion<sup>TM</sup> are its high cost, restricted temperature range (less than 100° C), and oxygen permeability.

### Microorganisms

The microorganisms are used as the biocatalysts to oxidize the substrate in the anode chamber and have been denoted as the powerhouse of MFCs. The electrons are transferred to the anodic (an electrode) surface, which are then directed to the cathode through an electrical connection. The electron transfer's effectiveness at the electrode surface depends mainly on the kinetics of organic matter oxidation at the anode and the reduction of oxygen at the cathode surface. Certain guilds of microbes have a physiological ability to generate an electric charge by oxidizing organic substances and donating electrons to metal ions that serve as an anode (Zhao, Slade, and Varcoe, 2009). The general term for these organisms is electrogens. Bacteria used in MFCs are called exoelectrogens. They are electrochemically active and can transfer electrons outside their cells. Exoelectrogens contain molecular machinery to transfer the electrons to an electron acceptor without any external assistance or accept the electrons from the electrode surfaces. Recently, MFCs populated by mixed microbial communities have garnered much attention owing to their stability, robustness due to nutrient adaptability, stress resistance, and general tendency to produce higher current densities than those obtained using pure cultures. However, in mixed-culture MFC systems, direct comparison is impossible unless all other conditions are kept the same. Contrarily, the use of single strains allows mechanistic and physiological details to be observed directly. There is a compelling need to identify pure cultures that can serve as appropriate models for electron transfer to the anodes of MFCs because little is known about this process's physiology. *Shewanella* species were the first organisms proposed to transfer electrons to the surface of electrodes via electron-transfer proteins. They are electrochemically-active bacteria that can oxidize various fermentation products and utilize an electrode as an electron acceptor.

### Extracellular electron transfer (EET) mechanisms

The current generation in MFCs depends on the exoelectrogenic community structure. Insight into understanding a microbial biofilm on an electrode surface is essential to enhance the power output and reveal extracellular electron transfer. So far, only two bacteria, namely, *Geobacter spp.* and *Shewanella spp.*, have been extensively investigated to explore the extracellular electron transfer (EET) mechanisms. Electrons can be transferred to the anode by electron mediators or shuttles, by direct membrane associated electron transfer, or by so-called nanowires produced by the bacteria, or perhaps by other as yet undiscovered means. Which mechanisms are the most important depend on the microorganisms and the thickness of the anode biofilm. Two types of EET mechanisms have been confirmed in both bacteria:

- DET: the direct electron transfer mechanism.
- MET: the mediated electron transfer mechanism.

Figure 1.2 illustrates the different EET mechanisms. The electrons reach the anode in one of three ways:

- Protein carriers can transport them on the cell surface.
- They can be exported through cell membrane projections (nanowires).
- They can be secreted in chemical solutions (mediators).

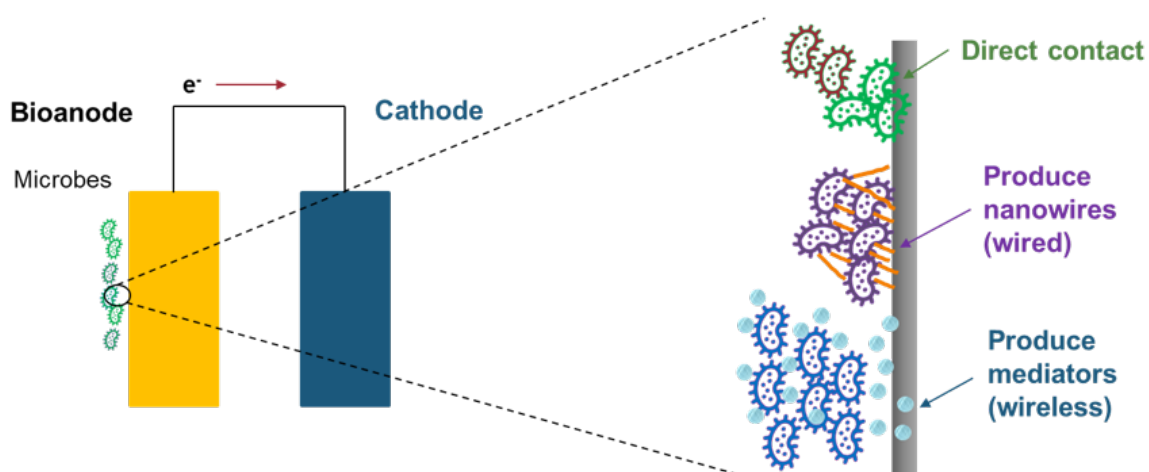


FIGURE 1.2: General principle of a double-chamber microbial fuel cell (MFC). Electrons can be carried by protein carriers, nanowires or mediators.

### MFC Losses

In the anode chamber of an MFC, the oxidation of organic matter by exoelectrogens results in a low redox potential, while in the cathode chamber, reduction of an electron acceptor, for example, oxygen, results in a higher redox potential. This difference in redox potentials drives the electrons to flow from the anode to the cathode, which consequently results in bioelectricity generation.  $E_A$  and  $E_B^o$  present the electrode potentials of the anode and the cathode, respectively. For MFC calculations, the reaction in the anode chamber is evaluated in terms of the overall cell electromotive force (emf),  $E_{\text{emf}}$  (V) defined as the potential difference between the cathode and anode:

$$E_{\text{emf}} = E_A^o - E_B^o \quad (1.3)$$

The open circuit voltage (OCV) is the cell voltage that can be measured after some time in the absence of current. Theoretically, the OCV should approach the cell  $E_{\text{emf}}$ . However, in practice, however, the OCV is substantially lower than the cell  $E_{\text{emf}}$ . Considering the losses mentioned below, the measured cell voltage can be described by the following equation, where  $R_{\text{int}}$  summarizes all internal losses of the MFC.

$$E_{\text{cell}} = \text{OCV} - R_{\text{int}} \quad (1.4)$$

- **Ohmic losses** include the resistance to the flow of electrons through the electrodes and interconnection, the resistance to the flow of protons via the PEM, and the anodic and cathodic electrolytes. Increasing the electrolyte's conductivity can reduce ohmic losses.
- **Activation losses** due to the energy needed for the oxidation-reduction reactions, occurring during the electron transfer from an organic matter to the electrode surface.
- **Bacterial metabolic losses** occur when the anode's potential is kept at a high or too low potential. The higher the difference between the substrate's redox potential and the anode, the higher the possible metabolic energy gain for the bacteria, but the lower the attainable MFC voltage.
- **Concentration losses** occur due to limited mass transfer between the electrode surface and any species in the anode chamber.

### 1.2.2 Factors affecting the MFC performance

MFCs utilize the organics in sludge to generate power. However, the low efficiency of organics utilization and limited power-output are the main challenges that need to be addressed. Improving the power performance remains the key focus of current research, hoping to move MFCs toward eventual practical applications. Generally, substrate degradation, electron transfer from the microorganisms to the anode, proton migration from anode to cathode through liquid media, and cathodic reaction rate are critical steps involved in MFC performance. Moreover, the main factors that impact the power generation in MFCs are:

#### Waste sludge

MFCs are a cost-effective system where energy is produced using microbes in the soil, wastewater, and waste sludge (Ozansoy, 2011). This latter constitutes a unique substrate for the current generation in MFCs due to its large combination of various organisms and nutrients capable of supporting certain bacteria's growth with MFCs (Cai et al., 2018). Most of the research tested the MFC performance using synthetic wastewater with sole carbon source of acetate, glucose, or cellulose under controlled experimental control conditions. Literature works stated that the solutions used were sterilized at high temperature to eliminate unknown bacteria's interference to the experimental results. Research conducted on the use of MFCs for wastewater treatment has shown that the contaminants and organic content of the wastewater can modify the MFC's anodic microbial community dynamically. The carbon source influences the anodic bacterial population in determining the operational performance of power generating MFCs. Furthermore, it is generally recognized that a specific ratio of nutrients is needed to metabolize anaerobes for optimal growth of bacteria. These findings indicate that various factors, including the Chemical Oxygen Demand (COD), influence the electrical current obtained from the MFC, the amount of electroactive and aerobic bacteria, and the nutrient ratios present that allow the bacteria's growth and metabolism. Being rich in COD, organic material broken down by the microorganisms could result in the formation of Volatile Fatty Acids (VFAs), however, altering the pH of the wastewater. Hence, this is the most likely reason to characterize the parameters such as pH, temperature, COD, Totale Dissolved Solids (TDS), and conductivity.

### **Electrochemically active bacteria**

It was found that the response of the MFC is positively correlated with the bacterial composition, in particular electroactive bacteria. It is well known that the bacterial population on the electrode plays a significant role in the electrical response of a microbial fuel cell. A mixed-culture biofilm community is typically and ideally a synergistic community with each species playing specific roles in a nutrient cycle ecosystem. For example, some of them digest nutrients while others contribute to the defense of the biofilm against harmful environmental conditions. Moreover, the anodic biofilm is dynamic in its microbial population, and its composition can change even after a long duration of stable operation. The availability of electroactive bacteria and aerobic versus anaerobic bacteria in the sample can cause changes in response because aerobic bacteria in the sample reduces the current generation. The interaction of the bacteria in the feed with the electrode and its biofilm can produce a synergistic effect, enhancing the conversion of organic matter in the feed to electrical current and affecting the MFC's performance. Based on this reasoning, not only is the electroactive bacterial content of the sample important, but the proportion of the aerobic bacteria is also critical in the electrical response of the MFC and its correlation with the COD. Furthermore, methanogens would otherwise use organic matter for methane production instead of electricity generation. Therefore, some pretreatments would be essential to change the biological properties of the used waste sludge.

### **MFC reactor configuration**

The traditional MFCs are two-chambered with an anaerobic anode and an aerobic cathode. This design presents numerous engineering problems, such as anode and cathode must be close to each other to facilitate the proton transfer and increase power outputs. The cathode cannot be anaerobic because oxygen is needed at the cathode surface to complete the reaction with the electrons and protons. The anode cannot be aerobic, as the bacteria that are capable of producing current do so under anaerobic conditions. Otherwise, they will be inactivated. In case of any oxygen leak, the efficiency of fuel's conversion to electricity goes down. In some other MFCs configurations, the PEM was removed. In this case, the anode is maintained anaerobic, and the cathode is aerobic. However, they should be separated by an optimum distance to allow for a gradient of oxygen and low resistance at the same time.

### **MFC operating conditions**

Since the anodic chamber in an MFC is generally anaerobic, especially under static conditions, many of them may be inactivated and unable to participate in the degradation of large organic matters to smaller ones to consume electroactive bacteria. It was previously reported that the anodic biofilm formation is active under specific ranges of temperature ( 5 to 45°C). The temperature has an impact on the initial biofilm formation process. Biofilms grown at higher temperatures tend to have higher electrochemical activity than those at lower temperatures. Besides, consideration of pH and its changes during MFC operation is among essential factors in power generation. Moreover, oxygen leakage through the cathodic chamber or from the anode chamber's surroundings is known to significantly impair MFC power output because of the biofilm usage of oxygen instead of the anode as the electron acceptor. The external resistance can afford the power performance of MFCs by regulating the electron flow from the anode to the cathode. The optimal external resistance for maximum power production in an MFC should approach its internal resistance. The external resistance can also affect the biofilm formation and thus the community structure.

To optimize and develop energy production by MFCs, full knowledge of the factors mentioned above is essential. Depending on the MFC's waste sludge and operational parameters, the bacteria use different metabolic pathways, which determines how bacteria use the anode as an electron acceptor and to what extent they generate electrical output. Researchers engaged in MFCs studies have endeavored many innovative efforts to increase the power output of MFCs. Many new MFC designs were developed using useful materials for the electrodes and membrane. Also, operating conditions have been treated at specific conditions. Moreover, inoculum treatment and electrode nanomodification have become a new trend to improve system performance. The main target to modify the electrodes in MFCs is to provide a high surface area for biofilm formation and increase the EET mechanisms. The anode chamber can also be modified by adopting a chemical treatment strategy to accelerate the electron transfer and thus improve the power performance of MFCs. Nanoparticle's addition can be a promising strategy to enhance the MFC system performance. It could help bacteria adhere to the electrode more efficiently, improve the anodic attachment, and transfer exoelectrogens.

## 1.3 $\text{Fe}^0$ Nanoparticles and Microbial Fuel Cell System

### 1.3.1 Nanoparticles

Metallic nanoparticles have been broadly applied in catalysts, biotechnology, biomedicine, optoelectronics, environmental remediation, and construction. Nanoparticles have a high surface-to-volume ratio and are typically in dimensions of 1 to 100 nm. This size range is making nanoparticles an interesting new type of material for studying their electronic, optical, catalytic, magnetic, and geometric features. The nanoparticles' role in these applications was only discovered recently with the advancement in microscopy. Metallic nanoparticles can be synthesized in various media: in the gas phase, in solution, supported on a substrate, embedded in a matrix, or a bacterial cell. Lots of experimental techniques have been used to characterize metallic nanoparticles. Metallic nanoparticles have also been widely used for environmental remediation. Their properties make them highly reactive with common organic pollutants and minimize the formation of unwanted toxic by-products. Their small size also provides an opportunity to deliver these remedial agents to subsurface contaminants in situ and provides access to contamination trapped in the smallest pores in an aquifer matrix.

Typically the nanoparticles were injected into the reactive treatment zone for remediation. Metallic nanoparticles can efficiently adsorb pollutants from the contaminated area before their removal from soil and groundwater. With magnetic metal nanoparticles, the recovery can be more manageable.  $\text{Fe}^0$  nanoparticles are a reactive and no longer active when all the  $\text{Fe}^0$  is oxidized. Other metallic nanoparticles not transformed during reactions are catalytic nanoparticles. Iron is one of the most frequently used metal for the treatment of contaminants present in water. It is the fourth most abundant element after oxygen, silicon, and aluminum present in the earth's crust. Iron is a reactive metal with standard redox potential  $E^0 = -0.44\text{V}$ , making it an effective reductant when reacting with oxidized contaminants. It is a useful and versatile tool for the purification of waters and soils owing to its: (i) environmental friendliness, (ii) high reactivity, and (iii) cost-effectiveness. When catalytic nanoparticles are used, an additional reductant or oxidant reagent like  $\text{H}_2$  reductant is used.

These metallic nanoparticles have a high affinity for concentrating the contaminants onto the particles. The contaminants are then removed along with the nanoparticles. The core primarily consists of metallic iron  $\text{Fe}^0$ , whereas a mixed valent ( $\text{Fe}^{2+}$  and  $\text{Fe}^{3+}$ ) oxide shell is formed as a result of oxidation of metallic iron.

The decrease of the iron particle size helps increase the number of atoms located on the surface of the particles. Therefore, their liability to adsorb, interact, and react with other particles will increase to achieve the charge stabilization (Alatraktchi, Zhang, and Angelidaki, 2014).  $\text{Fe}^0$  nanoparticles offer a grand promise for the environmental treatment of various contaminants and wastewater treatment (Yirsaw et al., 2016).  $\text{Fe}^0$  nanoparticles have been considered useful for wastewater treatment (Eljamal, Sasaki, and Hirajima, 2013; Eljamal, Khalil, and Matsunaga, 2017) due to their wide area distinctive reactivity combination, stability, and selectivity.  $\text{Fe}^0$  nanoparticles were successfully applied in degrading the chemical pollutants and cleaning wastewater. Krasae and Wantala, 2016 investigated the effect of  $\text{Cu-Fe}^0$  on nitrate reduction and its pathway utilizing nitrogen gas. Also,  $\text{Fe}^0$  was effective to remove nitrate in different contaminated- water bodies (Khalil et al., 2018). Results proved that the addition of  $\text{Fe}^0$ -based nanoparticles during the treatment significantly enhanced the nitrate removal. Furthermore, Eljamal, Okawauchi, and Hiramatsu, 2012 studied the removal of phosphorus from water using nanoparticle technology. Cesium removal from waters was also investigated, and the use of  $\text{Fe}^0$  nanoparticles greatly enhanced the removal efficiency (Eljamal et al., 2018). Besides, the microbial community's variation in the real waste sludge when exposed to  $\text{Fe}^0$  treatment was extensively studied. Results revealed that  $\text{Fe}^0$ -based nanoparticles could enhance bacterial growth when treated with optimal concentrations. Figure 1.3 illustrates a schematic design of bare iron nanoparticles.

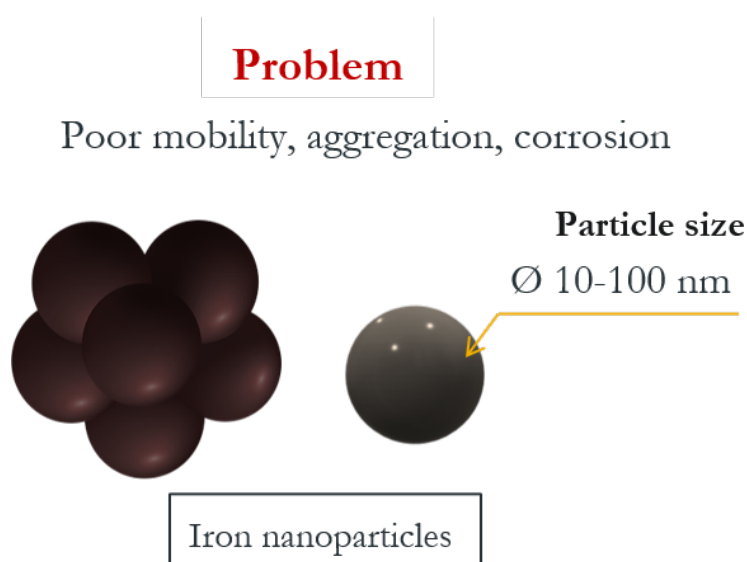


FIGURE 1.3: Bare  $\text{Fe}^0$  nanoparticles.

### 1.3.2 Literature review

Specific microbial strains have been exploited in the literature due to their high sensitivity and vulnerability to Fe<sup>0</sup>. In (Fajardo et al., 2013), the *Bacillus cereus* growth was recorded, and results showed that a complete inactivation was obtained when treated with 10 mg/mL of Fe<sup>0</sup> under aerobic conditions. The same impact was also observed for both *B. subtilis var. niger* and *P. fluorescens*. The study stated that there was still a complete deactivation for *P. fluorescens*, when the concentration decreased to 1, 0.1 mg/mL, whereas the toxicity effect decreased for *B. subtilis var. niger*. Moreover, in (Lv et al., 2017), *Pseudomonas putida* activation decreased with an increase in the dissolved oxygen concentration under Fe<sup>0</sup>/Pd treatment. (Pan et al., 2019) investigated the evolution of microbial community when exposed to Fe<sup>0</sup> nanoparticles. Results showed that the bacterial structure was modified, and methane production increased. Also, an abundance of *Bacillus*, *Paludibacter*, *Desulfovibrio* and *Lactococcus* species was observed in constructed wetlands microbial fuel cells (CW-MFC).

The influence of Fe<sup>0</sup> nanoparticles on biological activity was examined following the different bacterial growth phases (Chaithawiwat et al., 2016), and results showed that all the studied bacterial strains were highly resistant in the lag and stationary phases, whereas cells in exponential and death phases were rapidly inactivated. (Fajardo et al., 2012) provided a discussion about the effects exerted by Fe<sup>0</sup> nanoparticles on bacterial populations. Results suggested that the general impact is dose and species-dependent. All prior studies suggested that the impact of Fe<sup>0</sup> nanoparticles generally depends on the different microbial strains, their metabolites, and vulnerability. Also, the toxicity can be linked to the Fe<sup>0</sup> nanoparticles concentrations. Besides, the bacterial inactivation mechanisms can be classified into three categories (Lv et al., 2017): (i) the membrane disruption caused by the direct contact between Fe<sup>0</sup> nanoparticles and the bacterial cell surface, (ii) the high generation of the reactive oxygen species (ROS). Once accumulated inside the bacterial cell, all the proteins and nucleic acids are deteriorated and consequently cause cell inactivation, and (iii) the high release of Fe<sup>2+</sup> caused by Fe<sup>0</sup> oxidation.

In fact, the existence of bacteria has proven to be important in wastewater treatment plants for biological and wastewater treatments due to their potential in oxidizing the organic matter. Biogas production and more precisely methane gas production depends mainly on the methanogens and their behavior in the anaerobic digestors. Another application where bacteria and specifically exoelectrogens play an important role is the microbial fuel cells technology. Microbes are the biocatalyst that degrade the organic matter and electrons are released

as a product of the oxidation process. Microbes are the powerhouse of the microbial fuel cells technology which is based on electrochemical reactions to convert the organic matter present in the wastewater to electrical energy.

MFCs are not yet commercialized, but they show great promise as a wastewater treatment method and bioenergy generation. The power produced by these MFCs is currently limited, primarily by the high internal resistance. Nanoparticles can be used to improve the conductivity of the anode chamber due to its own high conductivity. The use of nanoparticles comes to seeking compatibility with the microorganisms and enhance power generation in microbial fuel cells.  $\text{Fe}^0$  nanoparticles have a promising potential for bioelectricity generation in MFCs. Many investigations on the effects of  $\text{Fe}^0$  on MFC's response have been achieved. A new manner of  $\text{Fe}^0$  based MFC-biosensor was developed in (Jia et al., 2017) for the properties of up-flow anaerobic sludge blanket (UASB-MFC) biosensor at different organic loading rates. The mechanism of the electron transport process was explored when  $\text{Fe}^0$  was added. The evolution of volatile fatty acids (VFA) in acidified reactors as the response to  $\text{Fe}^0$  addition was investigated to explore the process of the positive inhibition effect of  $\text{Fe}^0$ . Compared to the control group for the loading variation, the electrical signal response time shortened with the addition of  $\text{Fe}^0$  which maximum reached 2 hours with 30 mg/L  $\text{Fe}^0$  added compared to 5 hours of control reactor during the intermediate loading phase, and the response time elongated with the organic loading increased.

$\text{Fe}^0$  facilitated the anaerobic digestion process, helped buffer pH in a suitable range for exoelectrogen growth, and compressed electric double layer sludge effectively as well. The electrochemical analysis confirmed that the lower internal resistance and higher redox activity occurred in the  $\text{Fe}^0$ -biosensor, indicating that the direct interspecies electron transfer of the anode enhanced when anaerobic digestion intensified, and  $\text{Fe}^0$  plays a vital role in the sensing process. In (Cai et al., 2018), iron was doped into the anode electrode of a sludge MFC, and experiments showed an improvement in the electricity generation and wastewater treatment. This enhancement could be attributed to the substantial reduction of  $\text{Fe}^0$  particles, which improved the energy production. (Cai et al., 2019) proposed a method to enhance the performance of sludge MFC by adding the package of iron and carbon granules (FeC). In FeC-supported MFCs, the soluble and total chemical oxygen demand removal efficiencies were improved, thereby improving electrical performance. The study results reported that promoting the degradation of organics was beneficial to the enrichment of electrochemically active bacteria, especially typical exoelectrogens belonging to *Proteobacteria* and *Firmicutes*. In

(Zhang et al., 2014),  $\text{Fe}^{3+}$  ions were added to MECs to enhance both anaerobic digestion and anodic oxidation, resulting in good mineralization of volatile fatty acids. Besides, exogenous  $\text{Fe}^{3+}$  played a critical role in the biofilm formation and flavin secretion for *Shewanella oneidensis* MR-1 in MFCs and enhanced the power output (Wu et al., 2013). (Liu et al., 2018) described the response of microbial electrode biofilm communities to insoluble  $\text{Fe}^{3+}$  at different concentrations in MFCs. The results demonstrate that a low concentration of  $\text{Fe}^{3+}$  facilitated the power output of MFCs and shaped the electrode biofilm.

Optimizing the ecological conditions that facilitate exoelectrogen enrichment and the current output is essential for developing MFCs.  $\text{Fe}^0$  is a low cost and active metal with substantial reduction. When added to the anode in MFCs,  $\text{Fe}^0$  may prevent acid accumulation, maintaining the anaerobic system in neutral pH to reduce microbial activity inhibition.  $\text{Fe}^0$  is beneficial for enhancing the reductive atmosphere, thereby strengthening the electricity generation.  $\text{Fe}^0$  may constitute numerous micro galvanic cells with reduction, flocculation, adsorption, complexation, and electrode's position. The electrochemical performance of air-cathode MFCs supplemented with different ferric iron concentrations was investigated to evaluate insoluble ferric iron's effect on bacterial biofilms on electrode surfaces. Results indicated that  $\text{Fe}^{3+}$  at a lower concentration had an apparent positive effect on microbial extracellular electron transfer capacity. On the contrary, excess  $\text{Fe}^{3+}$  might compete for an electron with the anode and inhibit the biofilms' electrochemical activity. Furthermore, the cathode biofilms' bacterial community shifted substantially when higher concentrations of  $\text{Fe}^{3+}$  were present in the MFCs. The majority of dominant exoelectrogens in the anode biofilm of the MFCs were affiliated with *Geobacter*, and the relative abundance was 66–75 % in the  $\text{Fe}^{3+}$ -supplemented MFCs. Particular concentrations of the  $\text{Fe}^{3+}$  supplement substantially boosted the electrochemical activity of the MFCs during the start-up period.  $\text{Fe}^{3+}$  shifted the anode bacterial community and facilitated enrichment of exoelectrogenic bacteria.  $\text{Fe}^{3+}$  may form magnetite, which mediates EET in microbes.  $\text{Fe}^0$  nanoparticles, because of their small size, tend to agglomerate. Efforts have been made to improve the low suspension, high magnetic attraction, and the aqueous corrosion of  $\text{Fe}^0$  nanoparticles (Amen et al., 2018; Eljamal et al., 2019; Maamoun et al., 2020). Other noble metals were added to  $\text{Fe}^0$  forming the so-called bimetallic nanoparticles, where  $\text{Fe}^0$  acts as an anode, and the inert metal plays the role of a cathode, accelerating the corrosion rate of  $\text{Fe}^0$ . The metals added to the surface of  $\text{Fe}^0$  are expected to promote  $\text{Fe}^0$  nanoparticles' reactivity and provide adequate protection against

passivation corrosion. Iron is the crucial element of ferredoxin and plays a vital role as an enzyme activator in some anaerobic bacteria. Higher concentrations of  $\text{Fe}^{3+}$  have an inhibitory effect on the power outputs of the MFCs by increasing the anode's internal resistance or decreasing biodegradation substrates. Consequently, the microenvironment plays an essential role in shaping the microbial community and changing electrode reactions. Microbial communities response were present on the MFC biofilms in response to  $\text{Fe}^{3+}$ . Magnesium (Mg) was introduced to the MFCs for power generation. In (Li, Zhou, and Xu, 2017), graphene oxide aided with magnesium oxide (MgO) was used as a competent cathode catalyst for power production in a single chamber MFC. Results showed that the power density had a stable level after 20 cycles of running. A magnesium-air fuel cell electrocoagulation was also used for electricity production and phosphorus recovery from synthetic wastewater (Kim et al., 2018). Besides, MgO nanoparticles were prepared as cathode catalysts in an air-cathode MFC, and the power density was higher than the control by 58.3 %.  $\text{Mg}^{2+}$  reduced the electron transfer resistance and promoted the  $\text{H}^+$  adsorption (Liang et al., 2020).

## 1.4 Research interests

As it was mentioned previously, the effect of  $\text{Fe}^0$  nanoparticles on bacterial growth is still not confirmed yet, as well as the optimized level of  $\text{Fe}^0$  concentration that should be added to the wastewater reactor to guarantee the positive effect on the living microorganisms and on the wastewater treatment. The research studies have been focusing on the response and behavior of different living microorganisms due to the importance and utility of these bacteria in many technologies. The aim of this research study was to investigate the effect of bare  $\text{Fe}^0$  and iron-based nanoparticles on the behavior of a mixed culture bacterial cells collected from a domestic wastewater plant and to study the effect of the system condition variations on the microbial growth. In a first step,  $\text{Fe}^0$  nanoparticles were added to the wastewater reactor with three different concentrations. In a second step, the nanoparticles were impregnated with Ag, Cu, and Ni and their effects on bacterial growth and COD removal were evaluated. The added metals were chosen based on their environmentally friendless, cost effectiveness, and their performances in other studies.

Moreover, despite the improvements mentioned above in the performance of MFCs equipped with  $\text{Fe}^0$ , the low mobility, poor aqueous stability, longevity, and the aqueous corrosion of  $\text{Fe}^0$  nanoparticles, still limit their performance, and consequently, the current generation by

MFCs. It has been reported that around 35 pure cultures including *Geobacter*, *Pseudomonas* sp., *Rhodoferax*, *Shewanella*, *Cupriavidus basilensis*, *Lactococcus lactis*, and *Propionibacterium freudenreichi* have been effectively used in MFCs as exoelectrogens. Our study considered the use of actual sludge, which represents a wide range of microorganisms and nutrients capable of supporting the growth of certain bacteria with MFCs. Moreover, such a fuel would have a high organic matter content. The bioelectricity generation potential of a microbial culture cannot be compared with another unless and until all physical and chemical parameters are the same. In this thesis work, we have considered studying the effect of organic matter content, which is viewed as the source of mixed culture/anaerobic bacteria. However, microbial community changes are a dynamic and very complicated process during MFC operations. Other challenges arise when using real wastewater as the substrate. Various organic and inorganic toxic elements or compounds can be utilized as the electron acceptor in the anode chamber.

To the best of our knowledge, only a few studies have focused on using  $\text{Mg}(\text{OH})_2$  for MFC technology and none of them have investigated the effect of  $\text{Fe}^0$  nanoparticles coated with  $\text{Mg}(\text{OH})_2$  shell for bioelectricity generation. This study comes first to evaluate the response of a lab-scale microbial fuel cell to Mg/Fe nanoparticles treatment using real waste sludges. Coated  $\text{Fe}^0$  would protect the nanoparticles' reactivity and improve their performance by a temporary surface coating. Magnesium hydroxide  $\text{Mg}(\text{OH})_2$  coating shell can be considered an advantageous surface modification method (Liu et al., 2020).  $\text{Mg}(\text{OH})_2$  is a cost-effective and eco-friendly material, kinetically stabilized, and it is characterized by its large specific area and numerous active reaction sites. These latter contribute to the viability of treatment for multiple pollutants. Therefore, coated  $\text{Fe}^0$  with  $\text{Mg}(\text{OH})_2$  could be an attractive tool for power generation enhancement in MFCs technology. The  $\text{Mg}(\text{OH})_2$  coating layer is expected to prevent the  $\text{Fe}^0$  nanoparticles from aggregation and corrosion and reduce the toxicity towards bacterial cells. In addition, the dissolution of the  $\text{Mg}(\text{OH})_2$  shell would control the release of  $\text{Fe}^0$  reactivity. The  $\text{Mg}(\text{OH})_2$  shell could concurrently deal with the mobility problem of  $\text{Fe}^0$ . The  $\text{Mg}(\text{OH})_2$  coating provides a reliable and straightforward strategy to prolong the lifespan of  $\text{Fe}^0$  particles in actual field applications and guarantee its long-term decontamination efficacy. The  $\text{Mg}(\text{OH})_2$  coating not only protects the  $\text{Fe}^0$  cores from corrosion in water but also reduces the toxicity of  $\text{Fe}^0$  toward living microorganisms when exposed to  $\text{Fe}^0$  treatment.

## 1.5 Conclusion

Compared with other biomass degradation technologies, such as anaerobic digestion, the apparent difference is that MFCs exploit powerful exoelectrogens as catalysts to oxidize organic matter and convert the collected energy in Joules directly into direct current electricity. Generally speaking, microbial community changes are a dynamic and very complicated process during MFC operations. Substrate degradation, electron transfer from the microorganisms to the anode, and proton migration from anode to the cathode through liquid media, cathodic reduction reaction rate are critical steps involved in MFC performance. Other challenges arise when using real wastewater as the substrate. Various organic and inorganic toxic elements or compounds can be utilized as the electron acceptor in the anode chamber. Inoculum culture sources and substrate types, the MFC reactor configuration, operation conditions, electrode materials, external and internal resistances, and substrate types are essential parameters that affect microbial communities in MFCs. The following chapters investigated the MFC's performance under  $\text{Fe}^0$  nanoparticles treatment. In a double-chamber MFCs, a series of experimental strategies were executed to improve overall system performance, as shown in Figure 1.4 and Figure 1.5

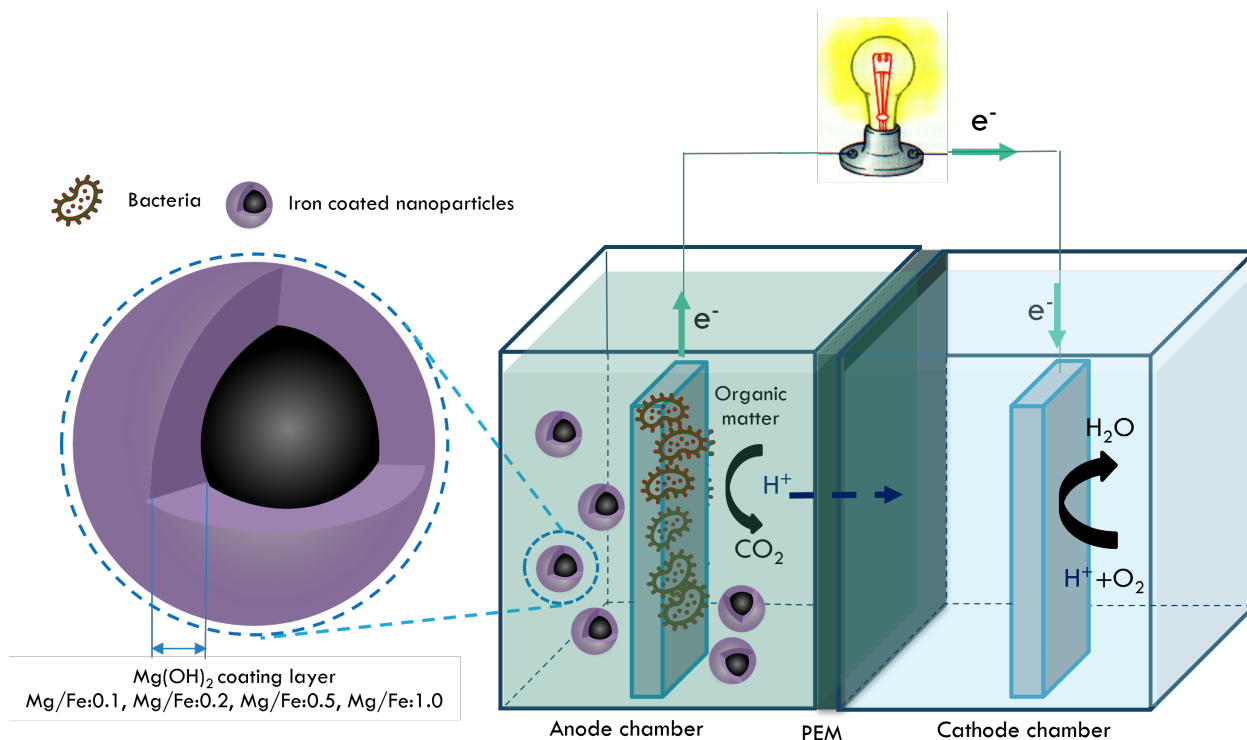


FIGURE 1.4:  $\text{Fe}^0$ -based nanoparticles introduced to a double-chamber MFC.

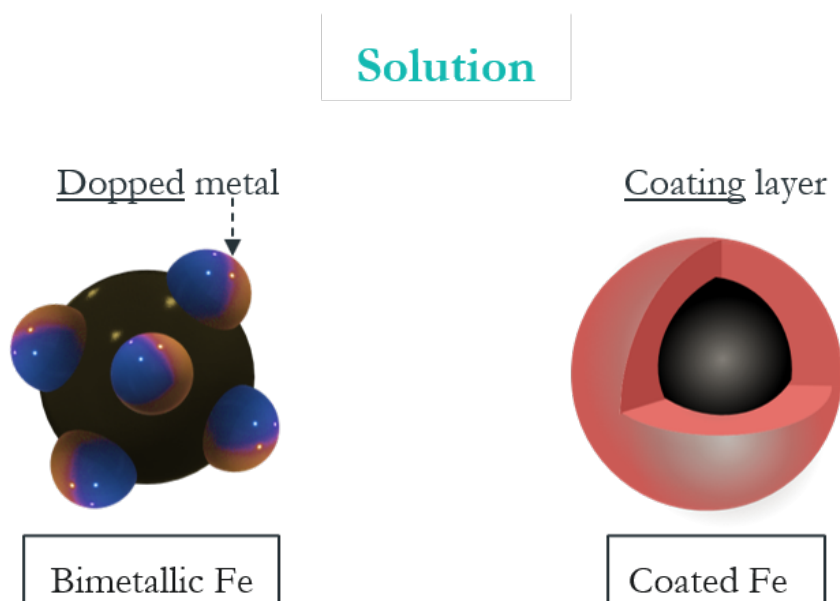


FIGURE 1.5: Schematic drawing of  $\text{Fe}^0$ -based nanoparticles.

The output of these experiments will be focused mainly on power output and MFC efficiency, as well as the solution conductivity, internal resistivity, the biofilm growth on the anode surface, and especially the electron transfer techniques. Usually, one batch of experiments lasts from 60 to 90 days. MFCs technology is a technology solution for cheap, fast, and simple. Many challenges will be addressed including a more detailed analysis in energy production, consumption, and application, understanding the relationship between the amount of electricity and contaminant removal, promoting the elimination of nutrients and optimizing system configuration and operators. Nanoparticles have been used in wastewater treatment and results proved that their use could be effective for toxic elements removal. In other studies, electrode surfaces were doped with nanoparticles and power output could be enhanced. Therefore, it is expected that adding nanoparticles will improve the MFC performance mainly by:

- Enhancing the biofilm structure
- Being a second source of electron
- Playing the role of an electron carrier
- Being a trace element for bacterial growth



## Chapter 2

# Materials and Methodology

### 2.1 Introduction

Referring to the literature, microbial fuel cells (MFCs) offer high reliability for wastewater treatment and energy generation. This is mainly due to the high organic matter content in waste sludge. With this said and considering the wastewater treatment costs, MFCs have cost advantages with regard to other wastewater treatment techniques. Several research projects are currently focusing on the development of cost-effective techniques in an attempt to make it fulfilling the required performances. To do so, the investigation of microbial fuel cells is carried out. The considered technology is characterized by:

- ★ Power density output,
- ★ Total volatile solids analysis,
- ★ Coulombic efficiency (CE).

The investigation was focused on the anode chamber's performance as it is one of the critical factors that determine power generation in MFCs. The experimental studies were carried out in lab-scale microbial fuel cells. Series of strategies were executed to improve overall system performance. The experimental procedure went through:

1. Construction of lab-scale MFCs (MFC's type, electrodes material),
2. Collection and characterization of waste sludge,
3. Synthesis and preparation of iron-based nanoparticles, and
4. Estimating bacterial growth improvement.

## 2.2 Microbial Fuel Cells Set-up

In our study, two configurations of double-chamber MFCs were used. The first configuration consisted of a rectangular double-chamber MFC designed and constructed in our laboratory. The MFC consisted of a two plexiglass chambers having a thickness of 5 mm. Each chamber had a volume of  $640 \text{ cm}^3$ . The two chambers were separated by a cation exchange membrane CEM (Nafion 117, thickness 0.007 in.) having a surface area of  $168 \text{ cm}^2$ . Carbon fiber tissue was used as the electrode material for both anode and cathode, with a surface are equal to  $24 \text{ cm}^2$ . The two chambers were connected through an external circuit with a resistance value equal to  $200 \text{ Ohm } (\Omega)$ . Figure 2.1 illustrates the principal functioning of the MFCs. Before the construction, we developed a mechanical drawing for the MFC unit, as shown in Figure 2.2. Figure 2.3 presents the fabricated double chamber MFC. Four MFCs were built for our study.

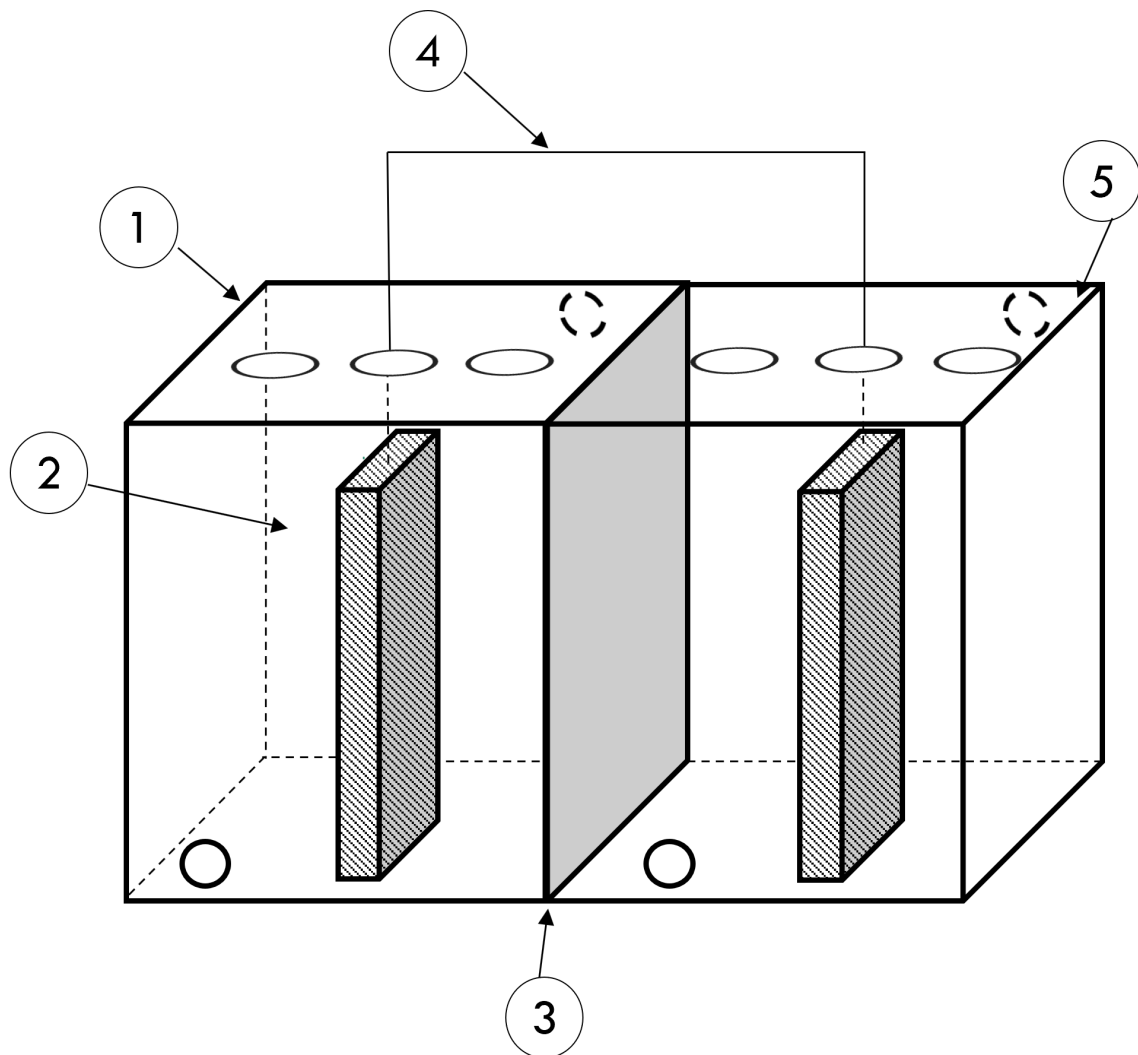


FIGURE 2.1: Schematic design of the lab-scale H-type microbial fuel cell (MFC).

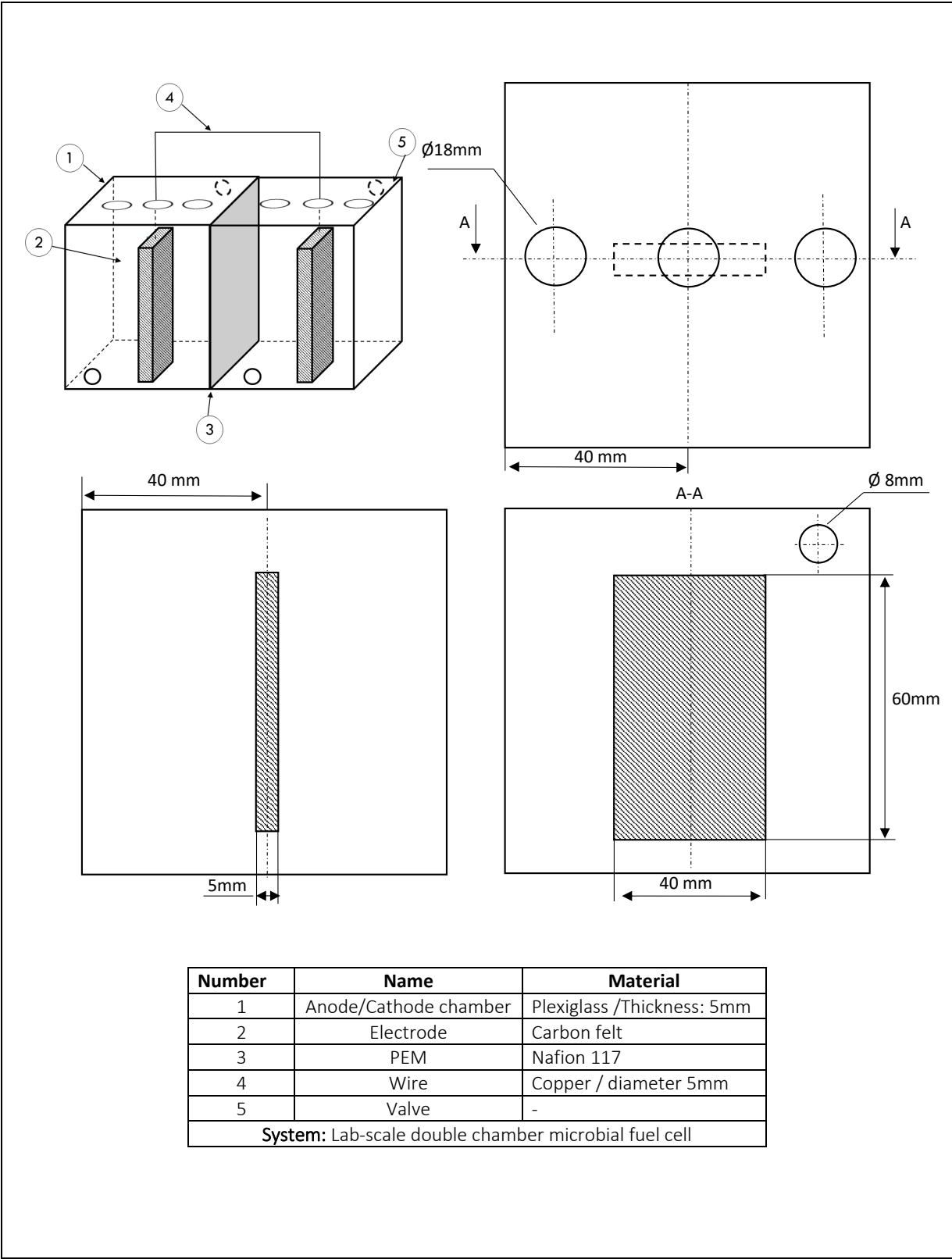


FIGURE 2.2: Mechanical drawing of the lab-scale H-type microbial fuel cell (MFC).

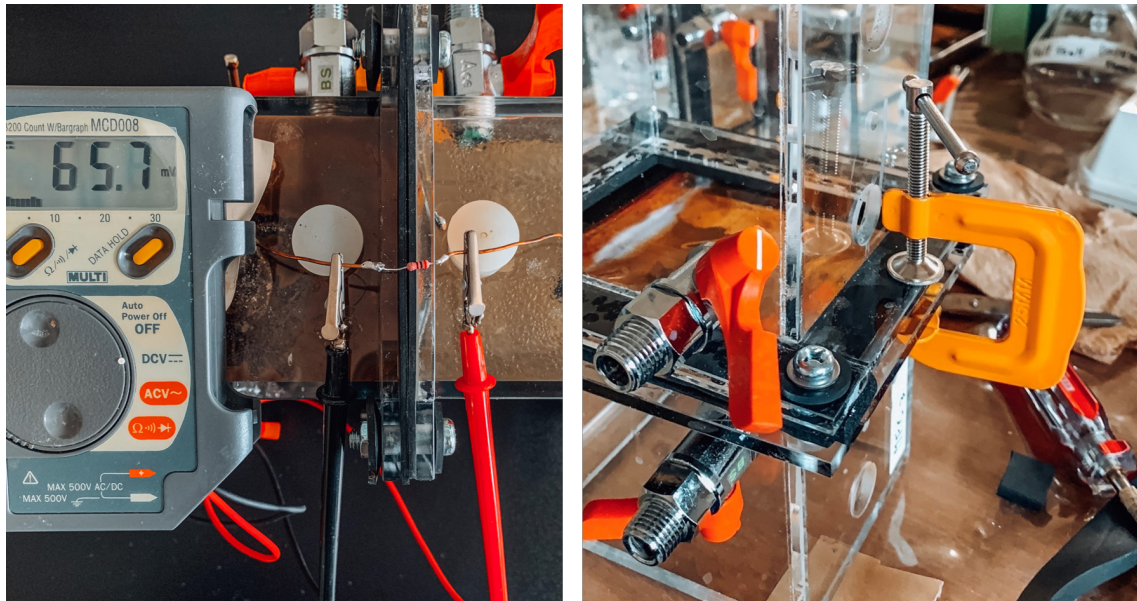


FIGURE 2.3: Construction of the rectangular double-chamber MFC.

The second configuration consisted of "H" type MFCs, containing two bottles with a total capacity of 500 mL, and disconnected by a Nafion 117 proton exchange membrane (PEM). Carbon felt was used for both anodic and cathodic electrodes, and a copper wire, connected via a resistance of  $200\ \Omega$ , was applied to close the electrical circuit. These MFCs are considerably inexpensive and applicable for basic research, such as examining the power production using new materials or types of sludge. However, they typically produce low power owing to the reduced surface of the proton exchange membrane. Figure 2.4 presents their schematic design, whereas Figure 2.5 shows the real H-type MFCs used for the experiments.

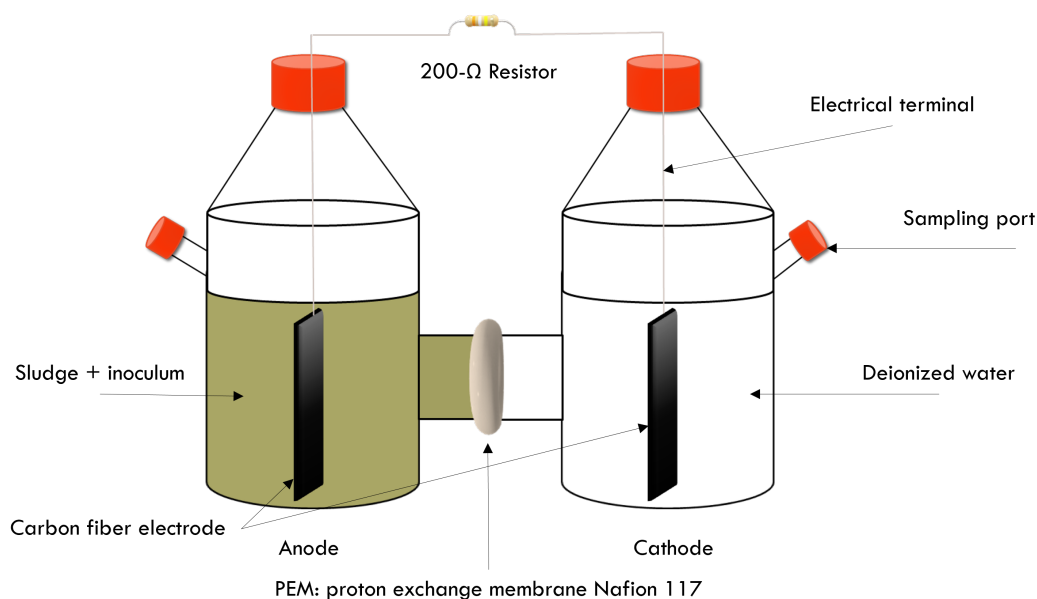


FIGURE 2.4: Schematic design of the lab-scale double chamber microbial fuel cell (MFC).

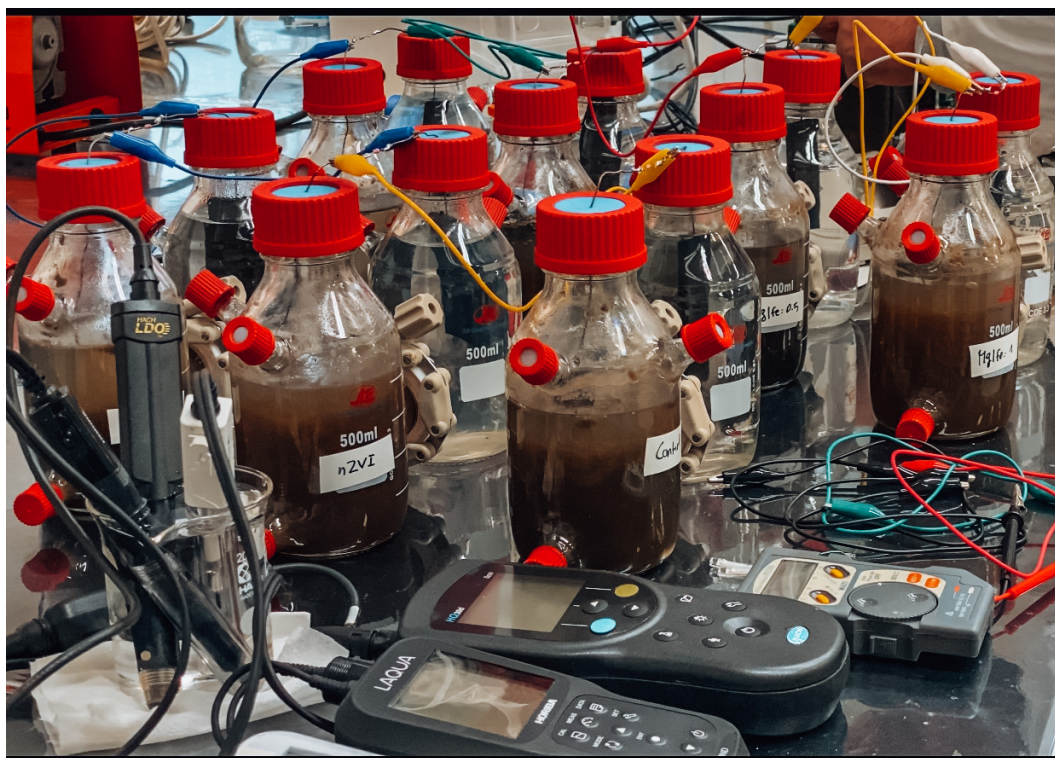


FIGURE 2.5: Real illustration of the the lab-scale H-type MFCs used for our study.

All MFCs were operated in a batch mode and incubated at a constant temperature (40 °C) for 45 days of operation. Cathode chambers were filled with water. All  $\text{Fe}^0$ -based nanoparticles were introduced to the anode solution with a concentration of 10 mg/L to evaluate their effect on MFC's performances. The temperature value was selected based on the system conditions' significant impact on the initial bio-film formation process. Bio-films grown at higher temperatures (5 to 45 °C) tend to be more electrochemically active than those at lower temperatures. A magnetic stirring was utilized to ensure a continuous mixing of the solution (500 rpm), which leads to a homogeneous medium and mass transfer resistance reduction. At the start of experiments, nitrogen gas  $\text{N}_2$  was bubbled into the anodic chamber for 10 min to ensure anaerobic conditions.

### 2.2.1 Waste Sludge Collection and Characterization

The anode chambers were fed with waste sludge from the Mikasagawa domestic wastewater purification center in Fukuoka, Japan as shown in Figure 2.6. Waste sludge samples were collected at different periods and analyzed. Table 2.1 illustrates the sludge characteristics.



FIGURE 2.6: Photo of Mikasagawa wastewater treatment plant in Fukuoka city, Japan.

TABLE 2.1: Initial waste sludges characteristics.

Sample name	Units	Sludge (S1)	Sludge (S2)	Sludge (S3)	Sludge (S4)	Sludge (S5)	Sludge (S6)
TS	g/L	4.785	34.46	4.37	3.69	2.92	4.54
TVS	g/L	3.82	27.68	3.60	2.96	2.19	3.71
TVS/TS	-	0.80	0.80	0.82	0.80	0.75	0.82
COD	mg/L	5561	37802	5849	4186	2975	6298
TDS	mg/L	358	0.04	397	248	252	176
pH	-	6.77	5.94	7.17	7.43	6.95	7.62
ORP	mV	-14	32	-38	-50	-24	-61
Conductivity	$\mu\text{S}/\text{cm}$	716	0.73	795	497	499	352.8
Resistivity	$\Omega.\text{cm}$	1000	2000	1000	2000	2000	3000
Salinity	ppt	0.3	0	0.2	0.2	0.5	0.2

The concentration of  $\text{Fe}^{2+}$ , the total dissolved  $\text{Fe}^0$  were measured using a UV spectrophotometer (Hach DR 3900, USA) (Figure 2.7 (A)). pH and ORP were controlled using a pH meter. Conductivity, resistivity, salinity, and total dissolved solids (TDS) were monitored using a conductivity meter. (Chemical Oxygen Demand) COD values were controlled using the chemical acids that oxidize organic and inorganic substances in the waste sludge sample. Figure 2.7 (B) shows an example of COD measurements. 2 mL of the tested waste sludge sample is injected in the vial then heated at 150 °C for 2 hours using a UV spectrophotometer (Hach DR 3900, USA). TS and TVS were determined following the four stages below:

1. A well-mixed sample of 20 mL is dried at 105 °C for 24 h.
2. The increase in weight of the dish ( $W_2 - W_1$ ) represents the total suspended solids of the sample, where  $W_1$  is the weight of the empty dish before adding the 20 mL of the sample and  $W_2$  is the weight of the dish after 24h.
3. The dish used for total suspended solids (TSS) testing is ignited at 550 °C for 30 min.
4. The weight loss on ignition of the solids ( $W_2 - W_3$ ) represents the total volatile solids (TVS) in the sample, where  $W_3$  is the weight of the dish after 30 min.

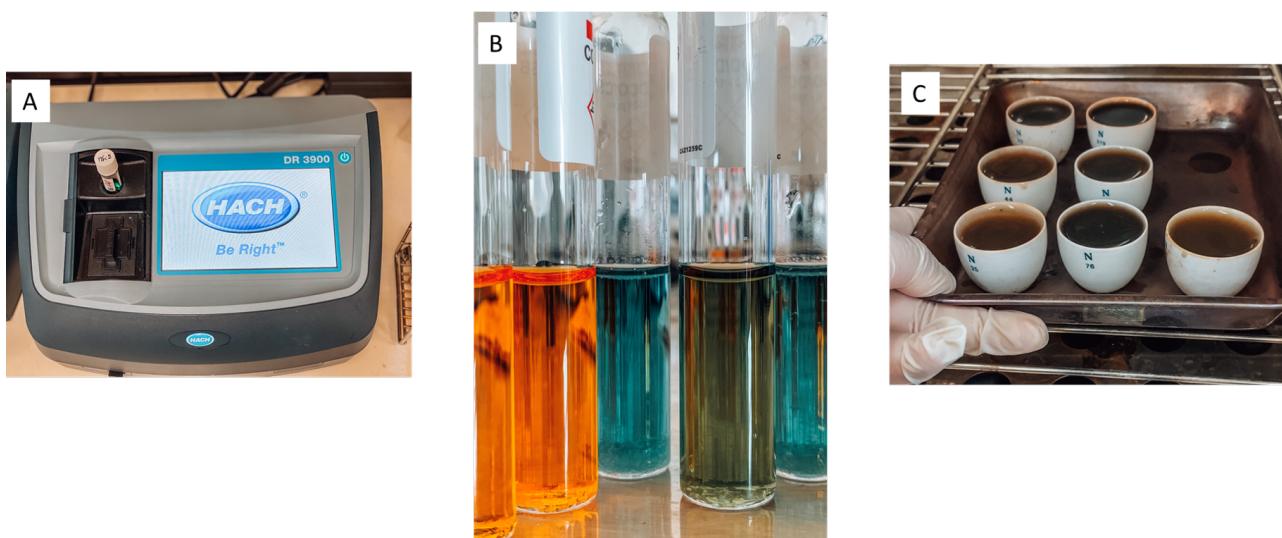


FIGURE 2.7: (A) UV spectrophotometer (Hach DR 3900, USA), (B) Various vials testing the COD values in different waste sludge samples. The vials change the color from orange to green based on the amount of oxidation. (C) Drying the mixed samples of waste sludge in the oven at 105 °C for 24 hours.

Analyses of COD are essential since it reflects the removal of the contaminants (biologically or chemically). COD represents the total measurement of all oxidized chemicals in the water. However, COD values are less specific since they measure everything that can be chemically oxidized rather than just biodegradable organic matter levels. The Biochemical oxygen demand (BOD) presents the amount of dissolved oxygen needed by aerobic biological organisms to break down organic material at a certain temperature over a specific period. Our study excluded the BOD measurements, owing to the long-time requirements (5 days), whereas we can obtain COD measurements within 2 hours. Moreover, solids in waste sludge can be viewed in two basic ways; particulate size or particulate composition. Total Solids (TS) present all solids contained in a measured volume of water and can be subdivided of:

$$TS = TVS + TFS \quad (2.1)$$

TVS are the Total Volatile Solids, solids that are organics and will volatilize during combustion. TFS, the Total Fixed Solids, are the inorganic solids and will not volatilize during combustion. Besides, solids can be measured by the concentration of particulate solids dissolved or suspended in the wastewater. TDS are the Total dissolved Solids, and TSS, the Total Suspended Solids.

$$TS = TDS + TSS \quad (2.2)$$

For solids composition characterization, TVS values were measured considering suspended and dissolved solids. The amount of TVS is essential since it reflects the strength of the waste. The more TVS, the stronger the waste sludge is. Besides, suppose the TVS/TS ratio reflects whether the waste sludge is mostly organic or not. In that case, the MFC operation's impact will be more significant if TS is primarily organic.

The conductivity in anode solution is a measure of the ability of anolyte to electric current. The more ions in the solution, the higher the anolyte's conductivity is. However, conductivity can be easily affected by the ion's concentrations and the substrate's type and dissolved solids used as a fuel in the anode chamber. Oxidative Reductive Potential (ORP) measurements can also indicate the degree to which a substance can oxidize or reduce another sense. ORP values can be: (i) positive when the essence is an oxidizing agent, or (ii) negative when the substance is a reducing agent. Our study aims to develop a strong anolyte that will be a good conductor of electricity, consequently, improve the MFC's response.

### 2.2.2 Data Measurements and Analysis

During the experiment, MFCs output voltage (V) was recorded in regular intervals using a multimeter. Following ohm's law, the current ( $I = V/R$ ) and power ( $P = V \times I$ ) were calculated based on the external resistance and voltage values. The power density was normalized to technical characteristics to compare the power output with other microbial fuel cell systems. Thus, to compare the system related to the MFC fuel like organic matter content in the anode chamber, the power output was normalized to the initial TVS value of the waste sludge as detailed in the following equation (Logan and Regan, 2006):

$$P_{g.VS} = V^2 / R_{ext} \times V_{an} \times TVS \quad (2.3)$$

The Coulombic efficiency (CE) was evaluated as the ratio between the electrons transferred from the microorganisms to the anode, to the theoretical one that can be attained if all organic substrates were digested by the microorganisms to generate electrons.

CE can be measured consequently for batch reactor conditions as shown in the equation below, where all the parameters are defined in Table 2.2:

$$CE = M \times \int Idt / F \times b \times V_{an} \times \Delta TVS \quad (2.4)$$

$$\Delta TVS = TVS_i - TVS_f \quad (2.5)$$

where,  $TVS_i$  is the initial value and  $TVS_f$  is the final value after 45 days of operation.

TABLE 2.2: MFC reactor constant parameters.

Parameter	Description	value
$V_{an}$	Anode chamber volume	500 mL
$R_{ext}$	External resistance	200 $\Omega$
$A_{an}$	Anode surface area	24 cm <sup>2</sup>
F	Faraday constant	96485.34 C/mol
M	Oxygen molecular weight	32 g/mol
b	Indicates the number of electrons exchanges per mole of oxygen	4

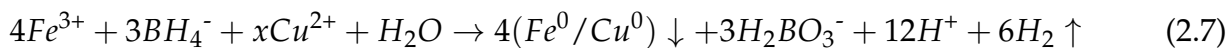
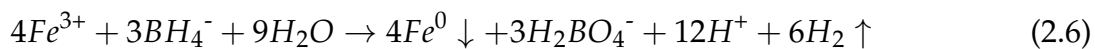
## 2.3 Nanoparticles Synthesis and Characterization

### 2.3.1 Reagents

The following reagents were used for Fe<sup>0</sup>, Cu/Fe<sup>0</sup>, Ni/Fe<sup>0</sup>, and Ag/Fe<sup>0</sup> synthesis, respectively: sodium borohydride (NaBH<sub>4</sub>>99.0 %, Junsei Chemical Co., Japan ) and ferric chloride (>99.0 %, Junsei Chemical Co., Japan), copper(II) chloride (Purity = 99.9 %, Sigma Aldrich, USA), nickel chloride hexahydrate (Purity = 99.9 %, FUJIFILM Wako Pure Chemicals, Japan), and silver nitrate (Purity = 99.8 %, JUNSEI, Japan). Magnesium nitrate hexahydrate (Mg(NO<sub>3</sub>)<sub>2</sub>·6H<sub>2</sub>O,>99.0 %, Sigma-Aldrich Inc., USA) were used for the preparation of magnesium (Mg<sup>2+</sup>) coating-ion solution. Sodium hydroxide (>93 %, Wako Co., Japan) and hydrochloric acid (35-37 %, Wako Co., Japan) were used for pH adjustment. Nitrogen gas was used for deoxygenating the deionized water through bubbling for 15 min before solutions could be prepared. Solutions were set up using ethanol (C<sub>2</sub>H<sub>5</sub>OH,>99.5%, Wako Co., Japan) and deoxygenated deionized water (DDIW, 18.2 M.cm, Milli-Q filter).

### 2.3.2 Synthesis

Fe<sup>0</sup> nanoparticles were prepared by the chemical reduction of 0.093 M FeCl<sub>3</sub>·6H<sub>2</sub>O by 0.58 M NaBH<sub>4</sub> according to the equation below. Figure 2.8 and Figure 2.9 illustrate the synthesis procedure. The sodium borohydride solution was supplemented to the ferric chloride solution dropwise (20 mL/min) using a peristaltic pump. A continuous nitrogen purging was granted to assure anaerobic condition. The 400 RPM vigorous mixing formed Fe<sup>0</sup> precipitates during the synthesis at 30 ± 0.5°C.



For the bimetallic nanoparticles preparation, to produce 1 g of Fe<sup>0</sup>/Cu<sup>0</sup> with the ratio (5% wt/wt), 0.1057 g copper chloride was mixed with 5 g of ferric chloride in 125 mL of distilled water. 5 g of sodium borohydride also was mixed in 125 mL distilled water and then was added drowsily into the mixture of copper-iron salts. Fe<sup>0</sup>/Cu<sup>0</sup> was synthesized following the reaction below, where, x is the number of copper moles. Vacuum filtration was used for separation after rinsing with deionized water (DIW). Ni/Fe<sup>0</sup>, and Ag/Fe<sup>0</sup> were prepared using nickel chloride and silver nitrate, respectively.

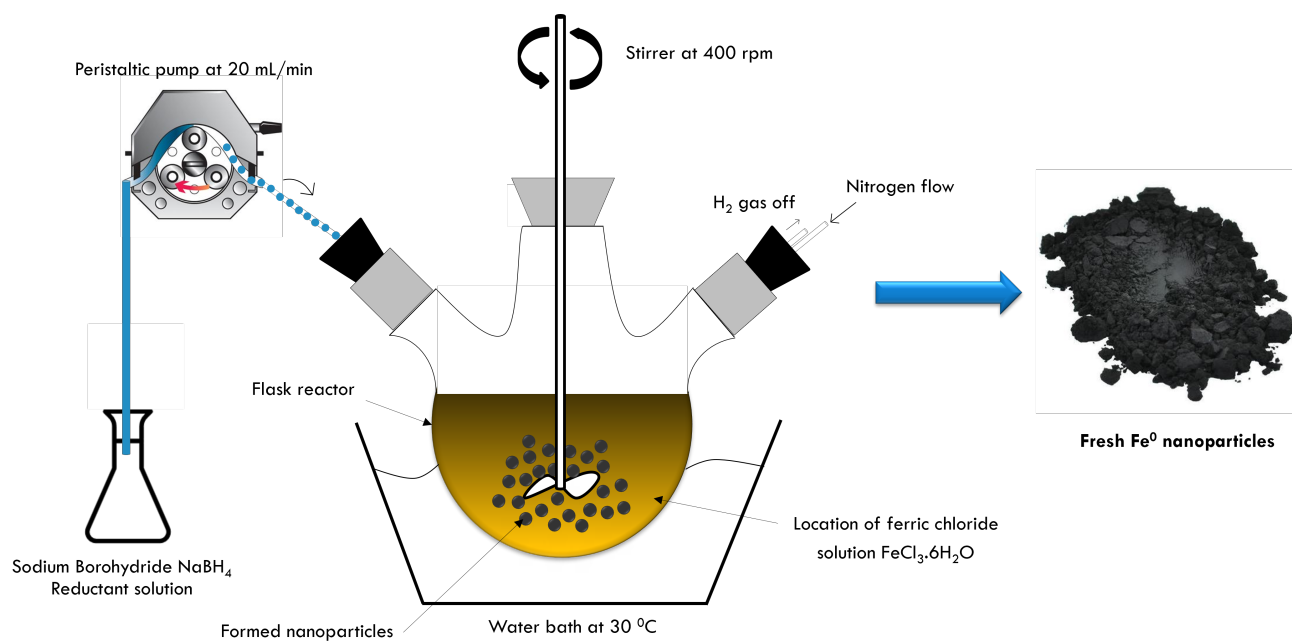


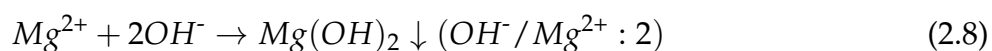
FIGURE 2.8: Schematic design of Fe<sup>0</sup>-based nanoparticles synthesis procedure.(A) Fe<sup>0</sup> nanoparticles synthesis, (B) freshly synthesized Fe<sup>0</sup>.



FIGURE 2.9: Synthesis of the Fe<sup>0</sup>-based nanoparticles in the laboratory.

$\text{Fe}^0$  @  $\text{Mg}(\text{OH})_2$  coated nanoparticles were synthesized applying the modified controlled thermal deposition (CTD) approach. Initially, 1 g/L  $\text{Fe}^0$ /ethanol solution was set up by disintegrating 0.1 g of  $\text{Fe}^0$  in 100 mL of ethanol for 30 min using the ultrasonication technique. Second, coating-ion  $\text{Mg}/\text{Fe}^{2+}$  solution and  $\text{OH}^-$ /ethanol were successively introduced into the  $\text{Fe}$ /ethanol mix at a precise infusion rate.

Ionic concentrations in the prepared mentioned two solutions were maintained constant, whereas the injected volumes were changed, aiming different coating ratios ( $\text{Mg}/\text{Fe}$ : 0.1, 0.2, 0.5, and 1.0 (wt/wt)), as well as keeping the molar ratios during the precipitation process as following:



Ultrasonication (38 kHz, 100 W) and nitrogen gas purging were maintained for the entire coating procedure at  $50 \pm 1.0$  °C as shown in Figure 2.10. After a 1-h aging time, the coated  $\text{Fe}^0$  precipitates were rinsed three times with ethanol and filtered through a 0.45 m paper filter (Millipore, Sigma- Aldrich Inc., USA) joined with three times washing by DDIW.



FIGURE 2.10: Ultrasonication (38 kHz, 100 W) and nitrogen gas purging for the preparation of coated iron nanoparticles.

### 2.3.3 Characterization

For morphology investigation, transmission electron microscopy (TEM, JEM-ARM 200F, JEOL Co., Japan) was used as presented in Figure 2.11 (A). Transmission electron microscopy (TEM) works like a slide projector. This latter shines a beam of light through the slide. As the light passes through, it is affected by the structures and objects on the slide. These effects would result in only certain parts of the light beam being transmitted through certain parts of the slide. Fourier transform infrared spectroscopy (FTIR) spectra were fulfilled with a Fourier transform infrared spectrometer (Magna-IR 750, USA).

The X-ray diffraction produces an interference effect so that the diffraction pattern gives information on the structure of the studied material or the identity of the crystalline substance. XRD characterization was achieved to evaluate the crystallinity and the chemical configuration of  $\text{Fe}^0$  and  $\text{Fe}^0$ -based nanoparticles using (XRD, TTR, Rigaku Inc., Japan) (Figure 2.11 (B)) with Cu K radiation at 40 kV/ 200 mA ( $\lambda = 0.15418 \text{ nm}$ ) and scanning rate of  $3 \text{ min}^{-1}$  over scanning range between  $3^\circ$  and  $90^\circ$ . The samples should be well powdered enough, so the XRD data gives all the d-spacing. Also, the analysis should not be too fast, so the peak data are accurate.



FIGURE 2.11: (A) Transmission Electron Microscope, (B) X-Ray Diffraction.

## 2.4 Culture and Analysis of Bacterial Growth

Physical and chemical conditions are necessary for bacterial growth, which depends on the availability of chemical nutrients and trace elements, the culture media, and the oxygen concentration. Our study focuses on using Mesophiles, which are middle-loving bacteria, growing at temperatures between 25 to 40°C. Also, most bacteria are best suited to neutral or slightly basic environments. We target the anaerobic bacteria cultured from real waste sludges, which are considered the powerhouse of microbial fuel cell technology. Anaerobic digestion is the organic matter decomposition achieved with no requirements for molecular oxygen. Therefore, the denitrification process will occur as a response to changes in the system's oxygen concentration.

Denitrification is a microbial process where nitrate is reduced to nitrite to gaseous forms of nitrogen. Bacteria use nitrate as an electron acceptor to oxidize the organic matter under such system conditions. The use of iron-based nanoparticles is expected to be trace elements that will improve bacterial multiplication and metabolism, enhancing the organic matter degradation and increasing the MFC's output. Bacterial growth rate was estimated by the plate count method using colony forming unit (CFU) technique. To do so, 1 mL from the original mixed culture inoculum was diluted 5 times in series to insure a countable plate. Then, 1 mL from each diluted sample was placed in the center of a Petri dish using a sterile pipette. The molten agar (15 mL) was poured into the Petri dish and mixed well. After solidification, the plate was saved for 24 hours overnight at 37 °C. Figure 2.12 illustrates the different steps for bacterial growth counting and Figure 2.13 presents the melted agar and an example of a real Petri dish after 24 hours. Each growth colony was carefully counted and represented a CFU:

$$CFU = CFU \times dilution\ factor \times 1/aliquot \quad (2.9)$$

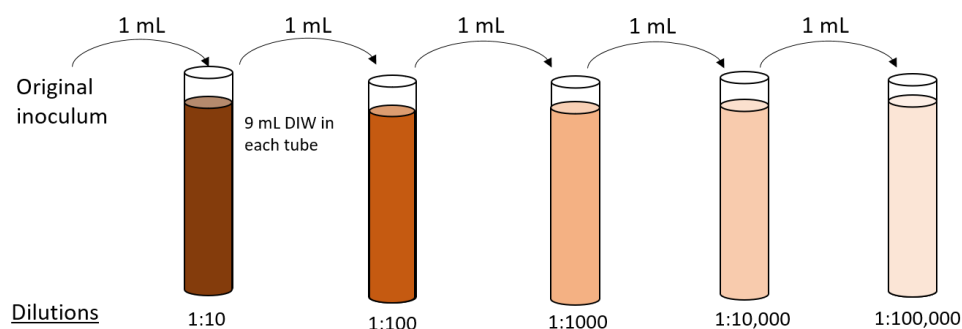


FIGURE 2.12: Pour plate method for bacterial growth measurements.

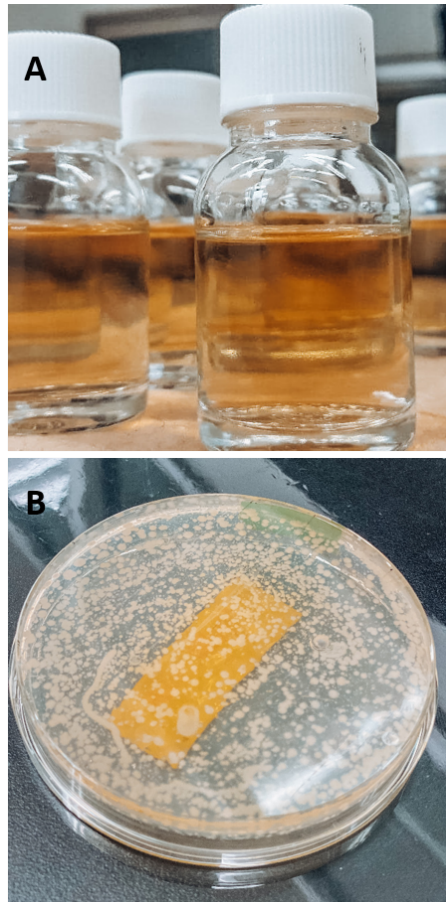


FIGURE 2.13: (A) Prepared standard plate count agar (APHA) CM0463 (OXOID LTD., England). (B) Bacterial colonies in a Petri dish after 24 hours.

In our study, bacterial growth was recorded for 12 days, and all sample results were presented as average data of triplicate experiments. Living microorganisms were treated as a black box, and the focus was mainly attributed to the bacterial growth analyses originated from a mixed culture medium. Figure 2.14 presents the typical bacterial growth cycle, and the different phases are defined below:

- The lag phase is the period of adjustment to new conditions. Little or no cell division occurs, and generally, the population size does not increase. This phase may last from one hour to several days.
- The log phase is the period where most of the rapid growth occurs. The number of bacterial cells produced is higher than the number of deadly bacteria. Also, cells are at their highest metabolic activity.
- In the stationary phase, the population size begins to stabilize, and the number of cells produced is equal to the number of cells dying. The cell division begins to slow down.

- The death phase is caused by: (i) the accumulation of toxic waste material, (ii) the acidic pH of the media, (iii) the limited nutrients, and (iv) the insufficient oxygen supply. The population size decreases, and the number of cells dying is higher than the number of cells produced since most of the cells start to lose their ability to divide.

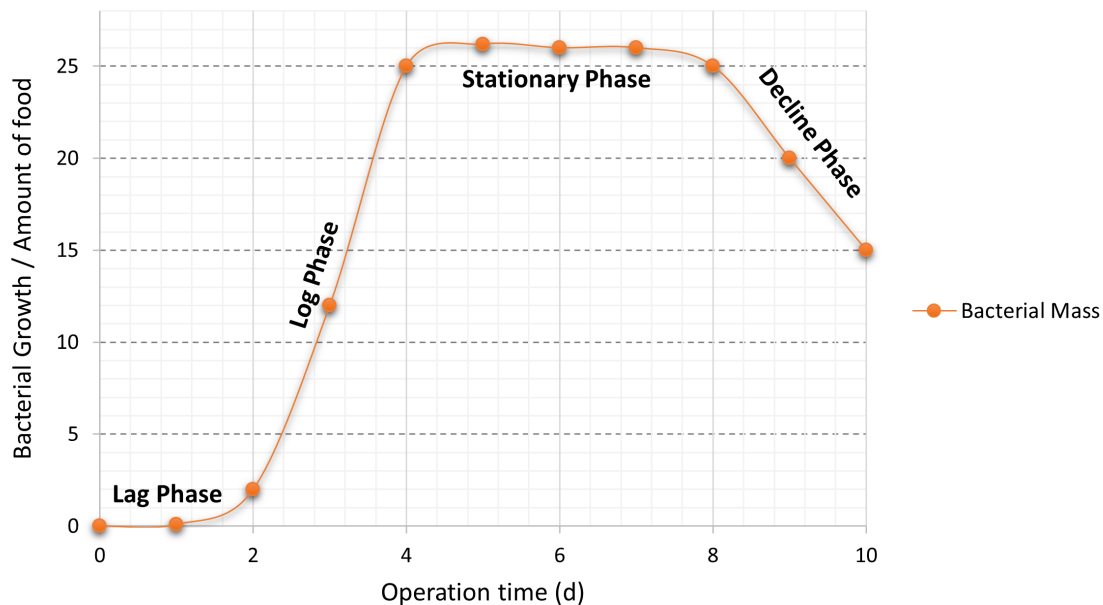


FIGURE 2.14: The bacterial growth cycle.

## 2.5 Conclusion

The second chapter aimed to illustrate the different methodologies and materials adopted for our research study. The MFC performance investigation goes through the voltage control, power density calculations, and organic matter degradation analysis. The waste sludge plays an essential role in MFC functioning, as it represents the fuel of the system and the source of bacterial communities. The waste sludge analysis is a crucial step that indicates the available nutrients and organic matter. Besides, iron-based nanoparticle synthesis and preparation are a delicate process, where leakage of oxygen can affect the nanoparticles' reactivity and affect overall system performance. Also, the bacterial development analysis will reflect the response of living microorganisms to the added iron nanoparticles.

## Chapter 3

# Investigation on The Effect of Iron-based Nanoparticles on Bacterial Growth

### 3.1 Introduction

Microbial communities' existence has been proved to be important in biological treatments due to their potential to oxidize organic matter in enriched wastewaters and generate renewable energies such as methane gas in anaerobic digestions (AD) and bioelectricity in MFCs. Microbes are the powerhouse of the MFC technology. Their types, metabolites, and activation are among the decisive parameters that affect the MFC performance. Therefore, with the widespread use of  $\text{Fe}^0$  nanoparticles in the environment, it becomes crucial to examine their potential risk and identify their consequences on the biological treatments and bioremediation processes to guarantee a sustainable and eco-friendly application. An excess of  $\text{Fe}^0$  would destroy the cell, whereas an optimum dosage will improve cell activation, regulate the pH system, and stimulate organic matter degradation and bioenergy generation. This chapter aimed to investigate the effect of  $\text{Fe}^0$ -based nanoparticles on the activation of mixed culture bacterial cells collected from real domestic wastewaters. The selection of mixed culture bacteria was based on such a community's high resistivity. The real-scale applications will also take place in real wastewater treatment plants, where it will be hard to select specific bacterial strains. Microbial activity performance was reflected by bacterial colony counting and COD removal efficiencies analysis.

### 3.2 Characterization of Fe<sup>0</sup> and Cu/Fe<sup>0</sup> Nanoparticles

TEM images characterized the surface morphology of Fe<sup>0</sup> and Cu/Fe<sup>0</sup> nanoparticles as shown in Figure 3.1. Fe<sup>0</sup> had a clear core-shell structure and spherical shape with a large specific area. These characterizations led to high reactivity and nanoparticles' ability to react with the wastewater's microorganism. However, Fe<sup>0</sup> nanoparticles were clearly agglomerated due to the natural magnetic effect and the high adhesion between the nanoparticles. Cu/Fe<sup>0</sup> presented higher dispersibility, more ductile chain, and lower agglomeration than Fe<sup>0</sup>. The bimetallic Cu/Fe<sup>0</sup> presented a larger surface area, which was mainly due to the non-homogeneity of the formed alloy. This latter will weaken the adhesion effect between the particles and inhibit the aggregation of Cu/Fe<sup>0</sup> particles, therefore improved the reactivity of Fe<sup>0</sup>. The obtained results were consistent with prior studies where the bimetallic nanoparticles showed a better performance than bare Fe<sup>0</sup> (Chen et al., 2020).

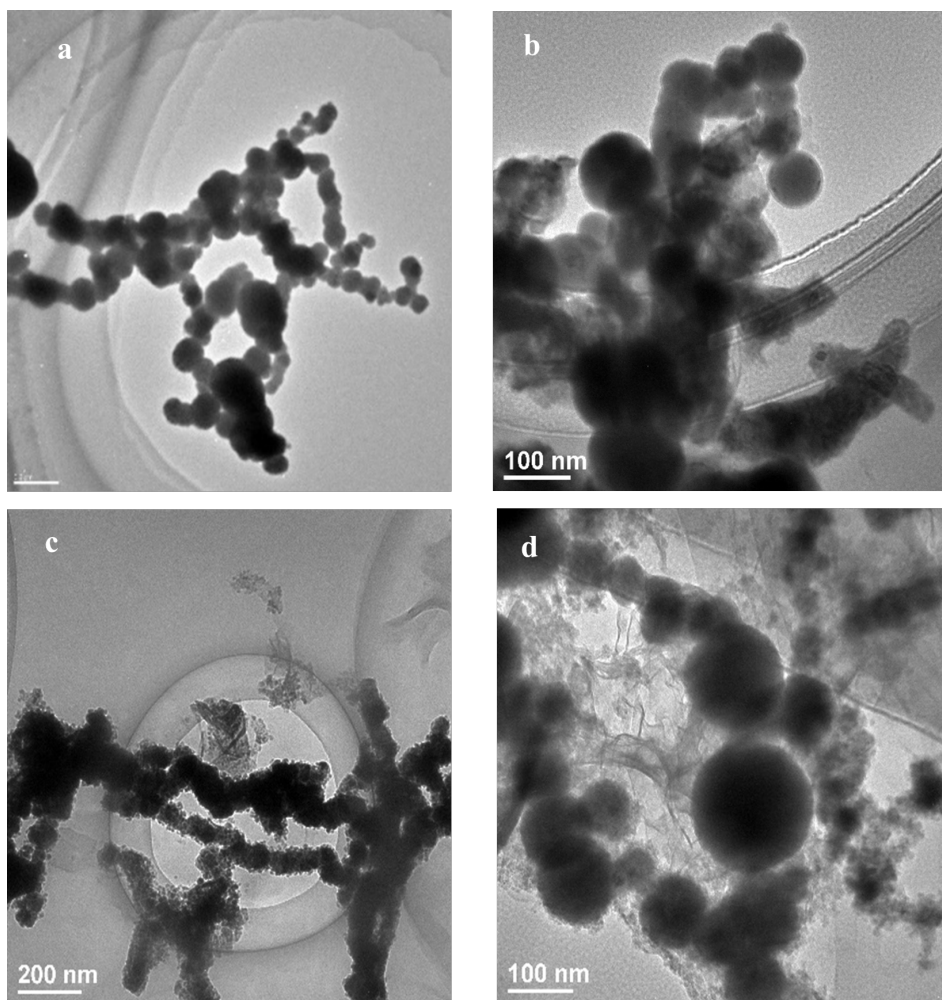


FIGURE 3.1: TEM characterization of the synthesized bimetallic nanoparticles: (a and b) Fe<sup>0</sup>, (c and d) Cu/Fe<sup>0</sup>.

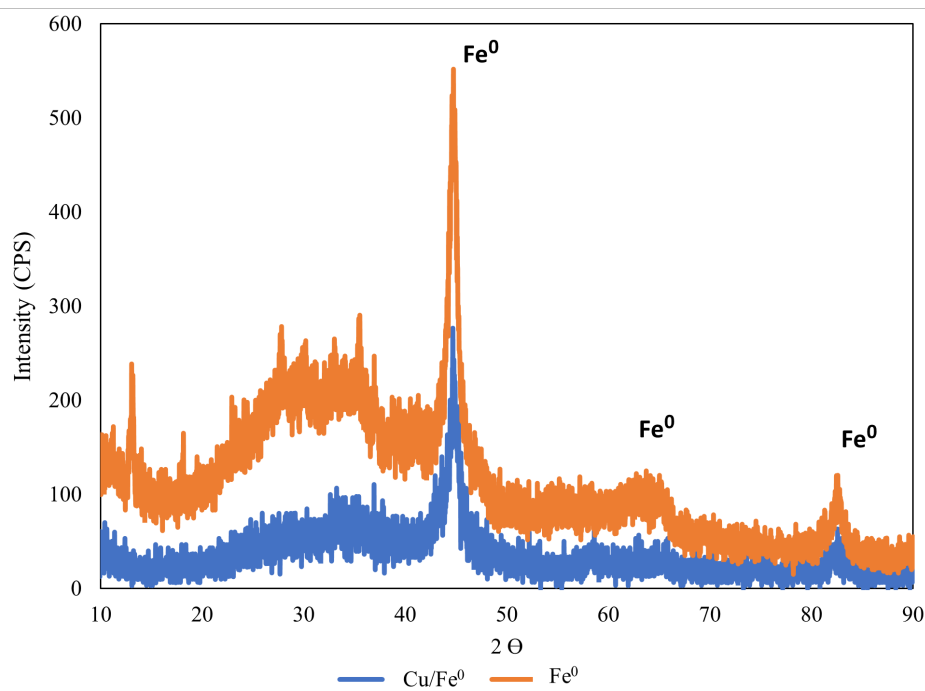


FIGURE 3.2: XRD characterization of the synthesized  $\text{Fe}^0$  and  $\text{Cu/Fe}^0$  nanoparticles.

The XRD analysis determined the chemical composition and crystallinity for the freshly synthesized  $\text{Fe}^0$  and  $\text{Cu/Fe}^0$  nanoparticles. Figure 3.2 showed a high peak intensity of  $\text{Fe}^0$  at  $2\theta$  of 44.7 and 82.3°, which indicated a pure and crystalline structure, whereas for  $\text{Cu/Fe}^0$ , the peak was less intense at  $2\theta$  of 48.02°. This result was attributed to the presence of copper particles, which led to an amorphous structure.

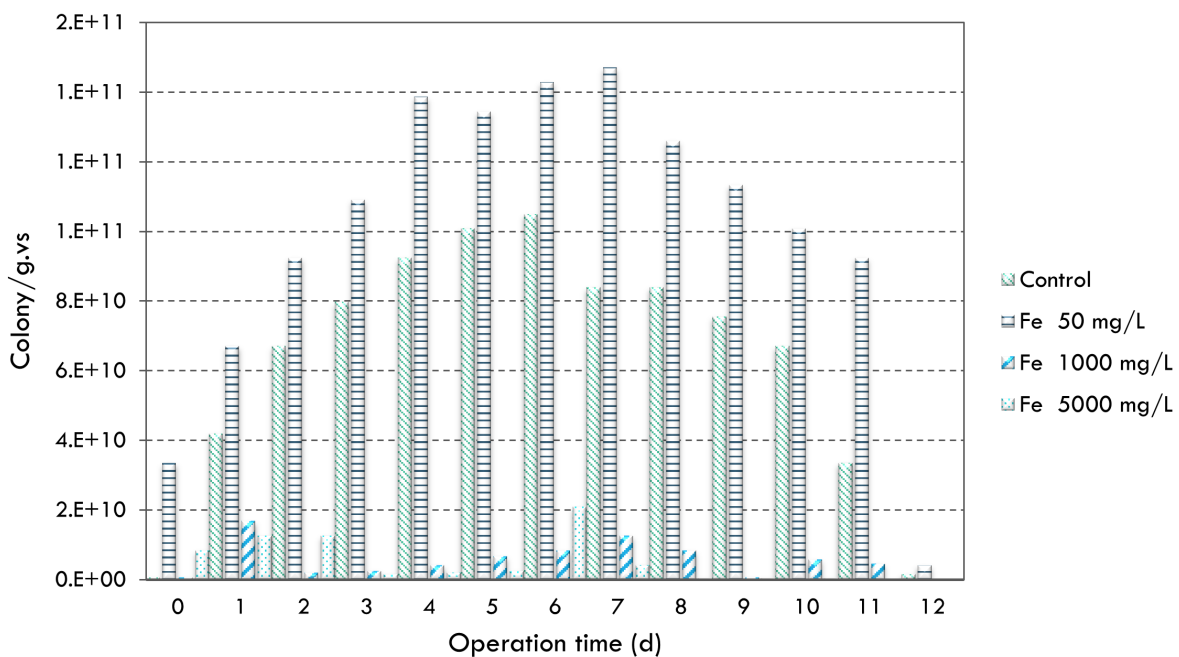
### 3.3 Bacterial Growth Response to $\text{Fe}^0$ -bimetallic Nanoparticles Treatment

#### 3.3.1 Effect of $\text{Fe}^0$ on bacterial cells at different concentrations

The bacterial activation was evaluated using different  $\text{Fe}^0$  concentrations 50 mg/L, 1000 mg/L and 5000 mg/L. Experiments were conducted to select the dosage level where  $\text{Fe}^0$  exhibits a non-toxic effect. Table 3.1 illustrates the properties of real domestic wastewater "1" used in this section. Figure 3.3 illustrated the different bacterial growth phases under anaerobic conditions. Results suggested that the activation increased when the  $\text{Fe}^0$  decreased from 5000 mg/L to 50 mg/L. Bacterial inactivity was significant ( $p = 0.0001 < 0.05$ ) at a high level of  $\text{Fe}^0$ . In contrast, the number of colonies increased significantly under 50 mg/L ( $p = 0.0278 < 0.05$ ) to be  $1.50\text{E}+11$  Colony/g.vs. compared to  $1.00\text{E}+11$  Colony/g.vs in control reactor.

TABLE 3.1: Wastewater 1 properties.

Characteristics	Units	Wastewater 1
COD	mg/L	792
TS	g/L	0.58
TVS	g/L	0.25
pH	-	7.74
ORP	mV	-71
Fe <sup>2+</sup>	mg/L	2.71
Total Fe <sup>0</sup>	mg/L	9.37

FIGURE 3.3: Activation of bacterial growth when exposed to Fe<sup>0</sup> nanoparticles with different concentrations under anaerobic conditions, T: 37 °C, pH=7.

Higher concentrations of Fe<sup>0</sup> has been observed to have higher toxicity for bacterial cells. Typically, Fe<sup>0</sup> nanoparticle is coated by a shell of oxides under specific conditions. Thus, there would be an optimal Fe<sup>0</sup> concentration where the bacterial cells would be less vulnerable to Fe<sup>2+</sup>. Under optimum dose, Fe<sup>0</sup> particles would be considered a trace element for bacteria. Fe<sup>0</sup> would aggregate and adsorb on the extracellular polymeric substance (EPS) around the microorganisms, and protect the microbial cells from any contact damage (Daraei et al., 2019). Zhou et al., 2020 showed that Fe<sup>0</sup> particles increased the abundance and the growth of some bacteria by providing a stable environmental conditions (pH, ORP) for their growth. In our study, pH values for control experiments decreased from 7.74 to 3.05 at the end of the cycle. This low pH was not favorable for the bacterial growth because microbes, generally, grow

best at neutral pH close to 7. With the addition of Fe<sup>0</sup> nanoparticles to the reactor, the pH values were kept in a range of 7.43 - 7.74, which indicated that Fe<sup>0</sup> maintained a neutral condition for bacterial growth. (Luo et al., 2014) explained that Fe<sup>0</sup> affected the pH of the system in two stages. First, it plays the role of as an acid buffer by the dissociation of Fe<sup>0</sup> and Fe<sup>3+</sup> in the early stage of contact. They also mentioned the release of the volatile fatty acids (VFAs) and their accumulation under the effect of Fe<sup>0</sup>, whereas in the second stage, the degradation of VFAs and the increase of ammonia nitrogen concentration led to increase pH values, which would maintain a favorable pH level for bacterial growth. The reason behind the pH variations could be explained by the following equations below:



Furthermore, ORP analysis showed that Fe<sup>0</sup> decreased the ORP level to be in a range of -70 ~ -58 mV, which offered a good condition for the survival and growth of bacteria (He et al., 2017). The presence of Fe<sup>0</sup> could decrease the level of ORP rapidly, and the generation of Fe<sup>2+</sup> might cause the wastewater to accumulate to form particles as it was described in (Liu, Zhang, and Ni, 2015). These environmental changes were suitable for the bacterial cells to adapt to the new reactor conditions. However, an excess of Fe<sup>0</sup> will block the cells and destroy their cellular membranes. In our study, Fe<sup>2+</sup> concentrations were 8.90, 91.74, and 164.65 mg/L for 50 mg/L, 1000 mg/L and 5000 mg/L of Fe<sup>0</sup>, respectively, after 12 days of operation. It was noted that the increase in Fe<sup>2+</sup> release had a toxic effect as it was previously described in section 3.1. Increasing the dose of Fe<sup>0</sup> led to increasing the release Fe<sup>2+</sup>. These latter will adhere to the cell wall, and cause the walls to form macroscopic flocs as it was described in (Lv et al., 2017). Also, the authors mentioned that the cell membrane was severely disrupted due to their interaction with Fe<sup>0</sup>-based nanoparticles and the dark spots were caused by the release of Fe<sup>3+</sup> oxide particles. Our study suggested that the bacterial growth activation depends on the dosages of Fe<sup>0</sup>. Using 50 mg/L of bare Fe<sup>0</sup> would be favorable for bacterial colonies enrichment. However, these nanoparticles still can easily be oxidized and possibly lose their reactivity. Therefore comes the point to adopt the Fe<sup>0</sup>-bimetallic nanoparticles and evaluate their contribution for improving the Fe<sup>0</sup> reactivity, increasing the bacterial multiplication, and enhancing organic matter degradation.

### 3.3.2 Effect of Cu/Fe<sup>0</sup>, Ag/Fe<sup>0</sup>, and Ni/Fe<sup>0</sup> on bacterial cells

Our study examined the different effects of Cu/Fe<sup>0</sup>, Ag/Fe<sup>0</sup>, and Ni/Fe<sup>0</sup> bimetallic nanoparticles on bacterial growth for 12 days of operation. Cell colonies were recorded and plotted over time in Figure 3.4. The maximum number of bacterial colonies was  $2.6 \times 10^{11}$ ,  $4 \times 10^{11}$ ,  $1.4 \times 10^{11}$ ,  $3 \times 10^{11}$ , and  $4.8 \times 10^{11}$  colony/g.vs under control, Fe<sup>0</sup>, Ag/Fe<sup>0</sup>, Ni/Fe<sup>0</sup>, and Cu/Fe<sup>0</sup> nanoparticles treatments, respectively. Ag/Fe<sup>0</sup> addition reduced the bacterial growth by 46.15 %, whereas it increased by 15.38 %, 53.85 %, and 84.61 % for Ni/Fe<sup>0</sup>, Fe<sup>0</sup>, and Cu/Fe<sup>0</sup>, respectively, compared to control reactor.

The above-mentioned results were consistent with prior studies. Ahmad et al., 2016 noted that Ag<sup>+</sup> interacts with the bacterial cells and alters the main function leading to the destruction of bacterial cells. Also, Argueta-Figueroa et al., 2014 highlighted the negative impact of Ni/Fe<sup>0</sup> which could be mainly attributed to the high released Fe<sup>2+</sup>. The positive impact was also reflected in COD removal efficiencies. The COD removal efficiencies were illustrated in Figure 3.5 and values were 33.21 %, 55.30 %, 61.24%, 58.21 %, and 51.77 % for control, Fe<sup>0</sup>, Cu/Fe<sup>0</sup>, Ag/Fe<sup>0</sup> and Ni<sup>0</sup>, respectively. Fe<sup>0</sup>-based nanoparticles enhanced the effectiveness of organic matter degradation by the production of a specific key enzymes which enhanced the fermentation process and thus improved the organic matter degradation (Pan et al., 2019).

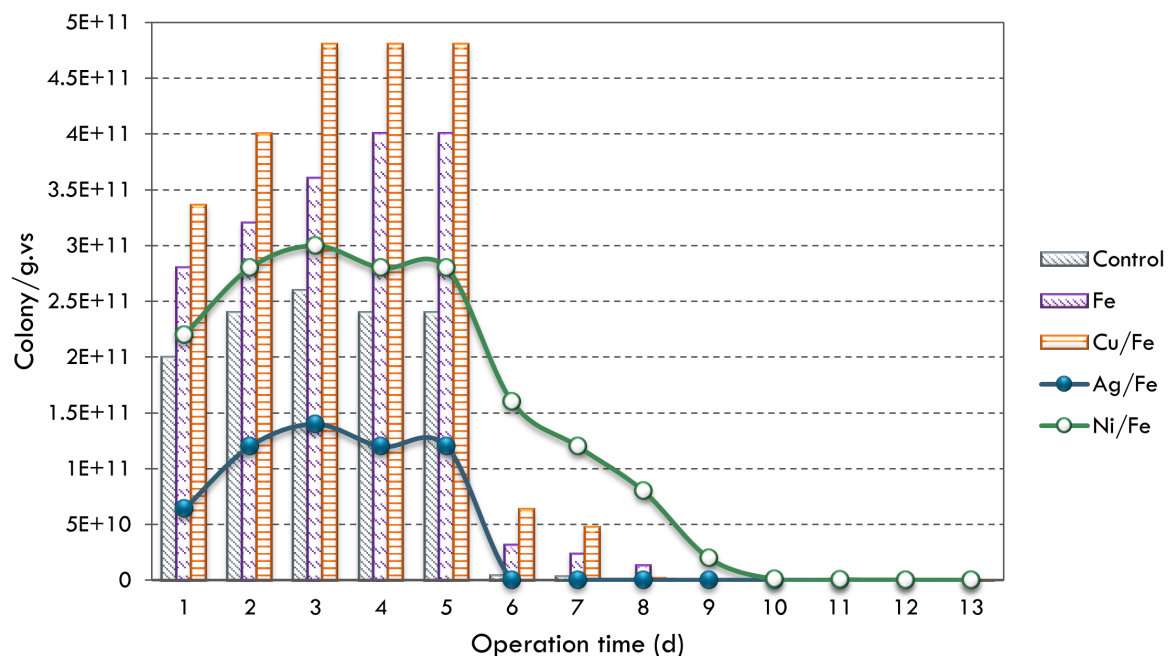


FIGURE 3.4: Effect of Fe<sup>0</sup>, Cu/Fe<sup>0</sup>, Ag/Fe<sup>0</sup>, and Ni/Fe<sup>0</sup> (50 mg/L) on the bacterial growth under anaerobic conditions, T: 37 °C, and pH=7 for 12 days of operation.

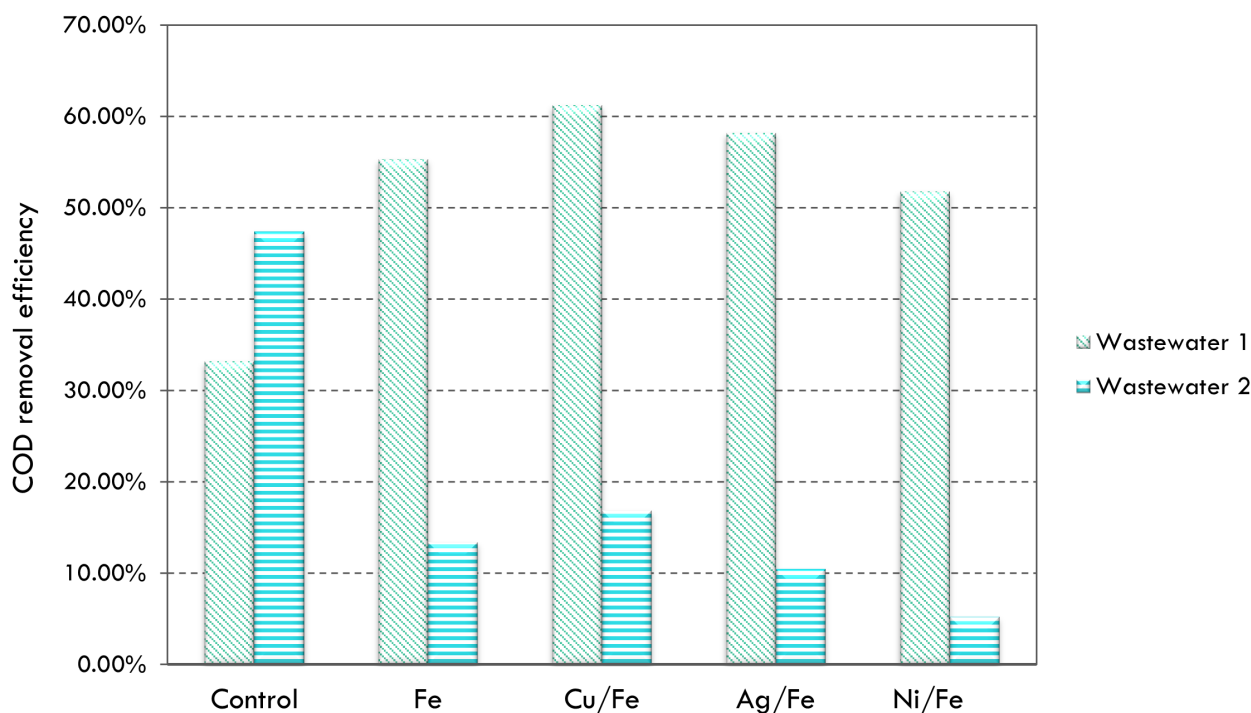


FIGURE 3.5: COD removal efficiencies under  $\text{Fe}^0$ -bimetallic nanoparticles treatment for the two studied wastewaters.

The bacterial activation obtained by  $\text{Cu}/\text{Fe}^0$  bimetallic nanoparticles could be explained by the presence of copper metal that could lower the corrosion rate of  $\text{Fe}^0$ , thus leading to an improved reactivity compared to the  $\text{Fe}^0$ . The high dispersibility and low agglomeration were responsible for enhancing  $\text{Fe}^0$  availability and interaction with bacterial cells, which consequently improved the organic matter degradation (Krasae and Wantala, 2016). Also, Amen et al., 2018 reported that introducing copper particles onto the surface of  $\text{Fe}^0$  will control the corrosion reaction of  $\text{Fe}^0$  particles, and the release of electrons would be considerably available enough to increase their reactivity. Surprisingly, COD removal increased with  $\text{Ag}/\text{Fe}^0$  addition, which was in consistence with (Najafpoor et al., 2020), where the COD removal increased from 25.80 to 41.15 %. This behavior could be partially due to Ag nanoparticles' presence, which was beneficial for contaminants removal and organic matter degradation. However, the direct contact and infiltration of  $\text{Ag}/\text{Fe}^0$  particles through the bacterial cell wall would lead to a higher sensitivity of the bacterial colonies. At the end of the experiments, small particles were formed under  $\text{Ag}/\text{Fe}^0$  treatment, which could be due to the agglomeration of nanoparticles. The adsorbent effective surface will be reduced; thus, the added nanoparticles will have a less toxic effect on bacterial cells, contributing to increase the COD removal at the end of the experiments.

It was clear in Figure 3.6 that the control reactor had an acidic environment at the end of the experiments, which could be attributed to the organic matter digestion and volatile fatty acids released. In contrast, bimetallic nanoparticles helped maintain a neutral system, owing to their buffer capacity, which was favorable for bacterial growth.

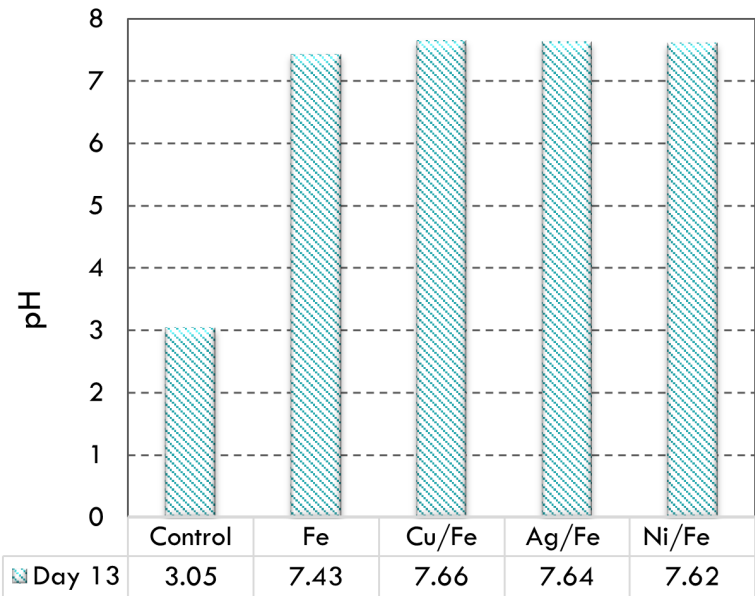


FIGURE 3.6: pH values after 13 days of the exposure of wastewater 1 to the bimetallic nanoparticle’s treatment with a concentration of 50 mg/L at 37 °C and under anaerobic conditions with an initial pH: 7,74.

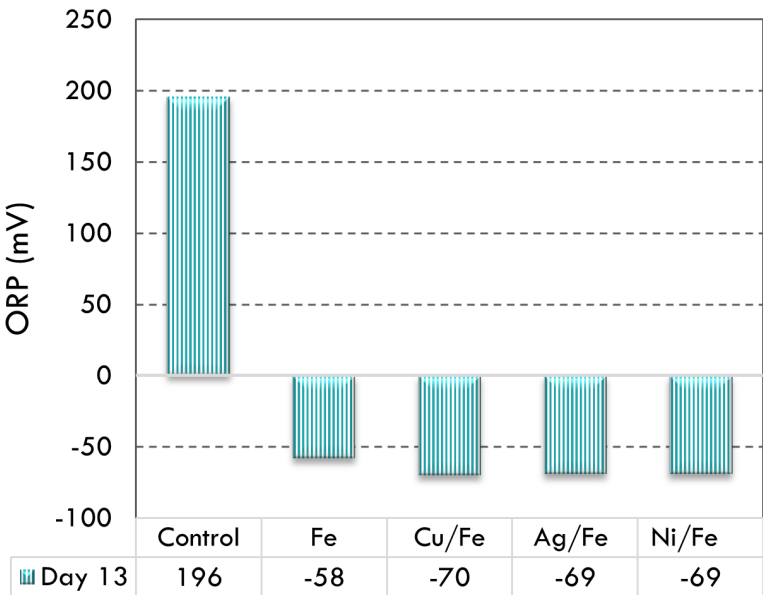


FIGURE 3.7: ORP levels after 13 days of the exposure of wastewater 1 to the bimetallic nanoparticles’ treatment with a concentration of 50 mg/L at 37°C, pH=7 under anaerobic conditions with an initial ORP value -106 mV.

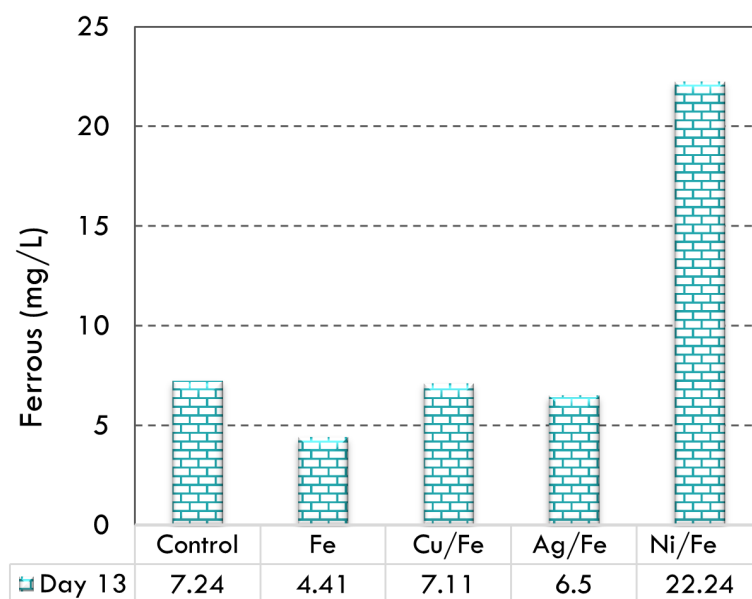


FIGURE 3.8:  $\text{Fe}^{2+}$  after 13 days of the exposure of wastewater 1 to the bimetallic nanoparticles' treatment with a concentration of 50 mg/L at 37 °C, pH=7 under anaerobic conditions with an initial  $\text{Fe}^{2+}$  value: 1,87 mg/L.

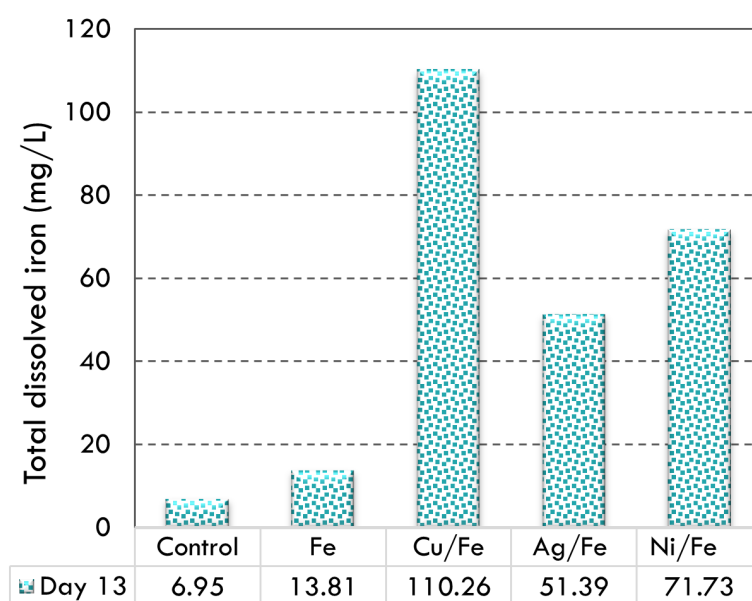


FIGURE 3.9: Fe concentration after 13 days of the exposure of wastewater 1 to the bimetallic nanoparticles' treatment with a concentration of 50 mg/L at 37 °C, pH=7 under anaerobic conditions with an initial  $\text{Fe}^{2+}$  value: 9.37 mg/L.

Iron concentration analysis were shown in Figure 3.8 and Figure 3.9. The difference in  $\text{Fe}^{2+}$  release played an important role in determining bacterial colonies' response during the bimetallic nanoparticles treatment. Considering an optimum dosage of  $\text{Fe}^{2+}$ , iron nanoparticles will be a trace element for bacterial multiplication. However, a high dosage will be toxic enough to destroy the EPS and deteriorate the bacterial cell.

The effect of  $\text{Fe}^0$  and  $\text{Cu}/\text{Fe}^0$  has been proved to be positive for a specific dosage level using wastewater 1. However, we can not confirm this impact for all tested wastewaters due to bacterial communities' diversity in real wastewaters. As mentioned in the literature review, the bacterial strains play an important role in identifying the consequences of  $\text{Fe}^0$  on bacterial growth. Therefore, another wastewater, "wastewater 2," as defined in Table 3.1 has been adopted to study the bacterial behavior when exposed to the bimetallic nanoparticles.  $\text{Fe}^0$ ,  $\text{Cu}/\text{Fe}^0$ ,  $\text{Ag}/\text{Fe}^0$ , and  $\text{Ni}/\text{Fe}^0$  were added separately with the optimum concentration of 50 mg/L, which has been already selected in section 3.3.1. The bacterial activity was reflected by the organic matter digestion rate expressed by COD removal efficiencies. As shown in Figure 3.4, it was clear that COD removal efficiencies decreased from 47.38 % in control to 13.37 % under  $\text{Fe}^0$  addition. This reduction in COD removal efficiencies reflected that the organic matter digestion was not favorable and bacterial cells were not active enough during their contact with the  $\text{Fe}^0$  nanoparticles. A high COD removal efficiency represents a low organic matter content at the end of the operation. Besides, a slight increase from 13.37 % to 16.86 % was observed with  $\text{Cu}/\text{Fe}^0$ , which confirms that the Cu particles could enhance  $\text{Fe}^0$  reactivity. These results highlight the need for studying the effect of system conditions on living microorganism's activity and their responses when exposed to  $\text{Fe}^0$  treatments.

### 3.4 Effect of $\text{Fe}^0$ -bimetallic Nanoparticles at Different System Conditions

Table 3.2 illustrates the properties of real domestic wastewater "2" used in this section. Clearly, the two wastewaters are different in the organic matter content reflected by COD and TVS values, which are essential parameters in biological wastewater treatment. TVS consists mostly of organic matter, and it is approximately equal to the concentration of bacterial cells living in the wastewater. In (Kelly Orhorhoro, 2017), eight different substrate samples were used with varied TS and TVS values to optimize bio-gas yield production. Results showed that the bio-gas production quantity increased with increasing the TS and TVS values and vice versa, and the maximum bio-gas generated was obtained at 10.16 % total solids. In another study, (Yi et al., 2014) focused on the effect of TS content on the implementation of the anaerobic digestion and revealed that any difference in the TS content would affect the microbial morphology of the system. In our case, the TVS/TS ratio values were 0.43 and 0.22 for wastewater 1 and wastewater 2, respectively.

TABLE 3.2: Properties of wastewaters used in this study.

Characteristics	Units	Wastewater 1	Wastewater 2
COD	mg/L	792	344
TS	g/L	0.58	0.50
TVS	g/L	0.25	0.11
pH	-	7.74	8.31
ORP	mV	-71	-106
DO	mg/L	0.45	0.45
$\text{Fe}^{2+}$	mg/L	2.71	1.87
Total $\text{Fe}^0$	mg/L	9.37	6.97

### 3.4.1 Effect of pH variation on COD Removal

Three batch reactors of wastewater two samples were conducted under three different pH values: 3, 7, and 12 to study the effect of  $\text{Fe}^0$  under acidic, neutral, and alkaline conditions. To each reactor, the bimetallic nanoparticles  $\text{Fe}^0$ ,  $\text{Cu}/\text{Fe}^0$ ,  $\text{Ag}/\text{Fe}^0$ , and  $\text{Ni}/\text{Fe}^0$  were introduced with 50 mg/L to examine their effect on the organic removal represented by the COD measurements. Figure 3.10 shows that COD removal efficiencies were not all improved compared to the control reactor when exposed to  $\text{Fe}^0$  based nanomaterial treatment. For example, acidic conditions slightly improved the removal efficiencies from 47.38 % to 48.55 % in control reactor and from 10.47 % to 22.09 % in  $\text{Ag}/\text{Fe}^0$  reactor, whereas COD removal was affected negatively in  $\text{Fe}^0$ ,  $\text{Cu}/\text{Fe}^0$ , and  $\text{Ni}/\text{Fe}^0$  reactors. This decrease can be justified by high sensitivity of bacterial cells under acidic conditions and  $\text{Fe}^0$  treatment. For alkaline conditions, the COD removal improved for  $\text{Fe}^0$  and  $\text{Ag}/\text{Fe}^0$  treatment but presented a negative effect on other reactors. This result showed that bacterial activity is delicate when exposed to high or low pH conditions. The activation and inactivation effects of bacterial cells could be explained by the high concentration of the released  $\text{Fe}^{2+}$ , which may have a toxic effect on the microorganisms in wastewater. Figure 3.11 illustrates  $\text{Fe}^{2+}$  and total iron concentrations for all reactors under different pH levels. It was noticeable that the variation in COD removal efficiencies could be linked to the different  $\text{Fe}^{2+}$  concentrations. For example, under acidic conditions, only control and  $\text{Ag}/\text{Fe}^0$  showed an increase in COD removal and low  $\text{Fe}^{2+}$  concentrations. In contrast, all other reactors had a high release of  $\text{Fe}^{2+}$  followed by low organic matter digestion. Besides, under neutral conditions, control showed the lowest  $\text{Fe}^{2+}$  concentration 0.68 mg/L and the highest COD removal, whereas  $\text{Ni}/\text{Fe}^0$  had the least organic matter degradation, which was caused by the highest  $\text{Fe}^{2+}$  equal to 6.10 mg/L. The  $\text{Cu}/\text{Fe}^0$  improved the digestion even though its  $\text{Fe}^{2+}$  content was higher than bare  $\text{Fe}^0$ .

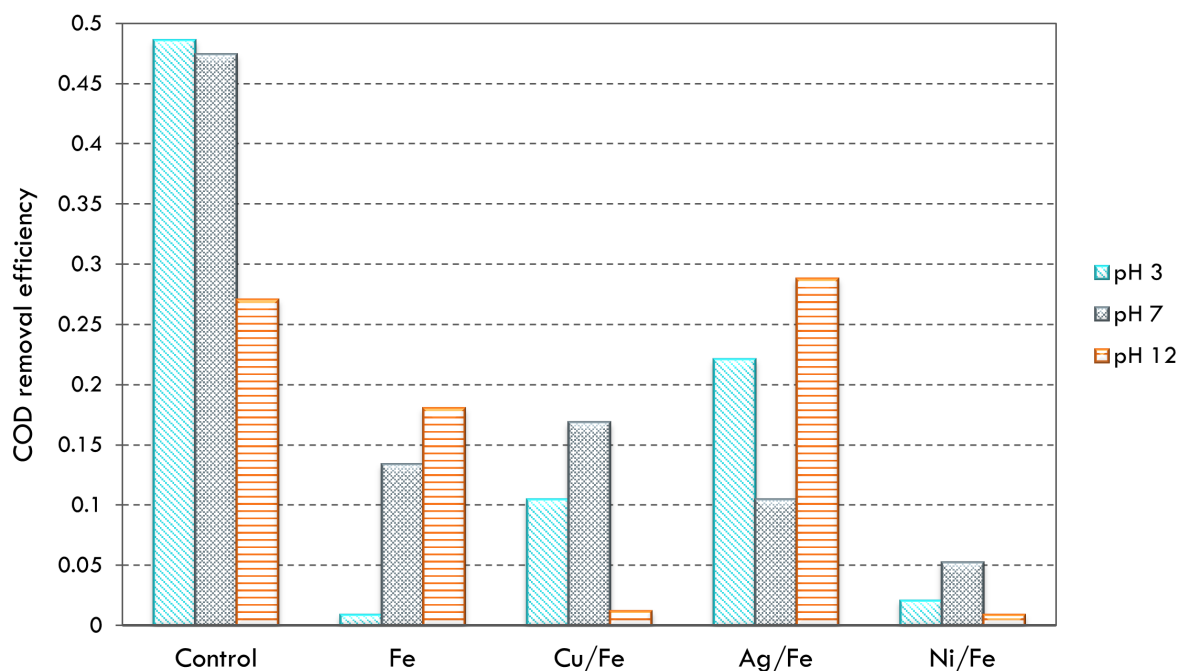


FIGURE 3.10: COD removal efficiencies of the mixed culture samples of wastewater 2 when exposed to bimetallic nanoparticles with a concentration of 50 mg/L for 12 days of operation with respect to the pH variation.

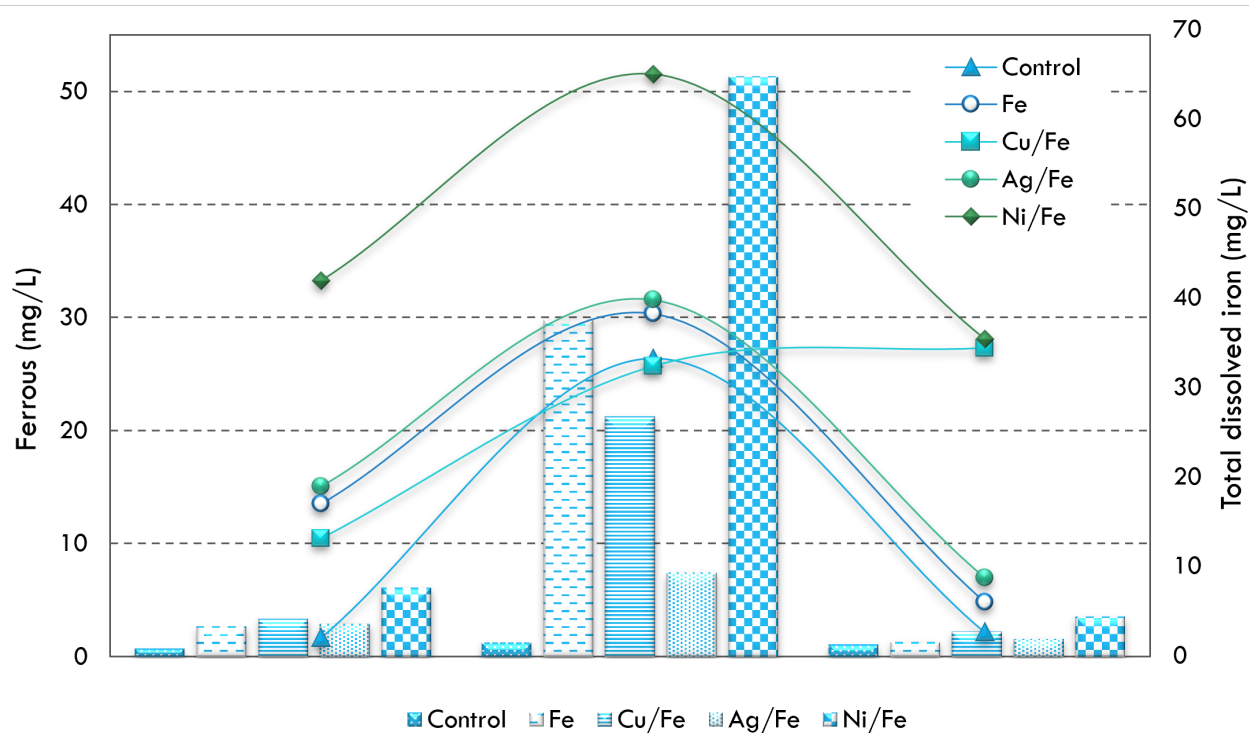


FIGURE 3.11: Iron concentrations after 20 days of operation using wastewater 2 under the bimetallic nanoparticles' treatment with a concentration of 50 mg/L at 37 °C and under anaerobic conditions.

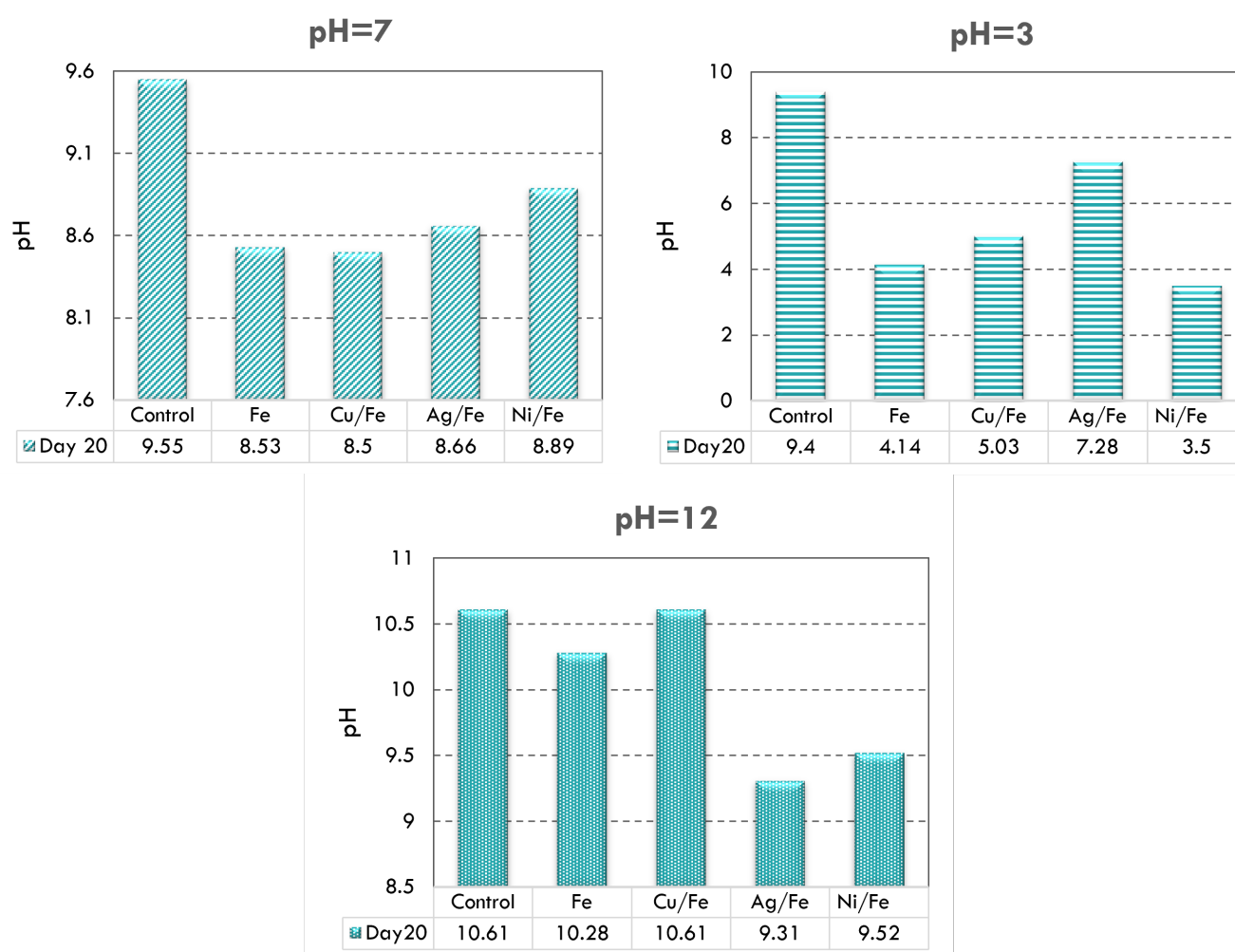


FIGURE 3.12: pH variations after 20 days of operation using wastewater 2 under the bimetallic nanoparticles' treatment with a concentration of 50 mg/L at 37 °C and under anaerobic conditions.

As shown in Figure 3.12, the pH of the three studied reactors tend toward neutral conditions. This enhancement can be associated with the presence of Cu particles to enlarge the bimetallic surface area and lower its accumulation on the cell membrane. These findings highlight again the toxic mechanism exerted by an excess of  $\text{Fe}^0$  toward living microorganisms. An excess of  $\text{Fe}^0$  would accumulate on the membrane cell and destroy the extracellular polymeric substance (EPS) that is responsible for protecting the bacterial cell membrane from any direct contact with  $\text{Fe}^{2+}$  when exposed to  $\text{Fe}^0$  treatment.

### 3.4.2 Effect of temperature variation on COD Removal

Three different temperatures (20 °C, 37 °C, and 50 °C) were tested to select the optimum conditions. Figure 3.13 illustrates the different COD removal efficiencies. Results showed

that the COD removal efficiencies increased under thermophilic conditions for  $\text{Fe}^0$ -bimetallic, whereas it decreased for control reactor. Generally, bacterial cells exhibit higher growth at relatively high temperatures ( $40 \sim 50 \text{ }^\circ\text{C}$ ). Therefore, COD values were slightly enhanced and the system showed almost the same pH values under the different temperature values (Figure 3.14).  $\text{Fe}^{2+}$  analysis were in consistence with the obtained results as shown in Figure 3.15. It was clear from Table 3.3 that  $\text{Fe}^0$ ,  $\text{Cu}/\text{Fe}^0$ ,  $\text{Ag}/\text{Fe}^0$ , and  $\text{Ni}/\text{Fe}^0$  reactors achieved their highest COD removal at  $T=55 \text{ }^\circ\text{C}$ , which corresponded to the lowest released  $\text{Fe}^{2+}$ .

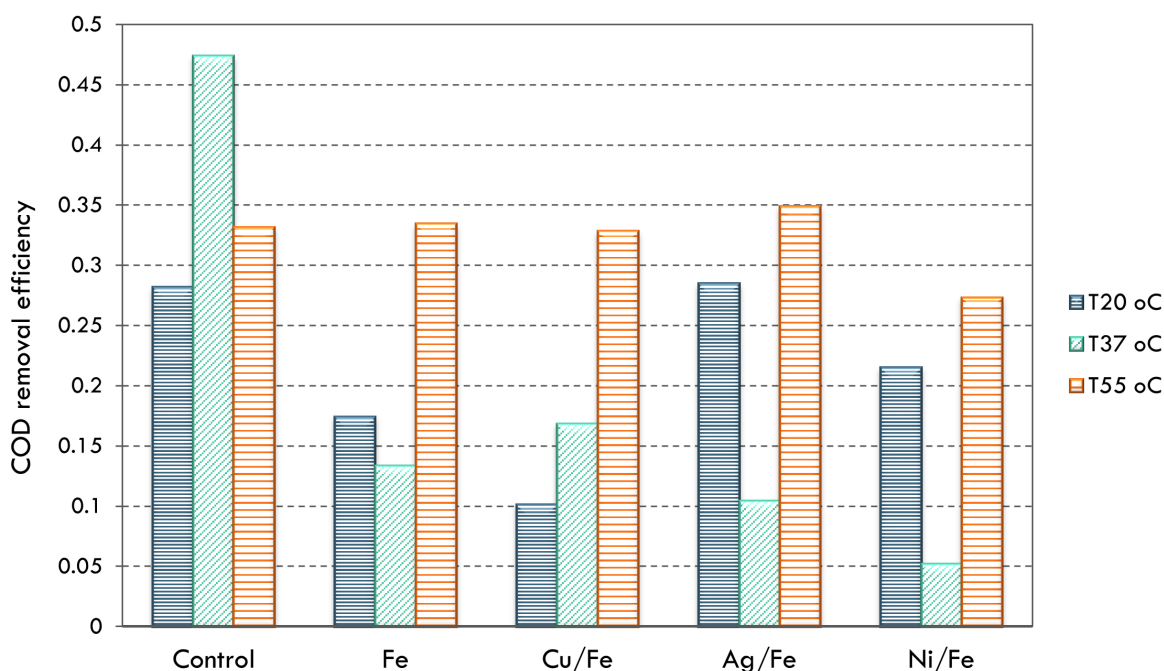


FIGURE 3.13: COD removal efficiencies of the mixed culture samples of wastewater 2 when exposed to bimetallic nanoparticles with a concentration of 50 mg/L for 12 days of operation with respect to temperature variation.

TABLE 3.3: Ferrous ions concentrations [ $\text{Fe}^{2+}$ ] for control,  $\text{Fe}^0$ ,  $\text{Cu}/\text{Fe}^0$ ,  $\text{Ag}/\text{Fe}^0$ , and  $\text{Ni}/\text{Fe}^0$  with respect to temperature variations.

Reactors	T= 20 °C	T= 37 °C	T= 55 °C
Control	1.09	0.68	1.27
$\text{Fe}^0$	5.72	2.69	0.73
$\text{Cu}/\text{Fe}^0$	5.54	3.32	1.45
$\text{Ag}/\text{Fe}^0$	3.12	2.88	1.13
$\text{Ni}/\text{Fe}^0$	5.13	6.10	3.37

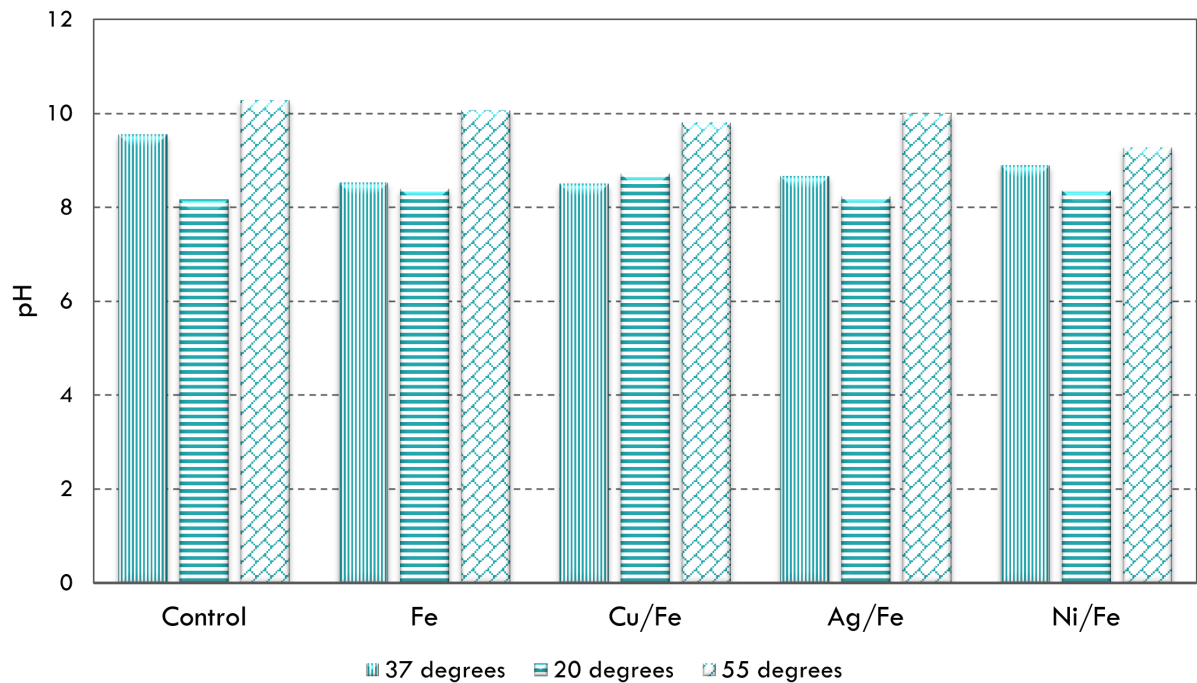


FIGURE 3.14: pH variations with respect to temperature variations after 20 days of operation using wastewater 2 under the bimetallic nanoparticles' treatment with a concentration of 50 mg/L.

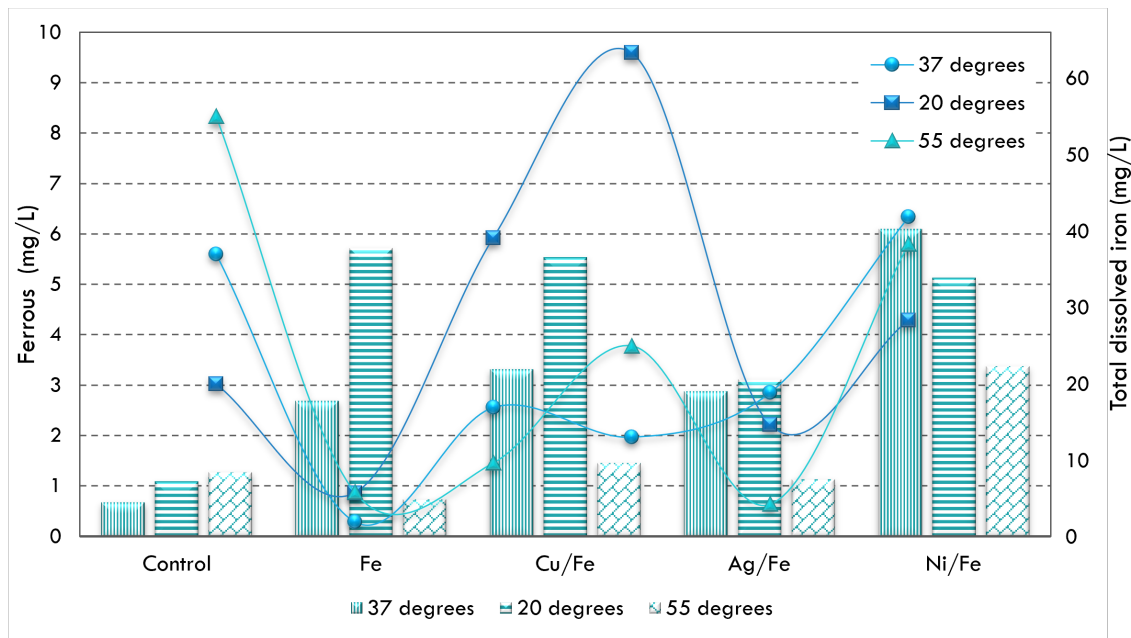


FIGURE 3.15: Iron concentrations after 20 days of operation using wastewater 2 under the bimetallic nanoparticles' treatment with a concentration of 50 mg/L, under anaerobic conditions.

### 3.4.3 Aerobic/anaerobic digestion and COD Removal

The oxygen concentration played an important role in bacterial activation. The toxicity significantly ( $p = 0.0026$ ) decreased with increasing the oxygen concentration in the reactor. The bacterial cells were less affected under aerobic conditions as shown in Figure 3.16. The bacterial cells were less threatened by nanoparticles treatment under aerobic conditions and COD removal efficiencies highly improved to be 59.30 %, 65.99 %, 46.22 %, and 50.58 % for  $\text{Fe}^0$ ,  $\text{Cu}/\text{Fe}^0$ ,  $\text{Ag}/\text{Fe}^0$ , and  $\text{Ni}/\text{Fe}^0$ , respectively. This improvement was attributed to the diverse bacterial community under aerobic conditions. Besides, oxygen played an important role;  $\text{Fe}^0$  is a strong reducing agent that can be easily oxidized in the presence of oxygen, which resulted in the decline in its toxicity and the improvement in bacterial growth. Figure 3.17 illustrates the pH variations after 20 days of operation. All pH values increased slightly under aerobic conditions owing to the increase of protons concentrations. Figure 3.18 demonstrates how the systems turn to be more reductive under aerobic conditions, which was favorable for reducing the ferrous toxicity and thus improved the bacterial activity and multiplication. The oxygen influenced the bimetallic  $\text{Fe}^0$  nanoparticles behavior, and the toxicity in the aerobic system was less strong.

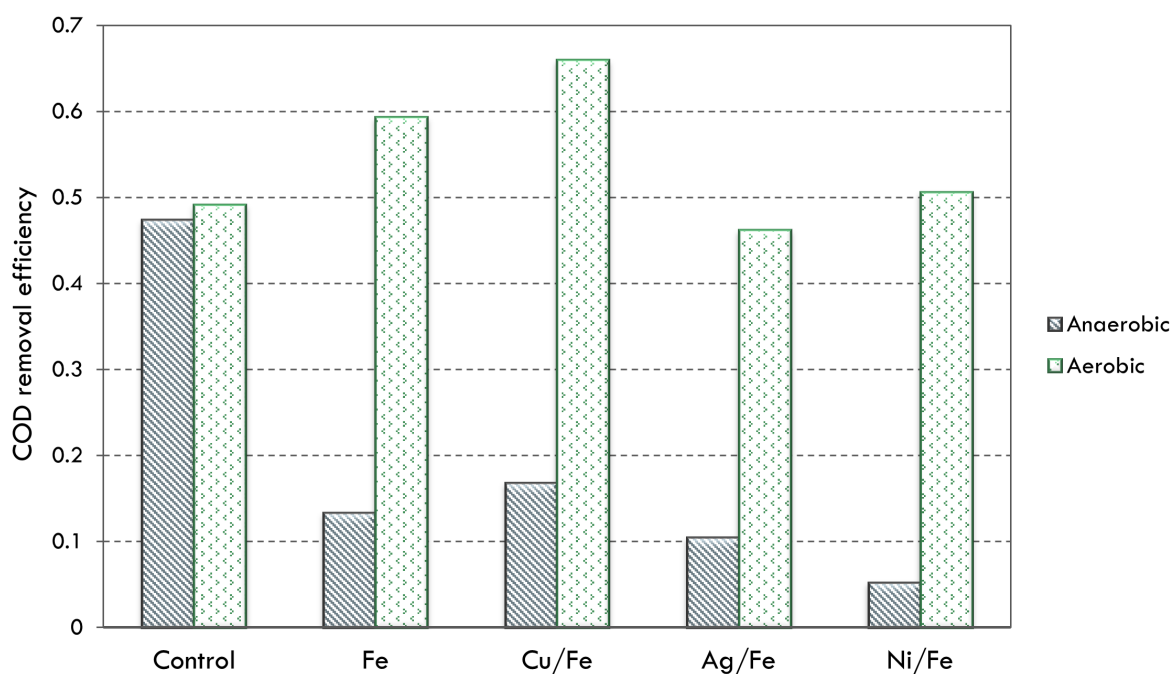


FIGURE 3.16: COD removal efficiencies of the mixed culture samples of wastewater 2 when exposed to bimetallic nanoparticles with a concentration of 50 mg/L for 12 days of operation under aerobic and anaerobic conditions.

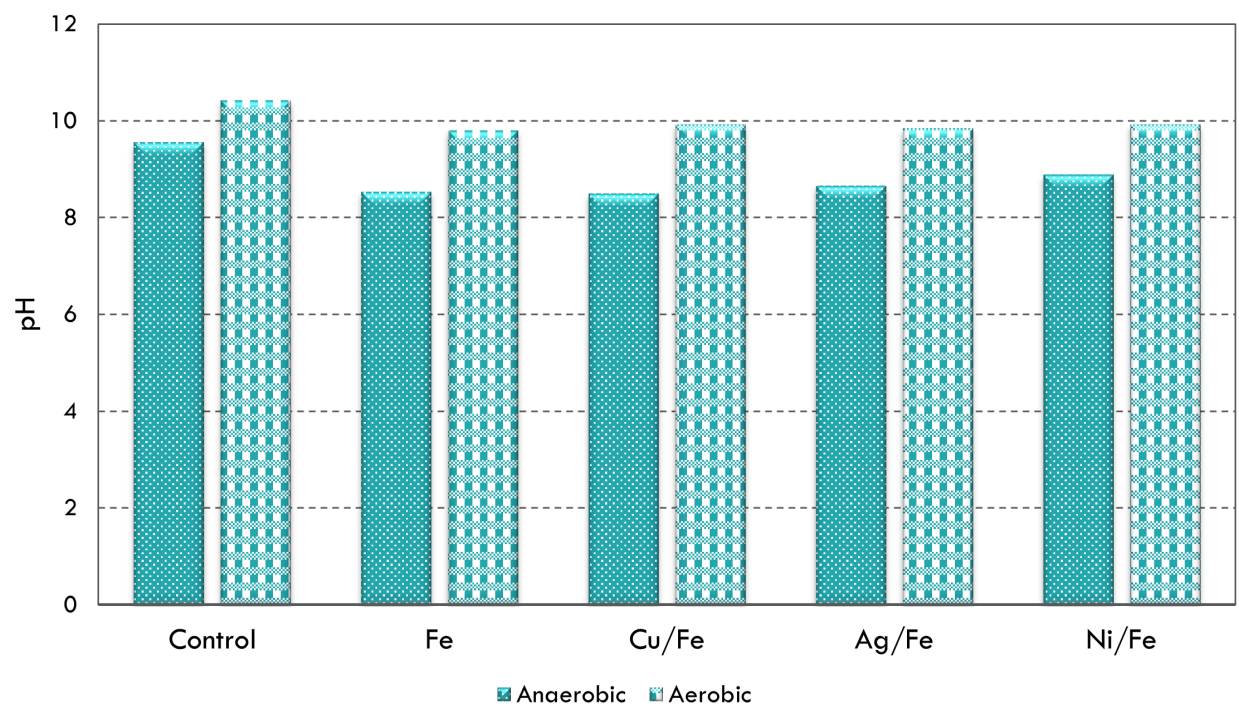


FIGURE 3.17: pH variations when exposed to bimetallic nanoparticles under aerobic and anaerobic conditions.

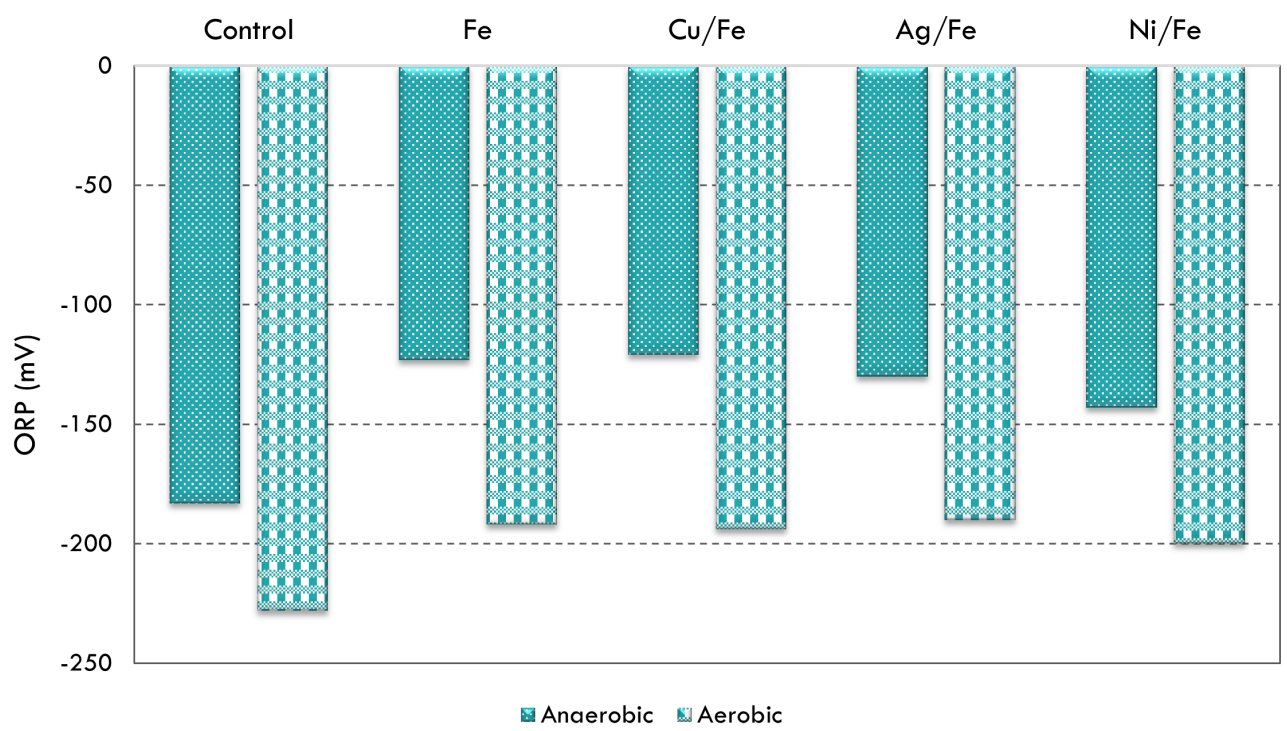


FIGURE 3.18: ORP variations when exposed to bimetallic nanoparticles under aerobic and anaerobic conditions.

Figure 3.19 describes the iron concentrations after 20 days of operation when wastewater 2 was treated by the studied bimetallic nanoparticles. It was clear that the amount of  $\text{Fe}^{2+}$  ions was reduced under aerobic conditions. The presence of oxygen increased the oxidation-reduction rate of  $\text{Fe}^{2+}$  ions, which would be favorable for reducing its negative impact on the living microorganisms in wastewater 2. Literature proved that the diffusion of oxygen would activate and enhance aerobic microorganisms' growth, which will favor organic matter degradation. Also, aerobic and anaerobic bacteria will present a resisting community toward any environmental changes such as  $\text{Fe}^0$  treatment. It was reported that practical bacterial community cooperation would stand against the toxic effects of the released ferrous ions, owing to their robustness and stability. They present a tendency to adapt to available nutrients. Therefore, the impact of nanoparticles will not be as harmful as it was for the anaerobic bacteria. Besides, more microorganisms will be available for organic matter degradation.

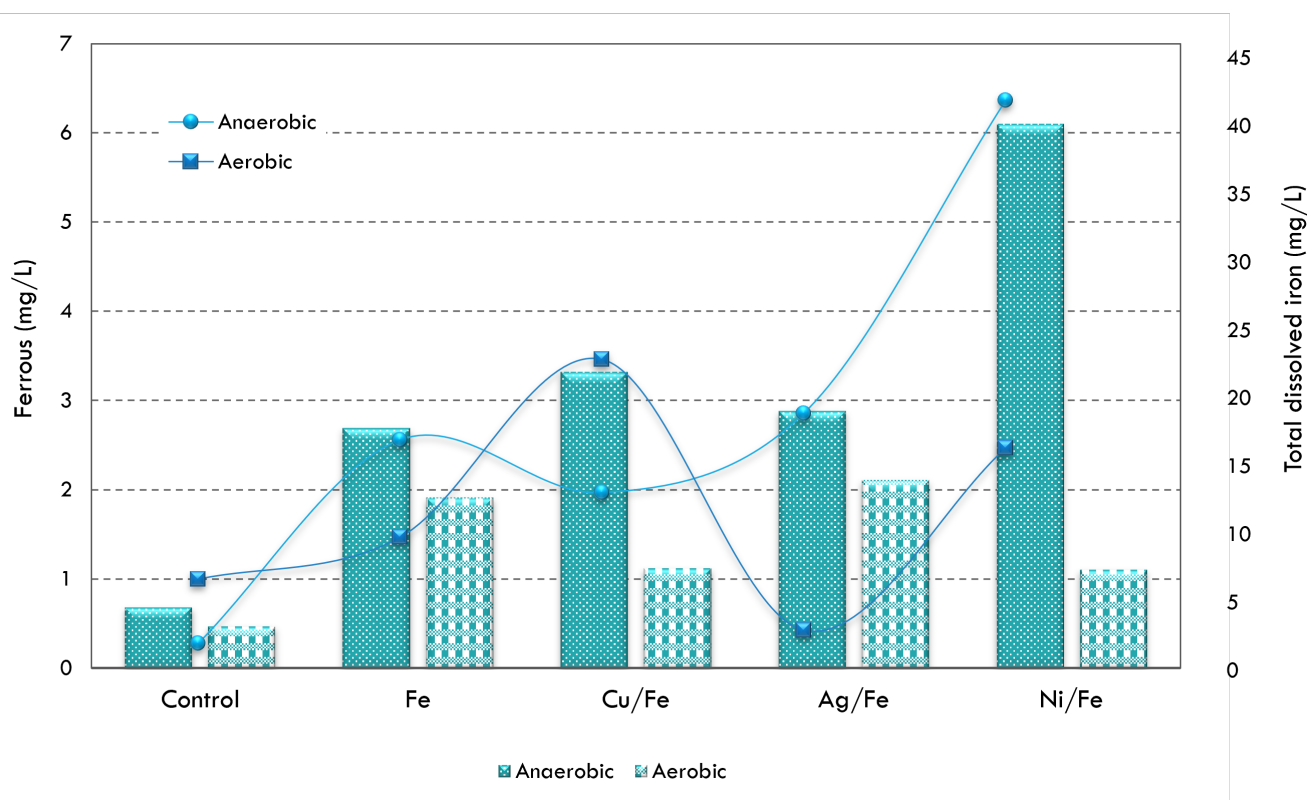


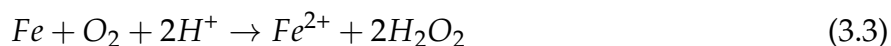
FIGURE 3.19: Iron concentrations analysis when exposed to bimetallic nanoparticles under aerobic and anaerobic conditions.

### 3.5 Conclusion

This chapter focused on examining the consequences of adding Fe<sup>0</sup> particles on bacterial growth and biological wastewater treatment. The bacterial communities were collected from real samples of wastewater, which were characterized by high microbial diversity. TEM characterizations showed that Fe<sup>0</sup> morphology had crystalline and pure structure. The introduction of Cu particles led to a larger surface area and more ductile chain. Living microorganisms were less sensitive to Fe<sup>0</sup> treated with an optimum concentration of 50 mg/L, and bacterial growth increased significantly by 50 %. In addition, Ag/Fe<sup>0</sup> addition reduced the bacterial growth by 46.15 %, whereas it increased by 15.38 %, 53.85 %, and 84.61 % for Ni/Fe<sup>0</sup>, Fe<sup>0</sup>, and Cu/Fe<sup>0</sup>, respectively, compared to control reactor. Furthermore, the COD removal efficiencies were 33.21 %, 55.30 %, 61.24%, 58.21 %, and 51.77 % for control, Fe<sup>0</sup>, Cu/Fe<sup>0</sup>, Ag/Fe<sup>0</sup> and Ni/Fe<sup>0</sup>, respectively. Fe<sup>0</sup>-based nanoparticles enhanced the effectiveness of organic matter degradation by the production of a specific key enzymes which enhanced the fermentation process and thus improved the organic matter degradation.

#### Effect of Fe on the anaerobic digestion at high concentrations

Fe<sup>0</sup> nanoparticles can be adsorbed on cell membranes of bacteria, or penetrate through them, which often leads to disturbances in the cell's functioning. In anaerobic digestion, Fe<sup>0</sup> can provide electrons due to its low oxidation-reduction potential (ORP) and serves as an acid buffer. The most recognized mechanism of Fe<sup>0</sup> bio-availability is linked to the corrosion-induced H<sub>2</sub>, which can be utilized to reduce CO<sub>2</sub> to methane by hydrogenotrophic methanogens. The Fe<sup>0</sup> corrosion process in water releases Fe<sup>2+</sup> irons, which contains a series of oxydrolisis and finally generates many types of hydrous ferric oxides. The Oxidative Oxygen Species (ROS) formed in that way may cause lipids' peroxidation and damage the DNA, and death. H<sub>2</sub>O<sub>2</sub> are hydrogen peroxide reactive species. OH<sup>•</sup> are hydroperoxyl radicals that go to interact with substituents. The listed toxicity mechanisms of Fe<sup>0</sup> can be summarized in: (i) DNA damage, (ii) string adsorption, (iii) block the cellular channels by the FeO(OH) precipitates coating on cells, (iv) reductive disruption of the cell membrane structures, and (v) enzyme inactivation caused by released iron ions (Lv et al., 2017).



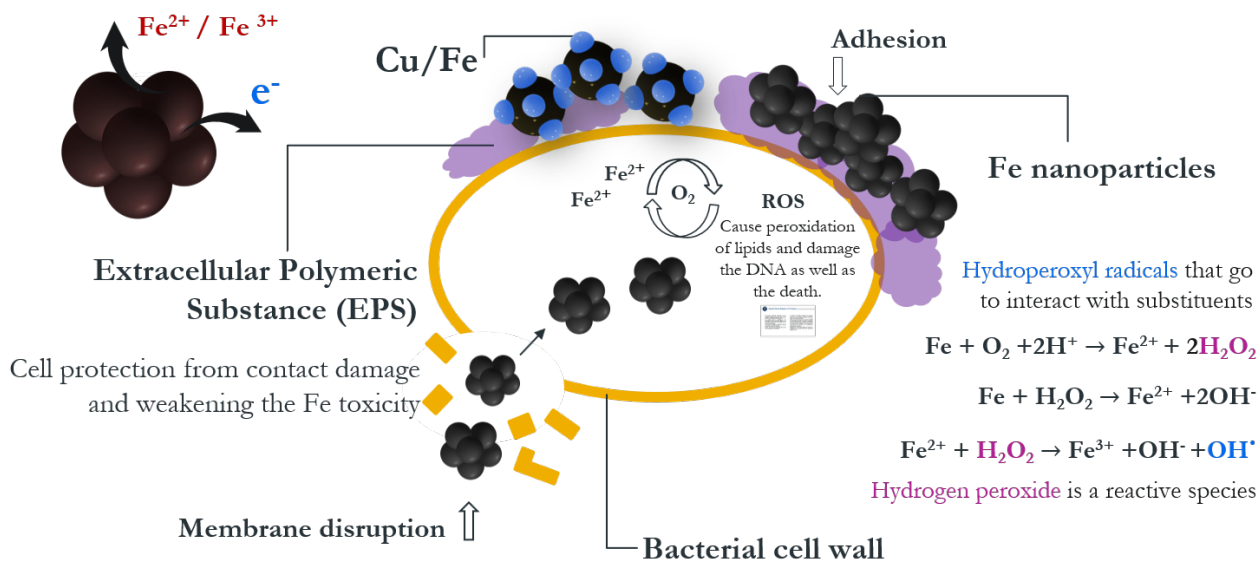
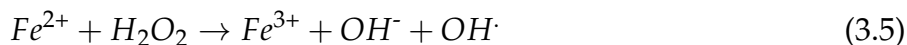


FIGURE 3.20: Fe<sup>0</sup> nanoparticles can be adsorbed on cell membranes of bacteria, or penetrate through them, which often leads to disturbances in the functioning of the cell.

### Effect of Fe on the anaerobic digestion at low concentrations

The presence of Fe<sup>0</sup> did not result in a remarkable reduction of species richness and diversities of microbial communities in anaerobic granular sludge. Conversely, the species richness of sludge exposure to Fe<sup>0</sup> was slightly higher than in the inoculum. The presence of Fe<sup>0</sup> promoted the digestion of organic matter substances in waste sludge (Zhou et al., 2020).

During the anaerobic digestion, Fe<sup>0</sup> could flocculate and adsorb on the Extracellular Polymeric Substances (EPS), which mainly protects the cell membranes from contact damage and destroying some decaying microbial cells membrane. The surrounded EPS located outer surface of anaerobic sludge could react with Fe<sup>0</sup> to accelerate the corrosion of Fe<sup>0</sup> and slow down H<sub>2</sub> release from Fe<sup>0</sup> dissolution, thus further weakening the toxicity of Fe<sup>0</sup> to anaerobic microorganisms. The addition of iron-based materials could increase the methane production rate by improving electron transfer. The main contents of EPS compounds, especially proteins, decreased after exposure to Fe<sup>0</sup>. The decrease in EPS concentration might arise from the reaction between Fe<sup>0</sup> and EPS or EPS adsorption onto oxidized iron surface due to the complex interaction between EPS and released Fe<sup>2+</sup> induced by Fe<sup>0</sup> dissolution. Interestingly, the Fe<sup>2+</sup> in the presence of EPS increased rapidly, indicating that the EPS could accelerate the

corrosion of  $\text{Fe}^0$ . EPS may partially contribute to weakening the toxicity of  $\text{Fe}^0$  to microorganisms. The addition of EPS inhibited  $\text{H}_2$  generation, which may be beneficial for the anaerobic process. The surrounded EPS located outer surface of anaerobic granule could react with  $\text{Fe}^0$  to accelerate the corrosion of  $\text{Fe}^0$ . Consequently, the toxicity of  $\text{Fe}^0$  to anaerobic sludge could be weakened because of its reaction with EPS before entering into the cell (He et al., 2017).

The presence of  $\text{Fe}^0$  could rapidly reduce the ORP in the digester. As a reducing agent,  $\text{Fe}^0$  can effectively consume oxidants in anaerobic systems, thereby maintaining a lower oxidation-reduction potential ORP in anaerobic systems. The formation of  $\text{Fe}^{2+}$  might cause the sludge to flocculate to form particles. Hence the flocculation of sludge could avoid the destruction of the bacterial filament structure during the moving process. This reaction decreased the ORP level, which is favorable for the survival and growth of methanogens.  $\text{Fe}^0$  could improve the methane production due to the reduced ORP.  $\text{Fe}^0$  could increase the abundances of bacteria with hydrolysis and acidogenesis.

In the early stage, the volatile fatty acids (VFA) would accumulate, which causes the pH to drop. Then, pH values would increase due to the rapid degradation of VFAs and the increase of ammonia nitrogen concentration.  $\text{Fe}^0$  particles have an adequate buffering capacity, which could avoid pH drop and provide a stable environment for methanogens.

The medium change effect was examined, and results showed that bacterial cells were sensitive to  $\text{Fe}^0$ -based nanoparticles exposition. The change of the nanoparticles' effect and the bacterial response could be attributed to the organic matter content in the mixed culture samples. The two samples were different in terms of the TVS content, representing the available organic matter and living microorganisms in the studied samples. The following chapter will implement the obtained results to investigate their effectiveness in bioelectricity generation using MFCs technology.

## Chapter 4

# Application of Iron-based Nanoparticles on Bioelectricity Generation Using MFCs

### 4.1 Introduction

MFCs are bioelectrochemical devices that permit bio-electricity during anaerobic respiration, based on bacterial behavior and metabolite. MFCs show promise in both wastewater treatment and bioelectricity generation. However, their power densities are still low for most envisioned applications. MFCs are still in the laboratory research stage, and their application on a commercial scale requires adopting necessary measures and scale-up testing to meet the implementation standards. The conversion of chemical energy to electrical energy via oxidation-reduction relies on the anode chamber's performance and efficiency. From an energetic perspective, ohmic losses in the anode solution, electrochemical losses at the electrodes, and bacterial metabolic losses limit the low power production. In the previous chapter, Fe-based nanoparticles significantly contributed to improving active bacterial growth, which are the primary contributors to substantial waste degradation for harvesting energy in MFC technology. The Fe-based nanoparticles' modification is a significant concern for seeking compatibility with microorganisms to enhance power generation. Most studies focus on using specific bacterial strains because pure cultures can be genetically modified for fundamental studies. This study explores the performance of the lab-scale MFCs enriched with mixed culture bacteria with a wide variety of living microorganisms needed for the system operation to meet the bioelectricity generation requirements from mixed communities. In the current chapter, three strategies have discussed the different Fe-based nanoparticles' role as an effective catalyst, owing to their large surface area and unique combination of reactivity, stability, and selectivity.

Research studies have been developed to understand the Fe nanoparticle's efficiency in lab-scale microbial fuel cells' anolyte. A series of experimental works examined the Fe-based nanoparticles' addition as detailed below:

- ★ First, we confirmed the design's working using two types of waste sludges with their mixed culture bacteria. We evaluated the response of double-chamber MFCs to the  $\text{Fe}^0$  addition in terms of the current generation using waste sludge (S1) and (S2) as described in Chapter 2, Table 2.1.
- ★ Second,  $\text{Fe}^0$  and  $\text{Cu}/\text{Fe}^0$  nanoparticles were added one by one with a concentration of 10 mg/L. Bimetallic nanoparticles  $\text{Cu}/\text{Fe}$  are a promising catalyst to be applied for power generation in MFC technology. It is supposed that the addition of  $\text{Cu}/\text{Fe}$  will increase the MFC output and contribute to the system development. Their performances were comparatively evaluated relating to current production and COD removal. Waste sludge (S3) was used for this study.
- ★ Third, Fe nanoparticles were introduced concerning their different valent states. The performance of MFCs were investigated with ferrous iron ( $\text{Fe}^{2+}$ ), ferric iron ( $\text{Fe}^{3+}$ ), and mixed  $\text{Fe}^{2+}/\text{Fe}^{3+}$  iron with a ratio of 50 %. All the iron ions were used separately, with a concentration of 10 mg/L to improve the anode chamber performance fed with waste sludge (S3) as described in Chapter 2, Table 2.1.
- ★ Finally, a new approach for power generation enhancement in MFCs from real waste sludge using Fe coated nanoparticles with  $\text{Mg}(\text{OH})_2$  shell has been developed. The study examined the use of bare and coated  $\text{Fe}^0$  nanoparticles with  $\text{Mg}(\text{OH})_2$ . Four different coating ratios were separately added to the anode chamber and comparatively evaluated. The study examined waste sludge (S4), (S5) and (S6), different pH, and aerobic enriched cathode chambers' effect on power generation.

Electricity generation in microbial fuel cells was reviewed in terms of cell voltage and power density measurements, organic matter degradation rate analysis, and bacterial growth rate improvement. The findings will bring the MFC technology a step closer to anaerobically digest the waste more effectively and collect environmentally friendly energy in the process. It is expected that adding the Fe-based nanoparticles will improve the microbial fuel cell technology performance mainly by: (i) being the second source of an electron, (ii) Playing the role of an electron carrier, and (iii) being a trace element for bacterial growth.

## 4.2 Evaluation of Double-chamber MFCs Response to $\text{Fe}^0$ treatment

In this section, the designed 4 MFCs were selected to examine their working using two different sludges (S1) and (S2) defined in Chapter 2, Table 2.1. The anaerobic sludges (S1) and (S2) were different in terms of organic matter content. Their COD values are 5561 mg/L and 37802 mg/L, respectively.  $\text{Fe}^0$  nanoparticles were added by 50 mg/L and the MFCs were operated for 80 days. The long operation time was due to the nature of the anaerobic reduction process, which always proceeds at a low rate. Figure 4.1 shows the daily voltage variation through the operation period. The maximum recorded daily voltage values were 60.20 mV and 41.30 mV for control S1 and Fe-supplemented S1 MFC. Table 4.1 summarizes the four MFCs characteristics after 80 days of operation. The maximum daily voltage obtained in the control MFC filled with S2 increased by 182 % compared to the MFC filled with S1. The addition of Fe nanoparticles reduced the daily voltage by 31 % and 9 % for the MFCs filled with S1 and S2, respectively. We executed COD measurements for the first 12 days of operation. The addition of iron could reduce the COD to 1429 and 824 mg/L for control S1 and Fe-supplemented S1 MFC, which proved the acceleration of the organic matter digestion in the anolyte compared to the other MFCs. Therefore, it is necessary to find a solution to increase the fraction of organic matter converted into electricity.

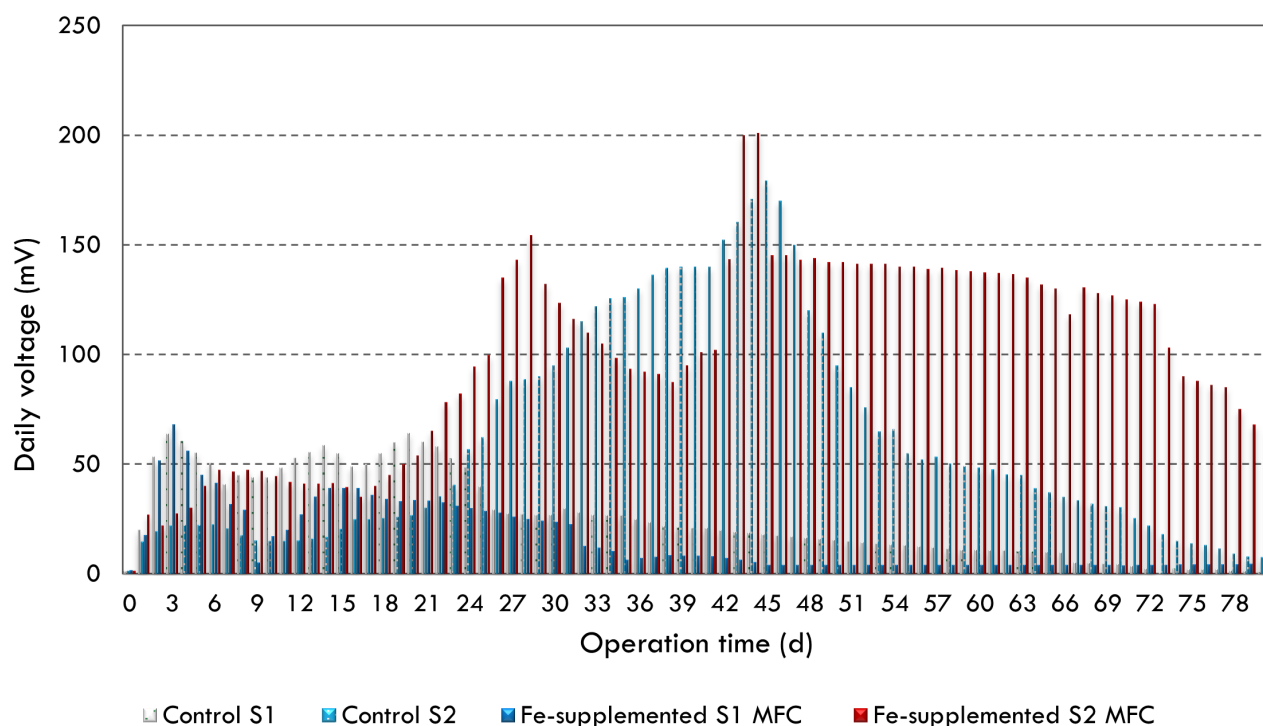


FIGURE 4.1: Daily voltage variation in MFCs using Fe nanoparticles.

TABLE 4.1: Measurements values recorded and calculated from the experiments.

parameter	Description	Control S1	Control S2	Fe-S1	Fe-S2
$V_{\max, \text{cell}}$	Maximum daily voltage measured (mV)	60.20	170.00	41.30	154.40
$P_{\max}$	Maximal daily power output ( $\mu\text{W}$ )	18.12	144.5	8.52	119.19
$I_{\max}$	Maximal daily current (mA)	0.30	0.85	0.20	0.77
$\Delta \text{COD}$	Reduction of COD concentration (mg/L)	4132	3861	47371	N
$P_{\text{An}}$	Maximum daily power output density ( $\text{mW}/\text{m}^2$ )	7550	60208	3550	49662
$P_{\text{g,VS}}$	Maximum daily power output density ( $\mu\text{W}/\text{g.vs}$ )	9.48	75.65	4.46	62.40

The voltage increased to reach 1.96 V (control S1) and 1.25 V (Fe-supplemented S1 MFC) after 80 days of operation. It was clear that  $\text{Fe}^0$  nanoparticles treatment reduced the overall voltage generation. As shown in Figure 4.2, the current generation was reduced by 36.27 % for Fe-supplemented S1 MFC compared to control S1. In contrast, the effect of  $\text{Fe}^0$  nanoparticles addition could improve the current generation by 63.08 % using (S2). During 80 days of operation, the voltage increased to 4.91 V and 8.01 V for control S2 and Fe-supplemented S2 MFC, respectively.

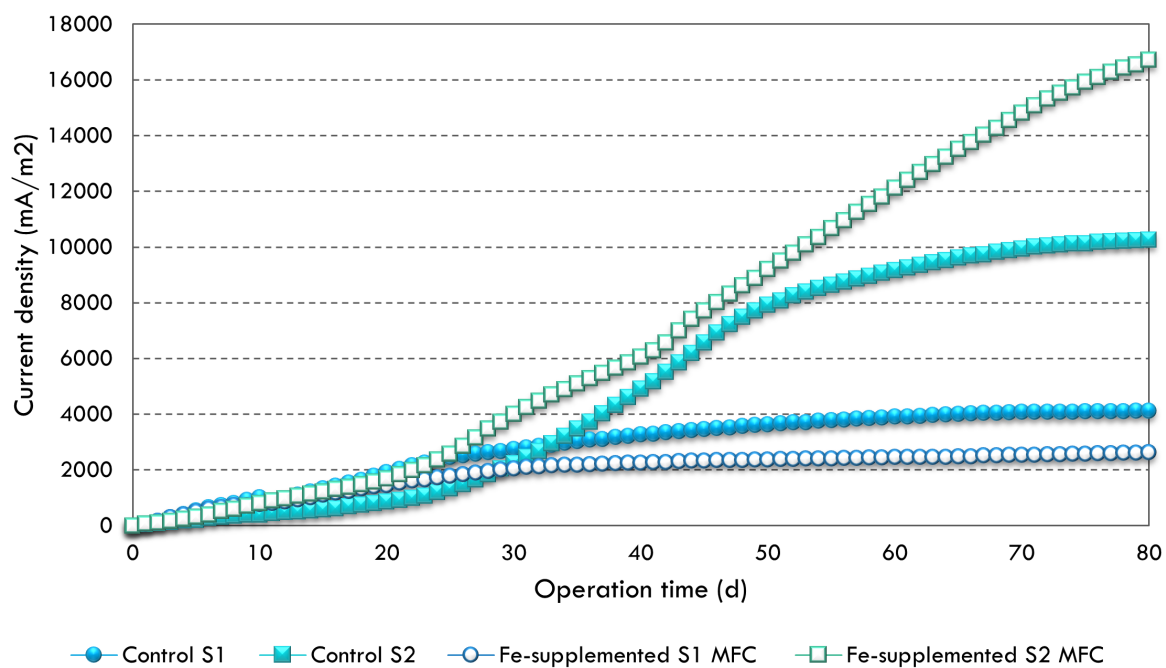


FIGURE 4.2: Daily voltage variation in MFCs using Fe nanoparticles.

Adding 50 mg/L enhanced the reactor's properties (resistivity, ORP, pH). In Figure 4.3, data measurement reported that resistivity values decreased by 24.07 % and 15.13 % for Fe-supplemented MFCs by S1 and S2, respectively. The system could be maintained around neutral conditions using waste sludge S1; however, pH values increased to 8.74 for control S2 as shown in Figure 4.4.  $\text{Fe}^0$  addition could lower the pH and maintain neutral conditions owing to its buffer capacity. ORP variations were recorded in Figure 4.5. Values could be reduced under  $\text{Fe}^0$  addition using S1. However, values comparatively increased using S2. The aggregation of  $\text{Fe}^0$  and organic matter sedimentation can explain the voltage output reduction. For the MFC working, the performance is affected by the anode surface, meaning the bacteria should be attached to the anode surface to release and transfer electrons to the anode during the organic matter digestion.  $\text{Fe}^0$  did not improve the voltage using waste sludge S1 because the anolyte was not homogeneous, whereas S2 possessed a highly compact and dense sludge, the anode surface was totally in contact with the sludge particles. Overall, control S2 generated a higher current than control S1. Fe-supplemented S1 MFC showed less resistivity to  $\text{Fe}^0$  nanoparticles, unlike Fe-supplemented S2 MFC, where the impact of  $\text{Fe}^0$  nanoparticles was positive. These results confirmed that the organic matter content affected the MFC response.

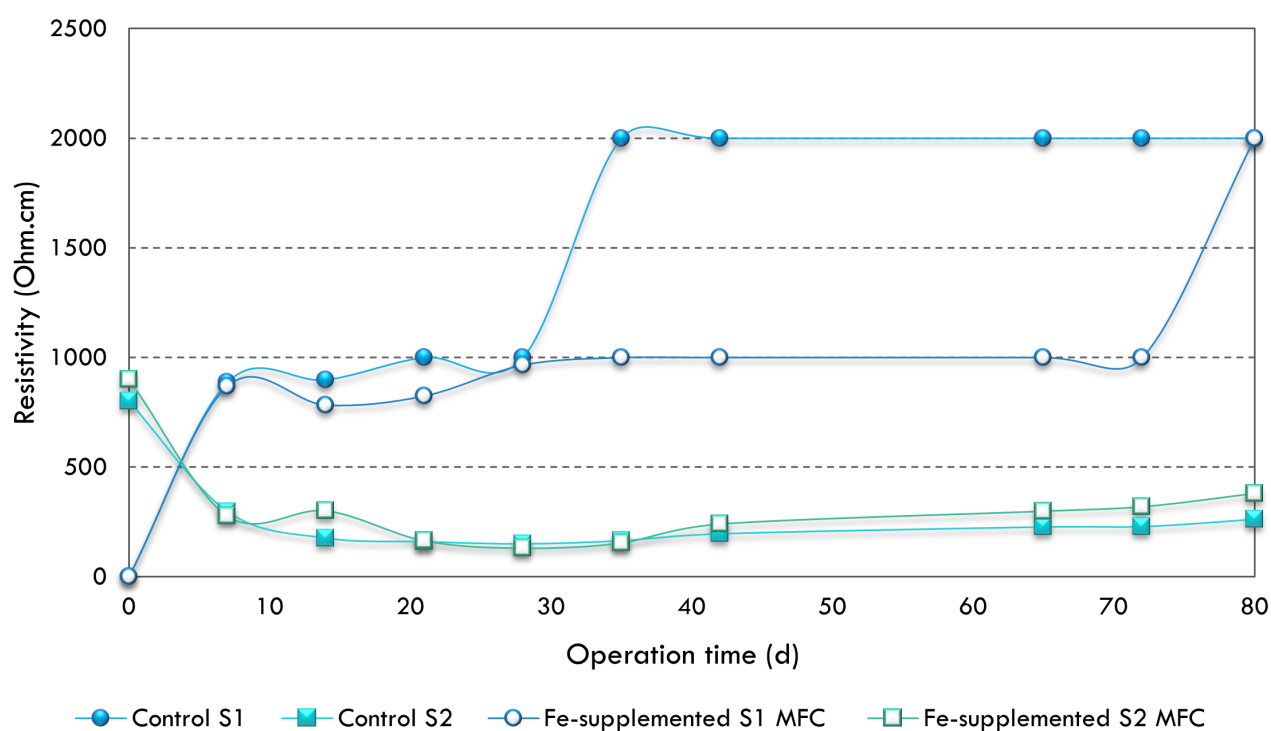


FIGURE 4.3: Resistivity variation throughout the days of operation.

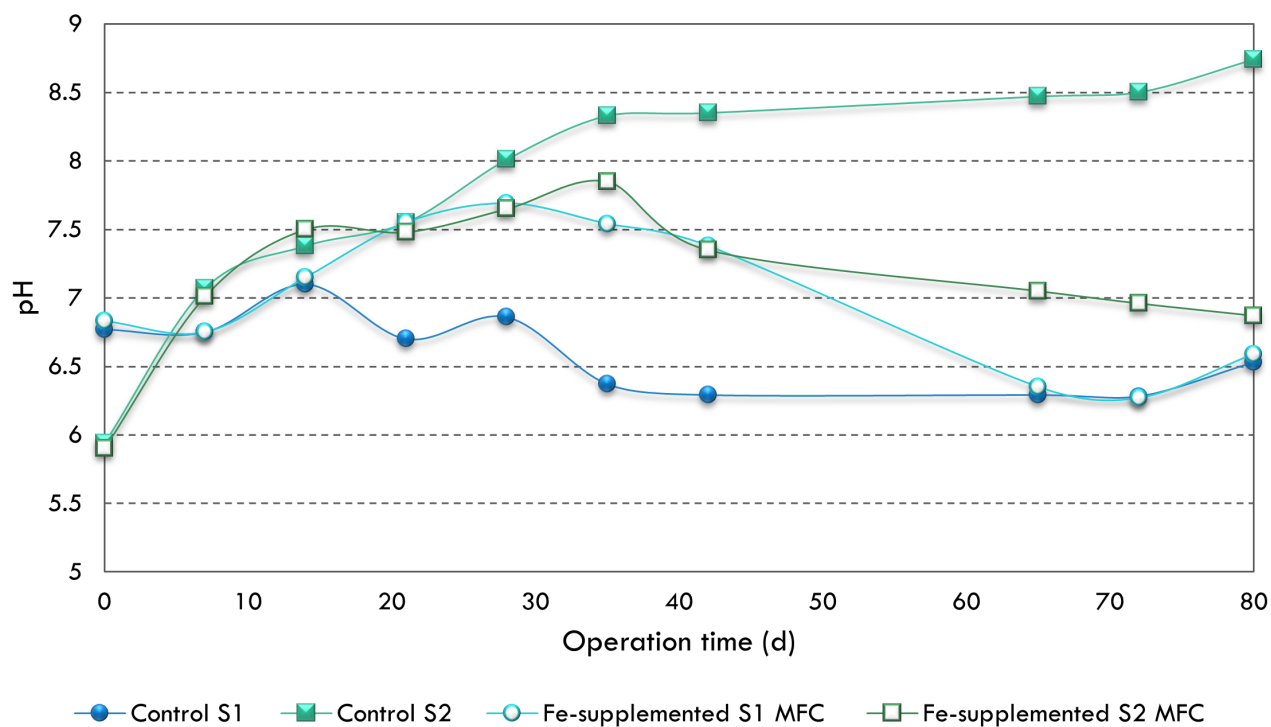


FIGURE 4.4: pH variations throughout the days of operation with an initial pH value 6.77 and 5.94 for S1 and S2, respectively.

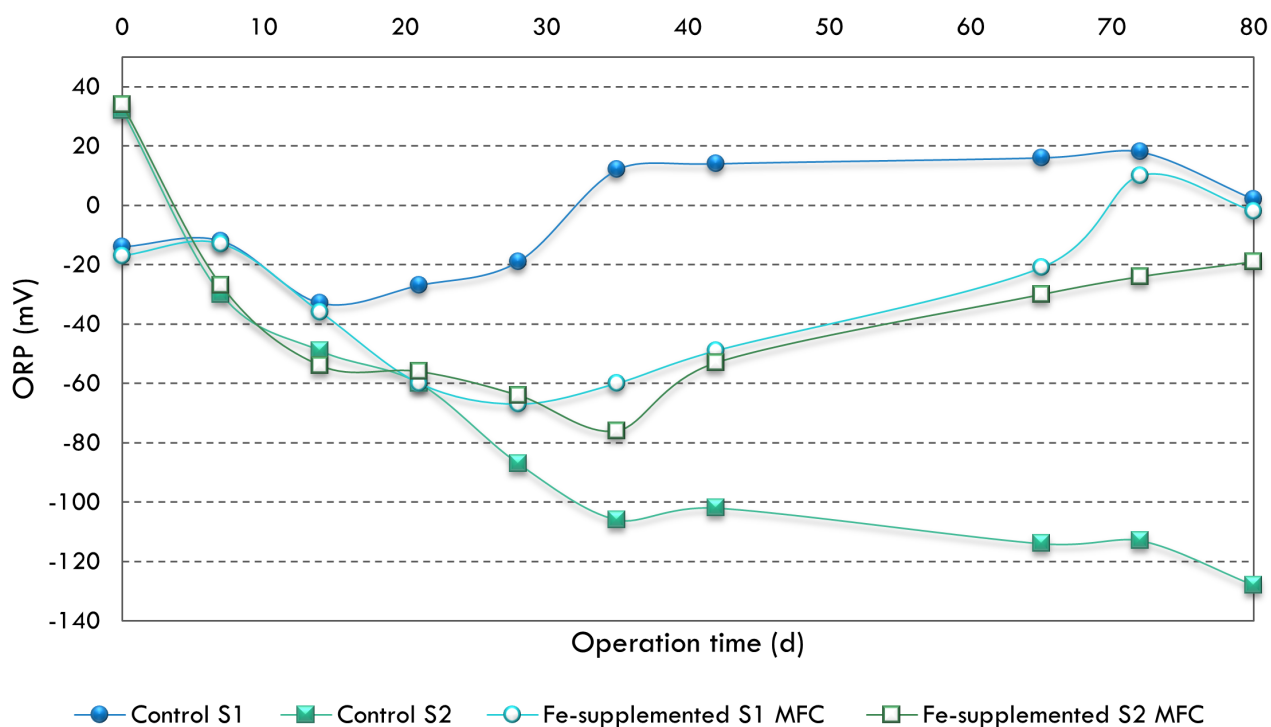


FIGURE 4.5: ORP variations throughout the days of operation with an initial ORP values -14 mV and 32 mV for S1 and S2, respectively.

The COD parameter can also be one factor determining the effect of iron nanoparticles on the current generation. Using a waste sludge with a high COD content could be suitable for electron transfer due to its compactness and richness in bacterial colonies; however, the internal resistivity is high. It requires more Fe dosages to achieve the needed organic matter degradation. In contrast, S1 is suitable for lab-scale applications. Due to the low organic content,  $\text{Fe}^0$  nanoparticles should be added with lower dosages. The anolyte should be mixed smoothly to inhibit the nanoparticles' aggregation and improve the bacterial attachment on the anode surface and the electron transfer.

Therefore, the use of double-chamber MFCs came to be challenging due to technical difficulties such as the lack of mixing. H-type MFCs were used in the following sections to examine their response toward  $\text{Fe}^0$ -based nanoparticles. A concentration of 10 mg/L was adopted for all experiments, and COD values ranged from 2000 to 6500 mg/L (S3, S4, S5, and S6). All MFCs were operated at a mixing speed of 500 rpm.

### 4.3 Application of $\text{Fe}^0$ and $\text{Cu}/\text{Fe}^0$ for Power Generation in MFCs

#### 4.3.1 MFCs performance in time

Figure 4.6 illustrates the daily voltage variation during the operation period. The maximum voltage value was equal to 25.6 and 54 mV using Fe and  $\text{Cu}/\text{Fe}$  nanoparticles. Therefore, adding iron nanoparticles to the anode chamber led to a decrease in the voltage output by 18.99 % compared to the control values, whereas using the bimetallic nanoparticles enhanced the voltage output by 43.33%. Figure 4.7 showed the accumulative cell voltages. Voltage values were recorded to be 892.40, 725.60, and 881.20 mV for control, Fe, and  $\text{Cu}/\text{Fe}$ -supplemented MFCs, respectively. The addition of Cu particles enhanced the voltage generation by 21.44 % compared to Fe nanoparticles. This improvement can be explained by promoting the Fe reactivity and decreasing the nanoparticles' agglomeration, as discussed in the previous chapter. Figure 4.8 comparatively illustrates the power density output. The maximal power density increased by 65.57 % in the  $\text{Cu}/\text{Fe}$ -supplemented MFC.

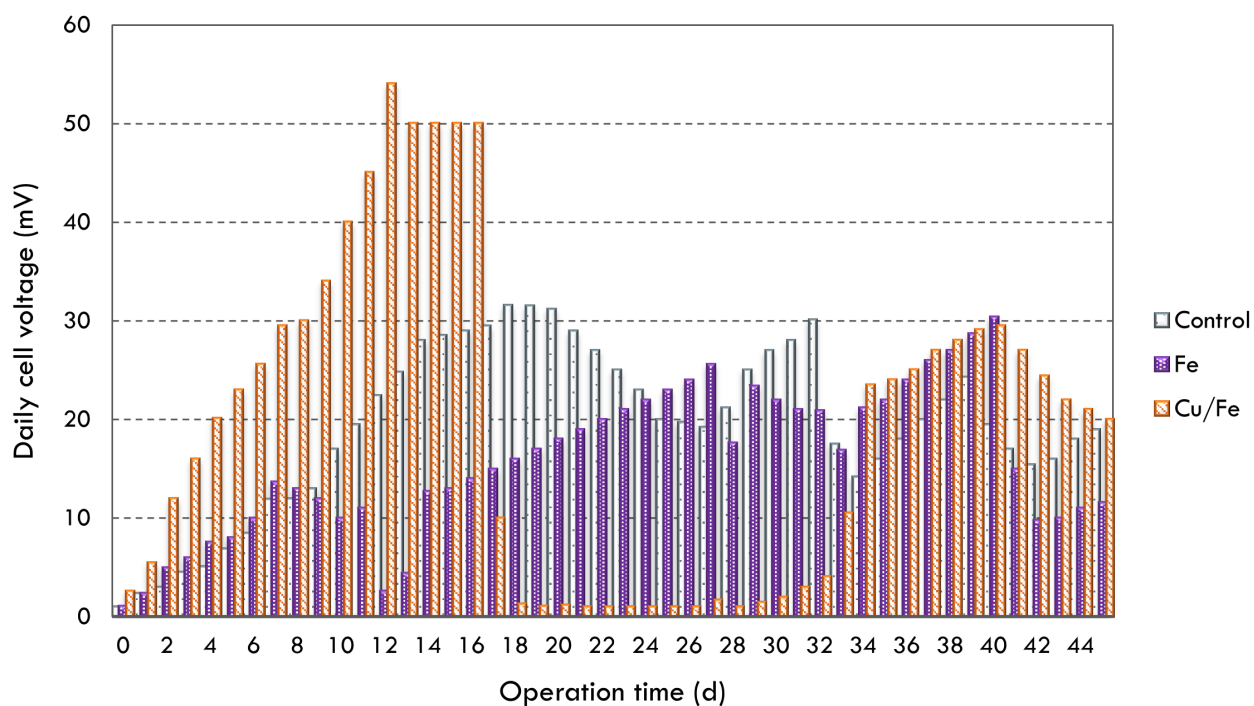


FIGURE 4.6: Daily voltage variation in MFCs using Fe and Cu/Fe nanoparticles throughout the operation period throughout the operation period.

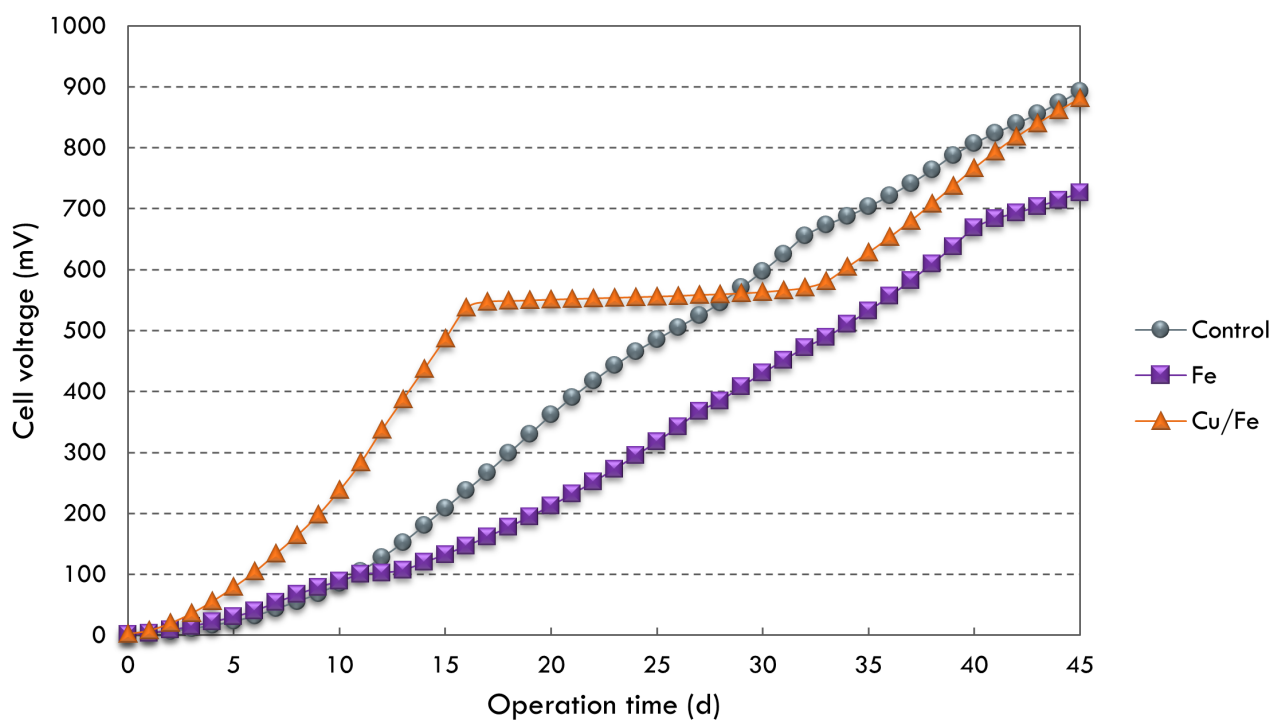


FIGURE 4.7: Voltage generation in MFCs using Fe and Cu/Fe nanoparticles throughout the operation period throughout the operation period.

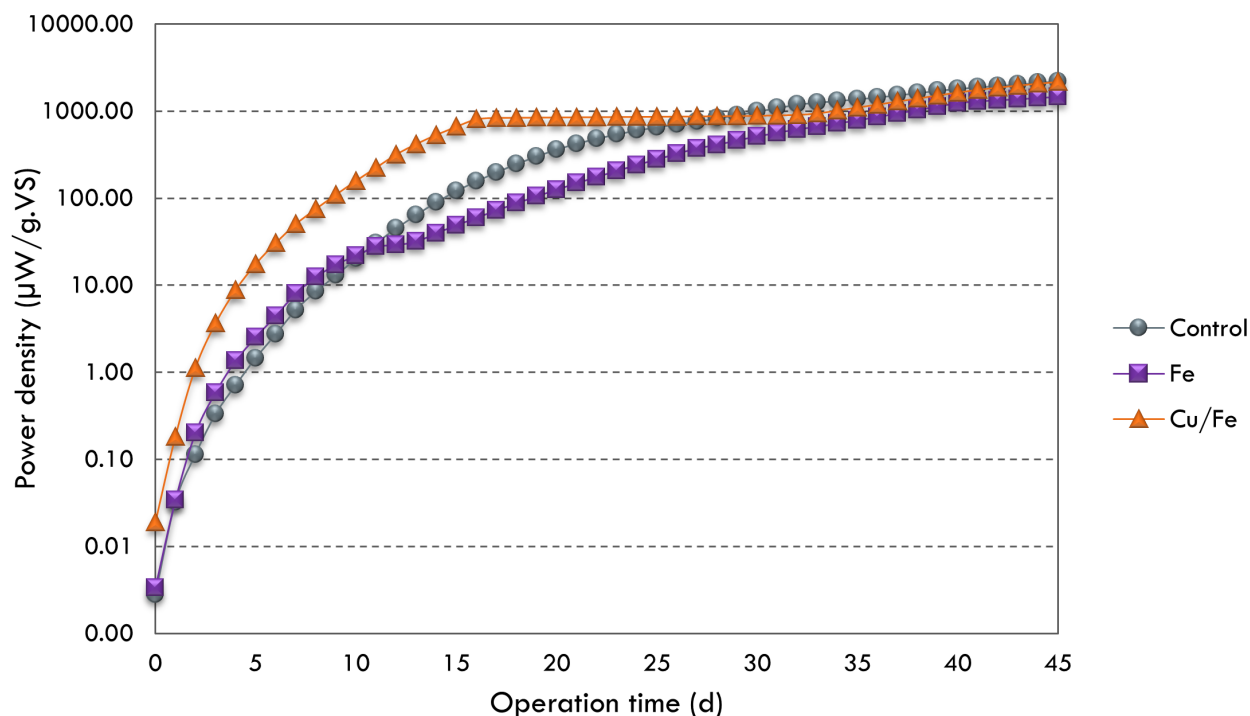


FIGURE 4.8: Power density in MFCs using Fe and Cu/Fe nanoparticles throughout the operation period.

#### 4.3.2 Iron concentration analysis

Figure 4.9 illustrates the iron concentration analysis. At the beginning of the experiments,  $\text{Fe}^{3+}/\text{Fe}^{2+}$  ions ratio was around 50 %, and then it decreased during the operation days to become almost null in control and Cu/Fe-supplemented MFCs.

The total iron was in the form of  $\text{Fe}^{2+}$ , which can be explained by the high reduction rate of  $\text{Fe}^{3+}$  ions throughout the experimental days. The reduction of the  $\text{Fe}^{3+}/\text{Fe}^{2+}$  ratio can be attributed to the high released electrons in the anode chamber resulted from the anaerobic digestion of the organic matter. As a result, a high reduction rate of  $\text{Fe}^{3+}$  occurred, which can explain that  $\text{Fe}^{3+}$  ions played an electron carrier's role in transferring electrons from the biofilm side to the anode surface.

#### 4.3.3 Wastewater treatment and organic matter removal

Table 4.2 summarizes the anolyte characteristics at the end of the experiments. It is clear that the Cu/Fe reduced the resistivity and improved the anolyte conductivity, which will be favorable for electron transfer and power generation.

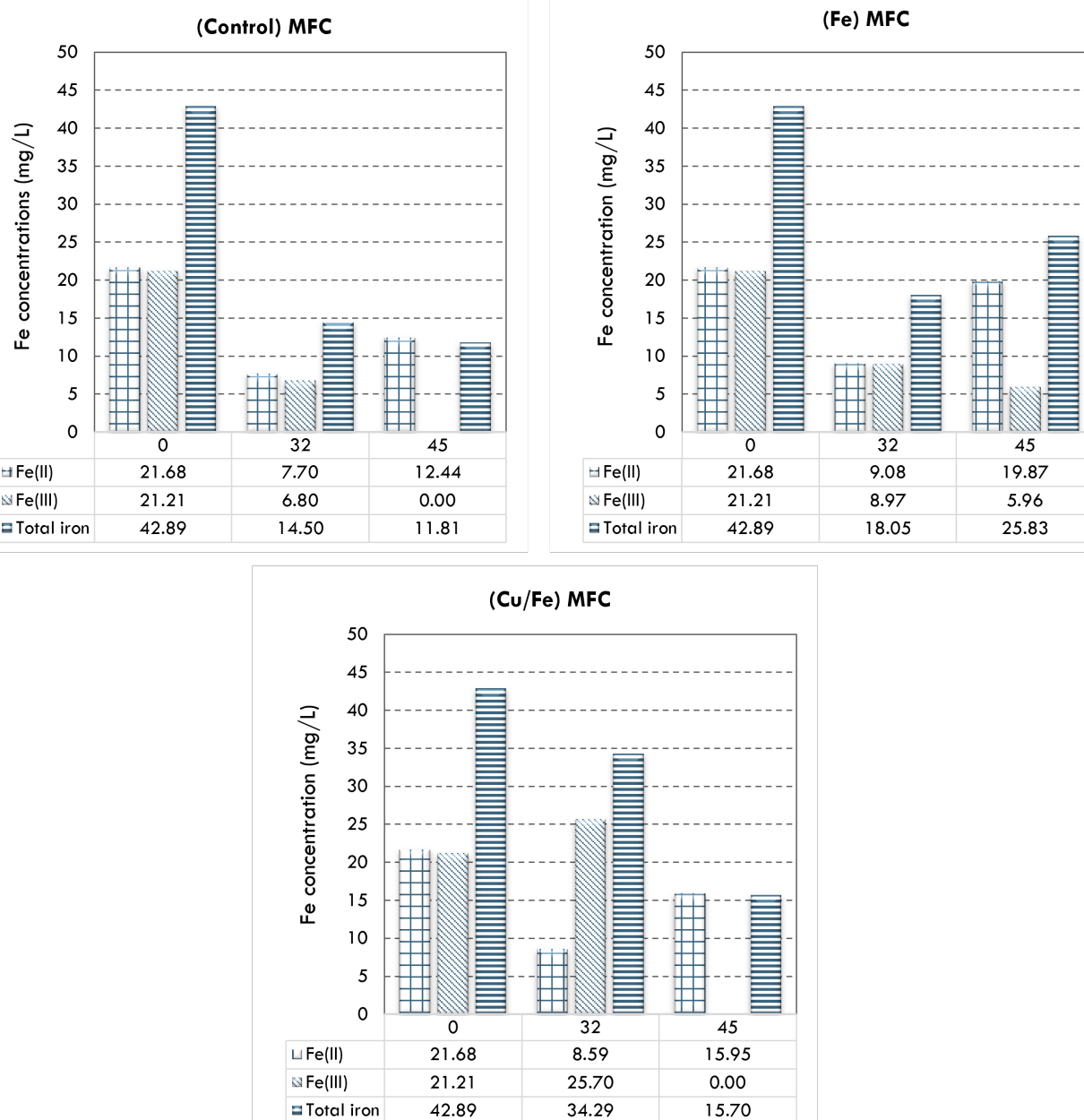


FIGURE 4.9: Iron concentration in the anode chamber throughout the operation period.

Although the anolyte characteristics are improved to the control MFC, the current generation was limited.  $\text{Cu/Fe}^0$  could maintain a lower ORP level and a neutral pH condition, which will be favorable for bacterial growth. As shown in Figure 4.10, the maximum number of colonies increased by 93.35 % and 95 % using  $\text{Fe}^0$  and  $\text{Cu/Fe}^0$ , respectively. Besides, the bacterial activity increased and the organic matter biodegradability reinforced. Figure 4.11 illustrates the COD removal efficiencies values on day 15, day 32, and at the end of the experiments. After 15 days of operation, the removal efficiency reached 46.62 %, 50.78 %, 37.07 %, and for control,  $\text{Fe}^0$ , and  $\text{Cu/Fe}^0$  MFCs, respectively.

At the end of experiments, the COD removal efficiency was 38.88 %, 38.26 %, and 52.40 % for control,  $\text{Fe}^0$ , and  $\text{Cu}/\text{Fe}^0$  MFCs, respectively. The increase in the bacterial cell number can justify the improvement in organic matter degradation. Total volatile solids measurements proved that the TVS was reduced by 30.83 %, 41.94 %, and 47.22 % for control,  $\text{Fe}^0$ , and  $\text{Cu}/\text{Fe}^0$ , respectively. The high matter degradation will enhance the number of released electrons as a product of the anaerobic digestion, and thus the power output will be enhanced.

TABLE 4.2: Anolyte characteristics when exposed to Fe and Cu/Fe addition after 45 days of operation.

MFC type	Units	Control	Fe-MFC	Cu/Fe MFC
Resistivity	$\Omega.\text{cm}$	979.0	848.0	748.3
Conductivity	$\mu.\text{cm}^{-1}$	1022.0	1184.0	1338.0
TDS	mg/L	511	593	670
Salinity	ppt	0.7	0.8	0.9
pH	-	7.12	7.26	7.17
ORP	mV	-34	-42	-36

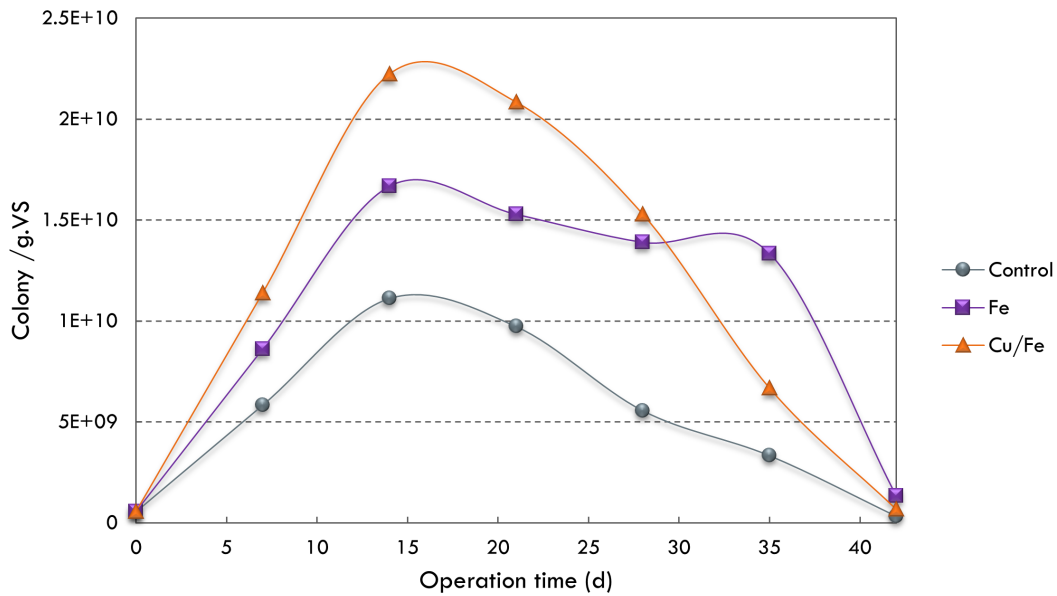


FIGURE 4.10: Bacterial growth in the anode chamber under anaerobic conditions during the operation period when exposed to: (a) the control MFC, (b) Fe MFC, and (c) Cu/Fe MFC.

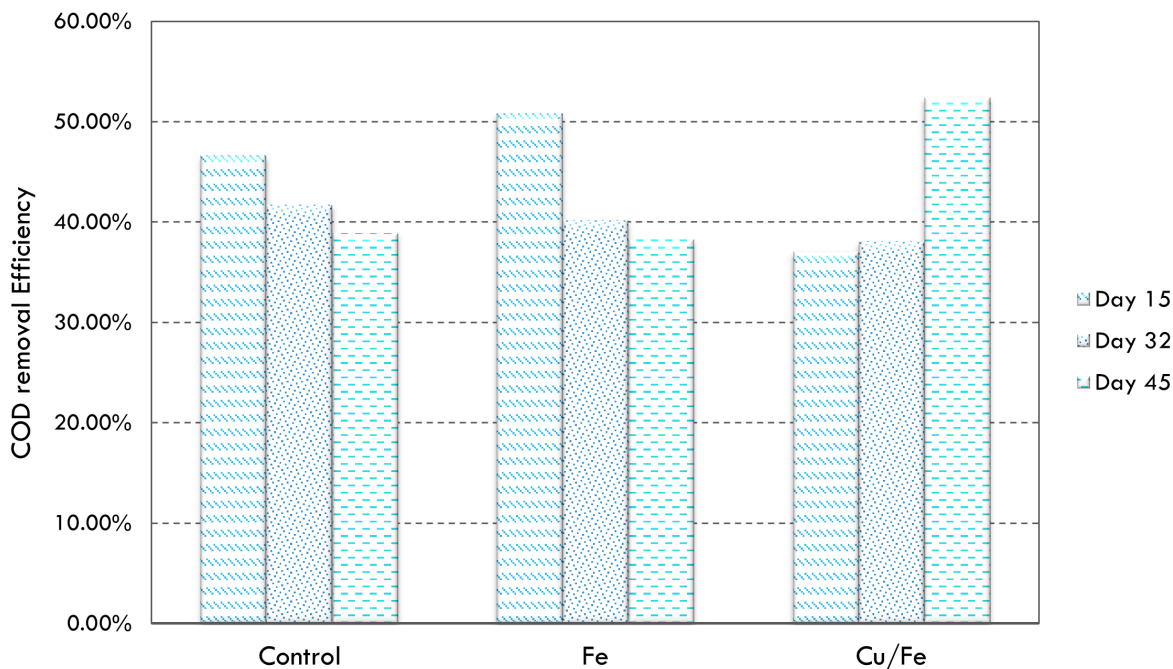


FIGURE 4.11: COD removal efficiencies in the anode chamber throughout the operation period.

## 4.4 Effect of $\text{Fe}^{2+}$ , $\text{Fe}^{3+}$ , and $\text{Fe}^{2+}/\text{Fe}^{3+}$ for Electricity Generation in MFCs

### 4.4.1 MFCs performance in time

The MFC performance improved in time and the voltage output rapidly increased in MFCs supplemented with  $\text{Fe}^{2+}$ ,  $\text{Fe}^{3+}$ , and  $\text{Fe}^{3+}/\text{Fe}^{2+}$  ions compared to the control MFC. Figure 4.12 illustrates the daily voltage evolution during 45 days of operation. Although the voltage was not stable all along with the experiments, it continuously increased in time. A steep increase in electricity production was observed starting from day 1, and the voltage reached its maximum values at day 14 and day 18 for  $\text{Fe}^{2+}$  and control MFCs, respectively, suggesting that the addition of iron ions accelerated the start-up of the MFCs. This shortened start-up time could be attributed to the promotion of the bacterial adhesion to the anode material. The daily voltage increased and maximum values were 31.6 mV (control), 57.8 mV ( $\text{Fe}^{2+}$ ), 67 mV ( $\text{Fe}^{3+}$ ), and 56.9 mV ( $\text{Fe}^{3+}/\text{Fe}^{2+}$ ). The accumulative cell voltages of all MFCs were illustrated in Figure 4.13. The voltage improvement was recorded to be 38.01 %, 98.86 %, and 82.29 % for  $\text{Fe}^{2+}$ ,  $\text{Fe}^{3+}$ , and  $\text{Fe}^{3+}/\text{Fe}^{2+}$ , respectively. The accumulative voltage increased continuously to reach 0.892 V (control), 1.231 V ( $\text{Fe}^{2+}$ ), 1.774 V ( $\text{Fe}^{3+}$ ), and 1.626 V ( $\text{Fe}^{3+}/\text{Fe}^{2+}$ ). Moreover, the power density and current values increased with time as shown in Figure 4.14.

Values increased in time and reached ( $2212.16 \mu\text{W/g.VS}$  ;  $1.859 \text{ A/cm}^2$ ), ( $4213.44 \mu\text{W/g.VS}$  ;  $2.565 \text{ A/cm}^2$ ), ( $8747.79 \mu\text{W/g.VS}$  ;  $3.697 \text{ A/cm}^2$ ), ( $7351.33 \mu\text{W/g.VS}$  ;  $3.389 \text{ A/cm}^2$ ) for control,  $\text{Fe}^{2+}$ ,  $\text{Fe}^{3+}$ , and  $\text{Fe}^{3+}/\text{Fe}^{2+}$ , respectively. Measurements showed that the power density values increased by 90 %, 295 %, and 232 % using  $\text{Fe}^{2+}$ ,  $\text{Fe}^{3+}$ , and  $\text{Fe}^{3+}/\text{Fe}^{2+}$ , respectively.

MFC supplemented with  $\text{Fe}^{3+}$  had the highest power density generation, followed by the highest daily voltage values and the highest accumulative cell voltage. Table 4.3 comparatively summarizes the MFCs performance in terms of power generation and organic matter degradation reflected by the reduction in COD values after 45 days of operation. A previous research study suggested that  $\text{Fe}^{3+}$  increased the initial start-up and electricity generation by being an essential element of ferredoxin, which played a vital role as an enzyme activator in some anaerobic bacteria (Wu et al., 2013). The study used a specific strain *Shewanella oneidensis* MR-1, whereas our works evaluate Fe ions' impact towards a mixed culture of bacteria.

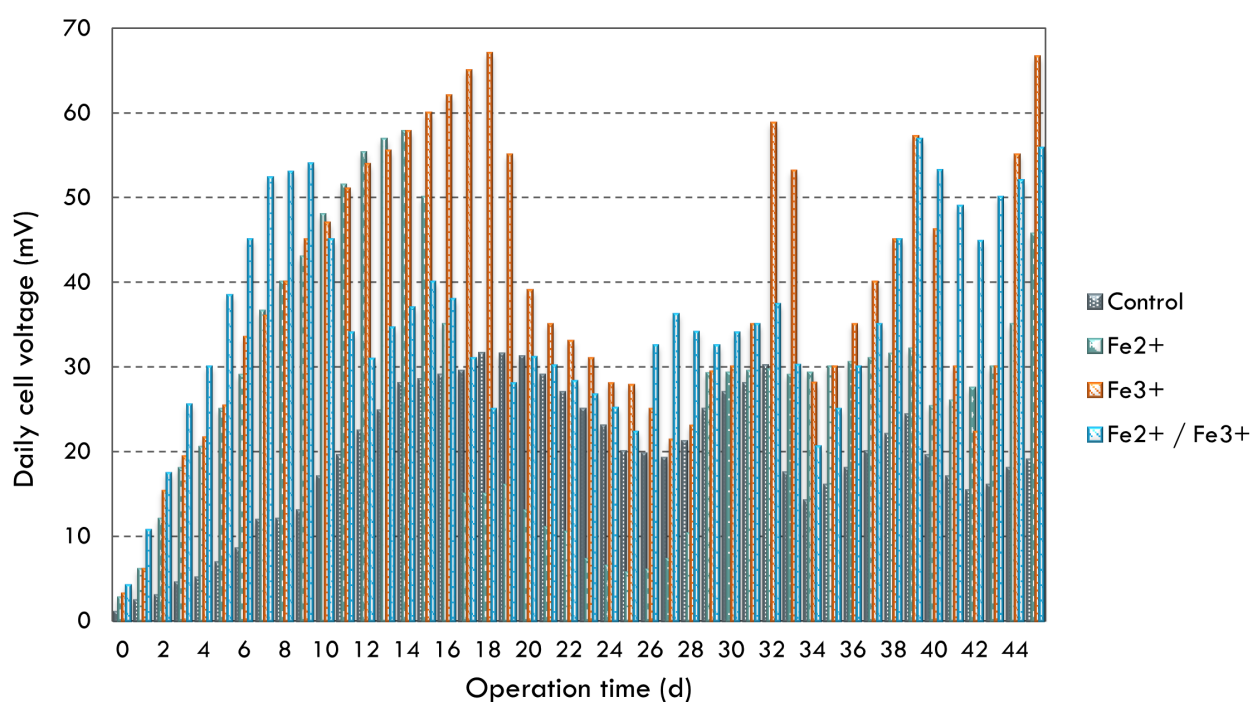


FIGURE 4.12: Daily voltage generation in MFCs using  $\text{Fe}^{2+}$ ,  $\text{Fe}^{3+}$ , and  $\text{Fe}^{3+}/\text{Fe}^{2+}$  iron salts with 10 mg/L at the anode throughout the operation period.

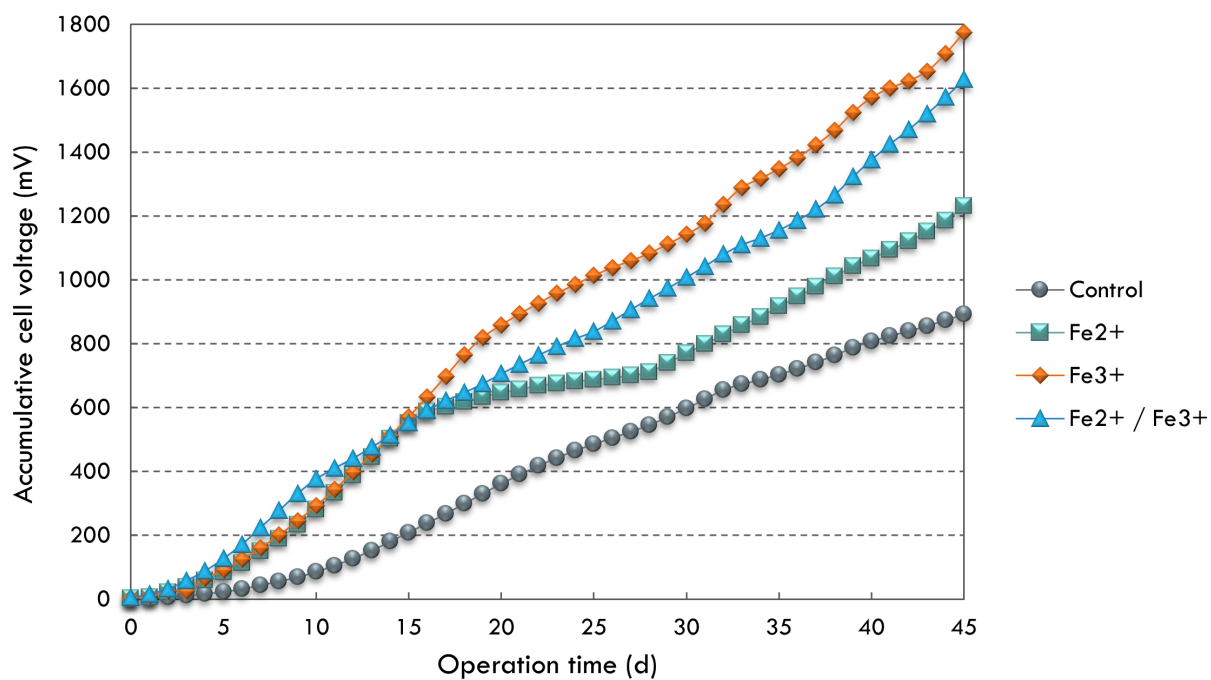


FIGURE 4.13: Accumulative voltage generation in MFCs with time using Fe<sup>2+</sup>, Fe<sup>3+</sup>, and Fe<sup>2+</sup>/Fe<sup>3+</sup> iron ions with 10 mg/L at the anode.

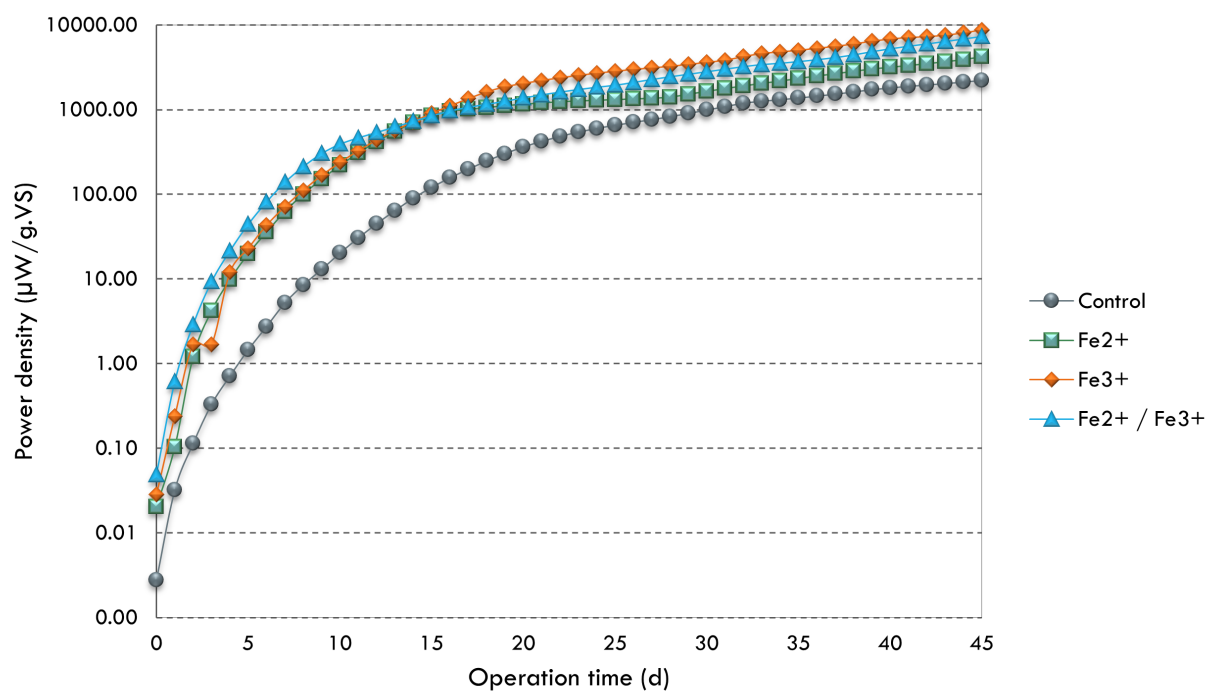


FIGURE 4.14: Power density variations of MFC using Fe<sup>2+</sup>, Fe<sup>3+</sup>, and Fe<sup>3+</sup>/Fe<sup>2+</sup> iron ions with 10 mg/L at the anode throughout the operation period.

TABLE 4.3: Measurements values recorded and calculated from the experiments.

parameter	Description	Control	$\text{Fe}^{2+}$	$\text{Fe}^{3+}$	$\text{Fe}^{3+}/\text{Fe}^{2+}$
$C_p$	Total coulombs measured (mA)	4.41	6.04	8.70	7.90
$V_{\text{max,cell}}$	Maximum voltage measured (mV)	31.60	57.80	67	56.90
$P_{\text{max}}$	Maximal power output ( $\mu\text{W}$ )	5.05	16.76	22.11	15.93
$I_{\text{max}}$	Maximal current (mA)	0.16	0.29	0.33	0.28
$\Delta \text{COD}$	Reduction of COD concentration (mg/L)	2274	3044	2911	2924
$P_{\text{An}}$	Maximum power output density ( $\text{mW}/\text{m}^2$ )	2.10	7.00	9.30	6.70
$P_{\text{g,VS}}$	Maximum power output density ( $\mu\text{W}/\text{g.vs}$ )	2.77	9.28	12.47	9.00

#### 4.4.2 Iron concentration analysis

The iron concentrations in the anolyte are shown in Figure 4.15. In the beginning of the experiments, the initial  $\text{Fe}^{2+}$ ,  $\text{Fe}^{3+}$ , and total iron concentrations were 21.68, 21.21, and 42.89 mg/L, respectively, at an initial pH equal to 7.17, 6.97, 7.00, and 6.46, respectively for control and iron ions-supplemented MFCs. The ratio of  $\text{Fe}^{3+}/\text{Fe}^{2+}$  was around 50 %, and it decreased in the end of the experiment, to be 90 % for control MFC, and 100 % for  $\text{Fe}^{3+}$ -supplemented MFC. It was clear that most of the iron was in the form of  $\text{Fe}^{2+}$  after 45 days of operation in control and  $\text{Fe}^{3+}$ -supplemented MFCs. Iron analysis showed that their  $\text{Fe}^{2+}$  concentrations were 12.44 and 17.81 mg/L, at pH values equal to 7.12 and 6.49 respectively. Therefore, the biological oxidation-reduction rate was good enough to sustain the produced current in the  $\text{Fe}^{3+}$ -supplemented MFC. The  $\text{Fe}^{3+}/\text{Fe}^{2+}$  ratio was always 50 % for the mixed  $\text{Fe}^{3+}/\text{Fe}^{2+}$  ions-supplemented MFCs, and their correspond iron ions concentrations at day 45 were 19.06, 18.15, and 37.21 mg/L for  $\text{Fe}^{2+}$ ,  $\text{Fe}^{3+}$ , and total iron at pH values equal to 6.29. Besides, iron analysis showed that the  $\text{Fe}^{2+}$ ,  $\text{Fe}^{3+}$ , and  $\text{Fe}^{3+}/\text{Fe}^{2+}$  concentrations were 15.93, 8.58, and 24.51 mg/L, respectively at a pH value equal to 6.80 for  $\text{Fe}^{2+}$ -supplemented MFC.

Iron analysis showed that iron ions concentration did not stay constant but decreased with time. The lower ratio  $\text{Fe}^{3+}/\text{Fe}^{2+}$  during the end of the experiments for  $\text{Fe}^{3+}$ -supplemented MFC may be caused by "the higher current density ( $3.697 \text{ A}/\text{cm}^2$ ) for which a higher reduction rate of ferric ions is needed. The iron oxidizers' limited activity resulted from higher  $\text{Fe}^{2+}$  concentrations, which can have an inhibitory effect on growth and oxidizing capacity.

A prior study, where the iron reduction process was investigated in the cathode chamber of a scaled-up MFC, showed that iron ions precipitated at the end of the experiments (Ter Heijne et al., 2011). This observation was a reasonable explanation for the decrease in the iron ions. The authors inspected the obtained precipitates under microscope analysis, and they proved that these precipitates consisted of yellow-orange rod-shaped microorganisms combined with iron salts structures. The study suggested that the yellow precipitates were a combination of the iron oxidizers with iron salts. The study highlighted the risk of iron precipitation, which should be further discussed. Besides, the diffusion of iron ions through the membrane from the anode chamber to the cathode chamber could limit the availability of iron ions in the anolyte, which would further lower the iron ions concentrations.

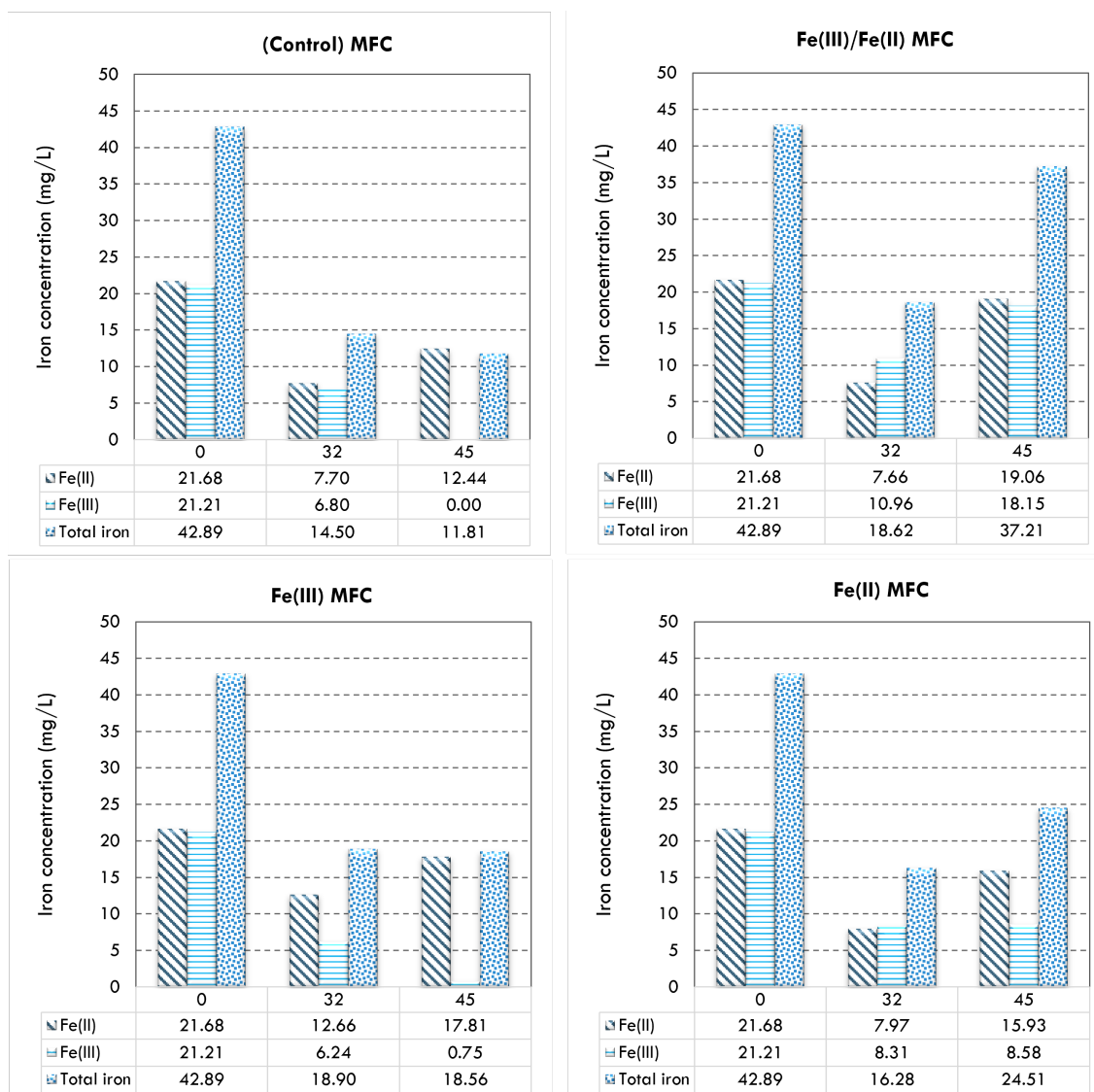


FIGURE 4.15: Iron concentration in the anolyte for control and iron ions-supplemented MFCs throughout the days of operation.

#### 4.4.3 Analysis of internal resistances

The measured cell voltage is lower than the theoretical MFC potential. A useful way to express the energy loss in the MFC system is to control the anode chamber's resistivity during the experiments. Figure 4.16 illustrates the anode resistance throughout the operation period. Results proved that the total resistance decreased from  $1000 \Omega \cdot \text{cm}^2$  to 699, 666, 815, and  $782 \Omega \cdot \text{cm}$  for control,  $\text{Fe}^{2+}$ ,  $\text{Fe}^{3+}$ , and  $\text{Fe}^{3+}/\text{Fe}^{2+}$ -supplemented MFCs, respectively. Measurements showed that the total resistance decreased by 30.1 %, 33.4 %, 18.5 %, and 21.8 % for control,  $\text{Fe}^{2+}$ ,  $\text{Fe}^{3+}$ , and  $\text{Fe}^{3+}/\text{Fe}^{2+}$ -supplemented MFCs, respectively, resulting in improving the MFCs performance with time. However, these results explained that the high internal resistance limits the amount of power generated in the studied MFCs. The growth of the electroactive biofilm could explain the high resistance. It contributed to the improved current generation but simultaneously increased the anolyte's resistivity. In Figure 4.17, results showed that iron ions stimulated the electrochemically active bacteria present in the mixed culture microbial community. The maximum values of colonies were  $1.42 \text{ E}+11$  colonies/g.VS for both  $\text{Fe}^{2+}$  and c-supplemented MFCs, whereas the  $\text{Fe}^{3+}/\text{Fe}^{2+}$ -supplemented MFC showed an increase up to  $1.83 \text{ E}+11$  colony/g.VS. The bacterial growth increased by 92.18 % using  $\text{Fe}^{2+}$  and  $\text{Fe}^{3+}$  ions compared to control MFC. The  $\text{Fe}^{3+}/\text{Fe}^{2+}$  enhanced the bacterial growth by 177 % compared to control MFC. These results demonstrated a superior influence of iron ions on the behavior and activity of bacterial communities. A recent study studied the effect of the presence of  $\text{Fe}^{3+}$  ions on *Shewanella oneidensis* MR-1 which are known as iron-reducing bacteria (Wurzler et al., 2020).

Electrochemical analysis proved that the biofilm is vital for the protection against local corrosion might occur during the experiments. Also, the multiplication of microorganisms that can completely oxidize the organic matter are the primary contributors to power production.

#### 4.4.4 Wastewater treatment and organic matter removal

The performance of the constructed MFCs was reflected in terms of COD removal efficiencies and total TVS degradation. As shown in Figure 4.18, the control MFC presented a removal efficiency of 46.62 %, whereas  $\text{Fe}^{3+}$ -supplemented MFC,  $\text{Fe}^{2+}$ -supplemented MFC, and the  $\text{Fe}^{3+}/\text{Fe}^{2+}$ -supplemented MFCs, the COD removal efficiencies were 78.49 %, 51.55 %, and 65.00 %, respectively at day 15. A decrease in the removal efficiency was observed at day 32, and then values increased at the end of the experiments.

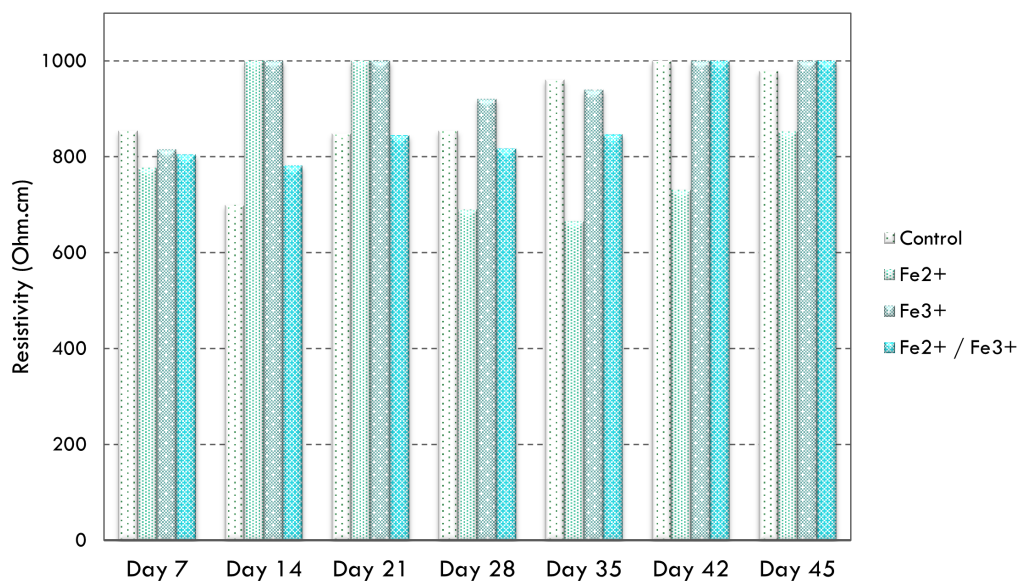


FIGURE 4.16: Resistance of the anode chamber of MFCs using Fe<sup>2+</sup>, Fe<sup>3+</sup>, and Fe<sup>3+</sup>/Fe<sup>2+</sup> iron salts with 10 mg/L throughout the operation period.

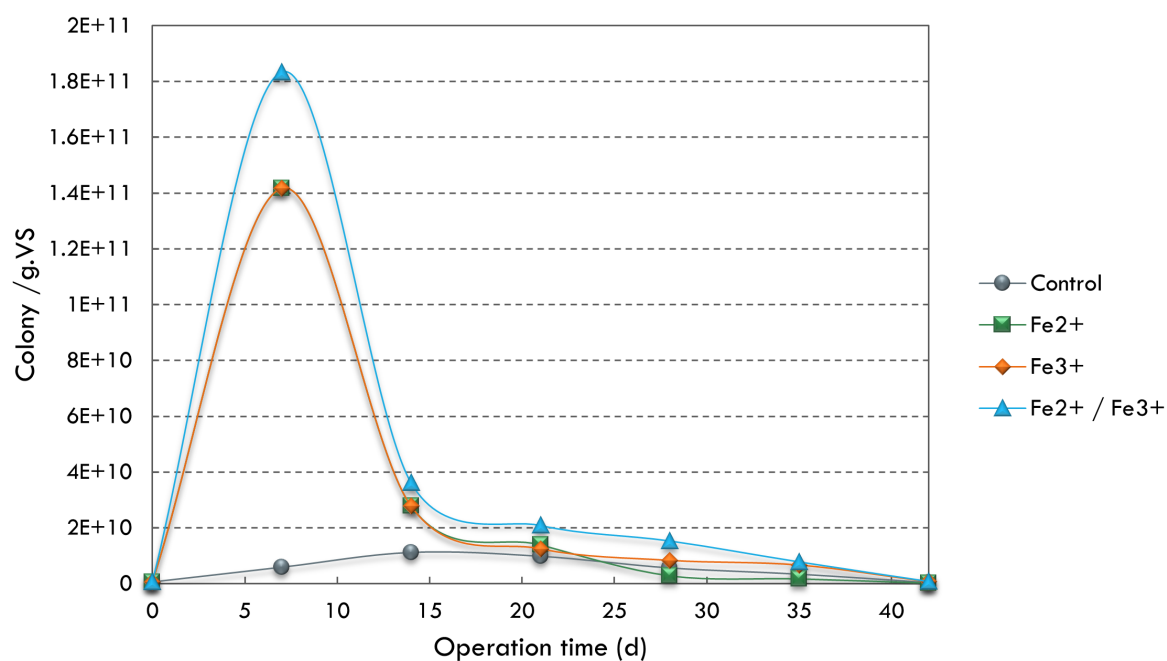


FIGURE 4.17: Bacterial growth with time using Fe<sup>2+</sup>, Fe<sup>3+</sup>, and Fe<sup>3+</sup>/Fe<sup>2+</sup> iron ions with 10 mg/L at the anode. The addition of iron ions was favorable for the enrichment of bacteria.

These variations in COD removal efficiencies could be attributed to the different phases of bacterial growth. An increase of bacterial colonies in the log phase would accelerate the organic matter degradation. However, a reduced number in the death phase will limit the digestion process, and thus COD values would remain high.

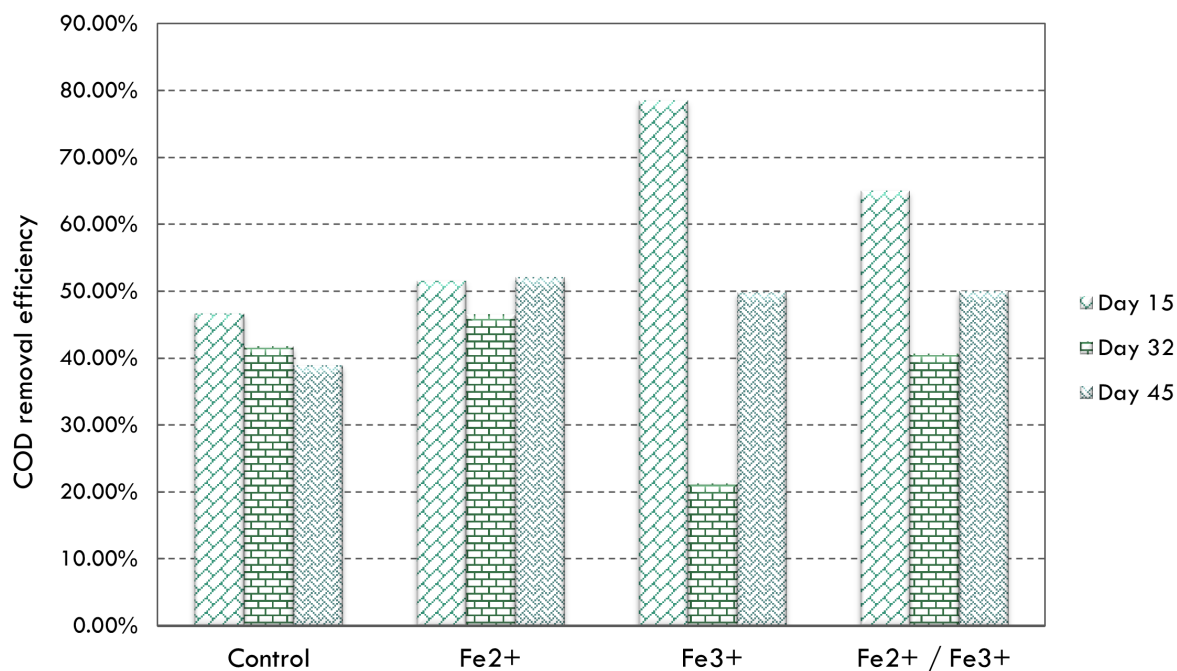


FIGURE 4.18: COD removal using  $\text{Fe}^{2+}$ ,  $\text{Fe}^{3+}$ , and  $\text{Fe}^{3+}/\text{Fe}^{2+}$  iron salts with 10 mg/L in the anode chamber throughout the operation period.

The high performance of  $\text{Fe}^{3+}$ -supplemented MFC might be attributed to the effects of redox reactions inside the anode chamber. Also, Microbes would be more activated when exposed to iron ions, which enhanced the degradation of the organic matter. Table 4.4 shows the total volatile solids variations during the experiments period. TVS concentrations were reduced by 48.05 %, 52.78 %, and 36.67 % by  $\text{Fe}^{2+}$ ,  $\text{Fe}^{3+}$ , and  $\text{Fe}^{3+}/\text{Fe}^{2+}$ -supplemented MFCs, respectively compared to 30.83 % in control MFC. These results highlight the promising effect of  $\text{Fe}^{3+}$  for promoting organic matter removal, enhancing bacterial growth, and increasing power generation in MFCs.

TABLE 4.4: TVS concentrations using  $\text{Fe}^{2+}$ ,  $\text{Fe}^{3+}$ , and  $\text{Fe}^{3+}/\text{Fe}^{2+}$  iron ions with 10 mg/L in the anode chamber throughout the operation period.

MFC type	day 0	day 32	day 45
Control	3.60	1.94	2.94
$\text{Fe}^{2+}$	3.60	1.91	1.87
$\text{Fe}^{3+}$	3.60	2.26	1.7
$\text{Fe}^{3+}/\text{Fe}^{2+}$	3.60	2.14	2.28

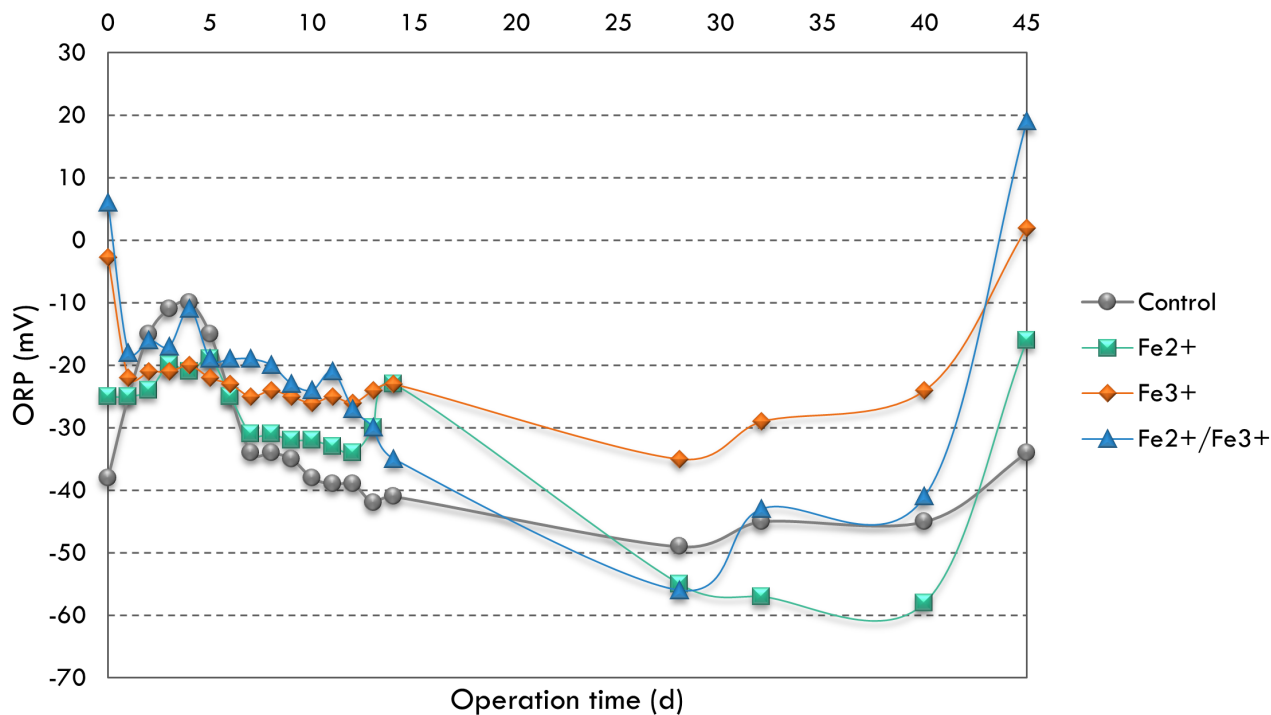


FIGURE 4.19: ORP variations for MFCs supplemented with Fe<sup>2+</sup>, Fe<sup>3+</sup>, and Fe<sup>3+</sup>/Fe<sup>2+</sup> iron salts throughout the operation period.

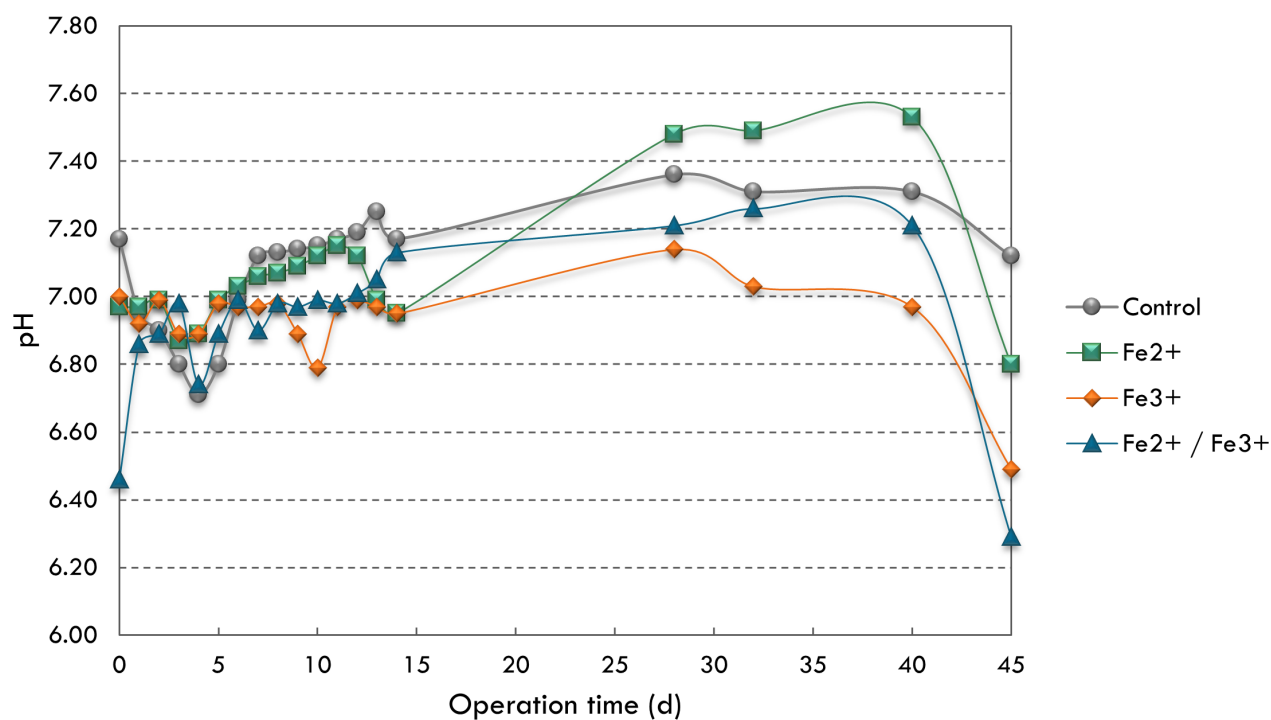


FIGURE 4.20: pH variations for MFCs supplemented with Fe<sup>2+</sup>, Fe<sup>3+</sup>, and Fe<sup>3+</sup>/Fe<sup>2+</sup> iron salts throughout the operation period.

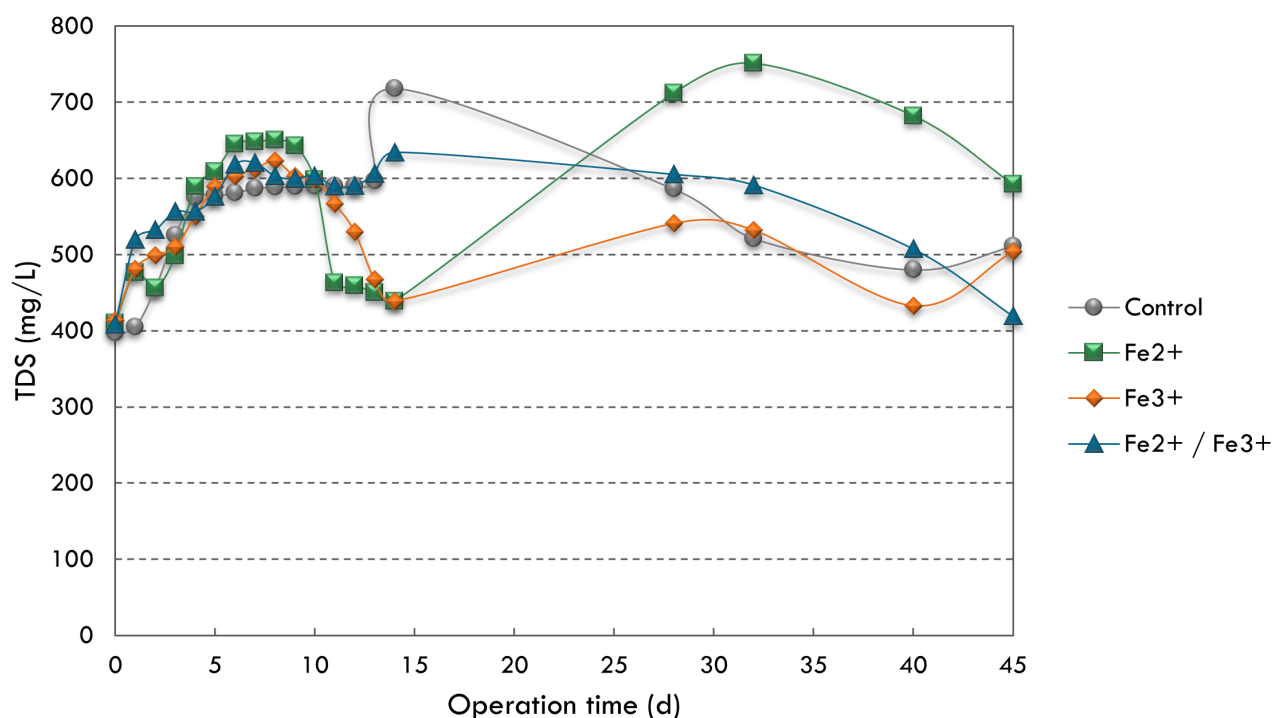


FIGURE 4.21: Total dissolved solids variations for MFCs supplemented with  $\text{Fe}^{2+}$ ,  $\text{Fe}^{3+}$ , and  $\text{Fe}^{3+}/\text{Fe}^{2+}$  iron salts throughout the operation period.

ORP values were illustrated in Figure 4.19. For the first ten days of operation, ORP values were almost similar, and their plots had the same trend. It was clear that  $\text{Fe}^{2+}$  showed the most reductive anolyte, whereas  $\text{Fe}^{3+}$  maintained almost the same level ranging between -20 to -35 mV. This stability was favorable for organic matter digestion and electron transfer. Moreover,  $\text{Fe}^{3+}$  helped maintain almost neutral system conditions during the operation period, as shown in Figure 4.20. pH values varied between 6.79 and 7.00. However, a sudden decrease occurred, and pH was equal to 6.49. The increase in TDS value could help explain the sudden variation in pH. At day 45, TDS values increased from 433 to 504 mg/L under  $\text{Fe}^{3+}$  treatment. The increase in organic matter digestion and release of dissolved solids would boost the release of volatile fatty acids as a by-product. The same phenomenon occurred with  $\text{Fe}^{2+}$ . The increase in pH values was linked to the increase in TDS values. The improved presence of dissolved solids was also reflected by the decrease in ORP values for  $\text{Fe}^{2+}$ -supplemented MFCs. The system would be more reductive, which means the anolyte is rich in reductive ions. The target resides in transferring the released electrons to the anode surface and, therefore, improving the MFC performance.

In this study, Fe ions' addition exhibited a higher power output and a shorter start-up time. The addition of iron ions was favorable for the enrichment of bacteria that could reduce  $\text{Fe}^{3+}$  by oxidizing organic matters through anaerobic respiratory metabolism. The results correlated with power generation enhancement as a combination of:

- Bacterial growth increase,
- Resistivity decrease, and
- Organic matter degradation improvement.

$\text{Fe}^{3+}$  ions would favor the multiplication of bacterial colonies and the biofilm formation in the anode chamber, which resulted in high protection for bacteria against any corrosion effect. Besides, it will further promote organic matter degradation due to the strengthened activity and metabolic rate of electroactive bacteria, and power output would increase. However, a low removal efficiency could be obtained due to limitations in the electron donor's mass transfer to the microbes and the anodes. The amount of power generated in these MFCs was limited by the system's high internal resistance and the biological  $\text{Fe}^{3+}$  iron reduction rate that was high enough to limit the produced current. Therefore, suggested studies would be elaborated to:

1. Control the oxidation-reduction rate of iron ions in the anolyte,
2. Improve the electron transfer rate,
3. Reduce the resistivity of both anodic and cathodic chambers, and
4. Increase the bio-energy produced in MFC technology.

The following section presents an attempt to promote the MFC output via improving the Fe nanoparticles reactivity when introduced for power generation. Considering iron's high oxidation-reduction rate, a magnesium hydroxide coating shell will be applied for bare Fe nanoparticles. It is supposed that the coating layer would control the iron ions release and, therefore, improve the development of microbial fuel cell technology.

## 4.5 Power Generation Enhancement Using $\text{Fe}^0$ Coated with $\text{Mg}(\text{OH})_2$

### 4.5.1 Characterization of bare and coated $\text{Fe}^0$ nanoparticles

The morphological characteristics of the prepared bare  $\text{Fe}^0$  and coated Mg/Fe were described through TEM. As shown in Figure 4.22, the  $\text{Fe}^0$  nanoparticles were aggregated due to the magnetic attraction, which consequently decreased the particles' mobility, whereas in the case of the coated  $\text{Fe}^0$  nanoparticles, the clouds of  $\text{Mg}(\text{OH})_2$  maintained the particles' discreteness, which enhanced their mobility and thereby decreased their magnetic attraction. The use of different Mg/Fe coating ratios was evident through the difference in the volume of  $\text{Mg}(\text{OH})_2$  clouds surrounding the  $\text{Fe}^0$  nanoparticles. Figure 4.22 (e) showed that using a ratio of Mg/Fe:1.0 led to obtaining the thickest coating layer, which further led to obtaining the least aggregated particles compared to the other coating ratios as it was clear in Figure 4.22 (b),(c), and (d). TEM results confirmed that Mg/Fe nanoparticles had a smooth surface, an adequate particle size, and a spherical shape. This latter will result in higher dispersibility and more availability of the nanoparticles in the anolyte solution, which will be favorable for the solution's conductivity.

**A**

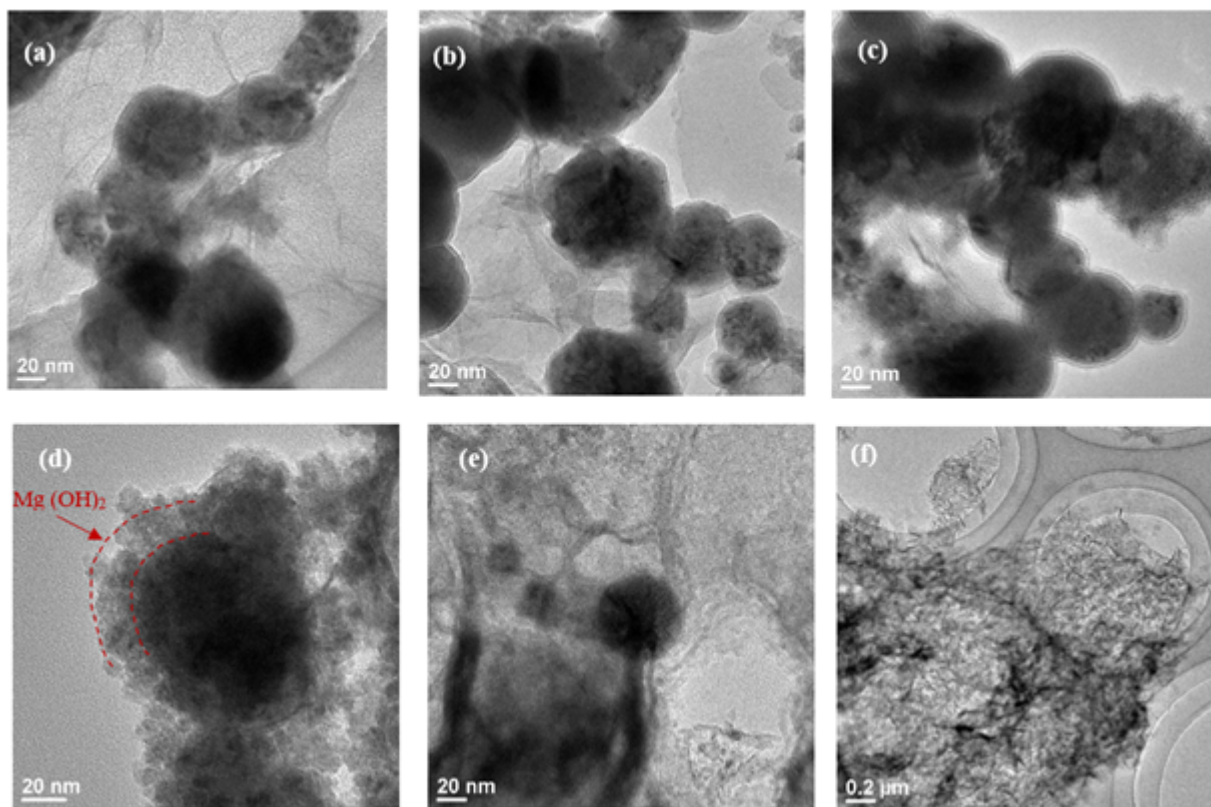


FIGURE 4.22: TEM characterization of the synthesized bare and coated  $\text{Fe}^0$

The modification of  $\text{Fe}^0$  nanoparticles composition was apparent through XRD analysis. Figure 4.23 (A) illustrates the different peaks of crystallinity for the bare and coated  $\text{Fe}^0$  nanoparticles. Two typical peaks at  $2\Theta = 44.8^\circ$  and  $2\Theta = 82.16^\circ$  were detected in the bare  $\text{Fe}^0$ , whereas peaks of brucite were detected on the coated nanoparticles' surface.

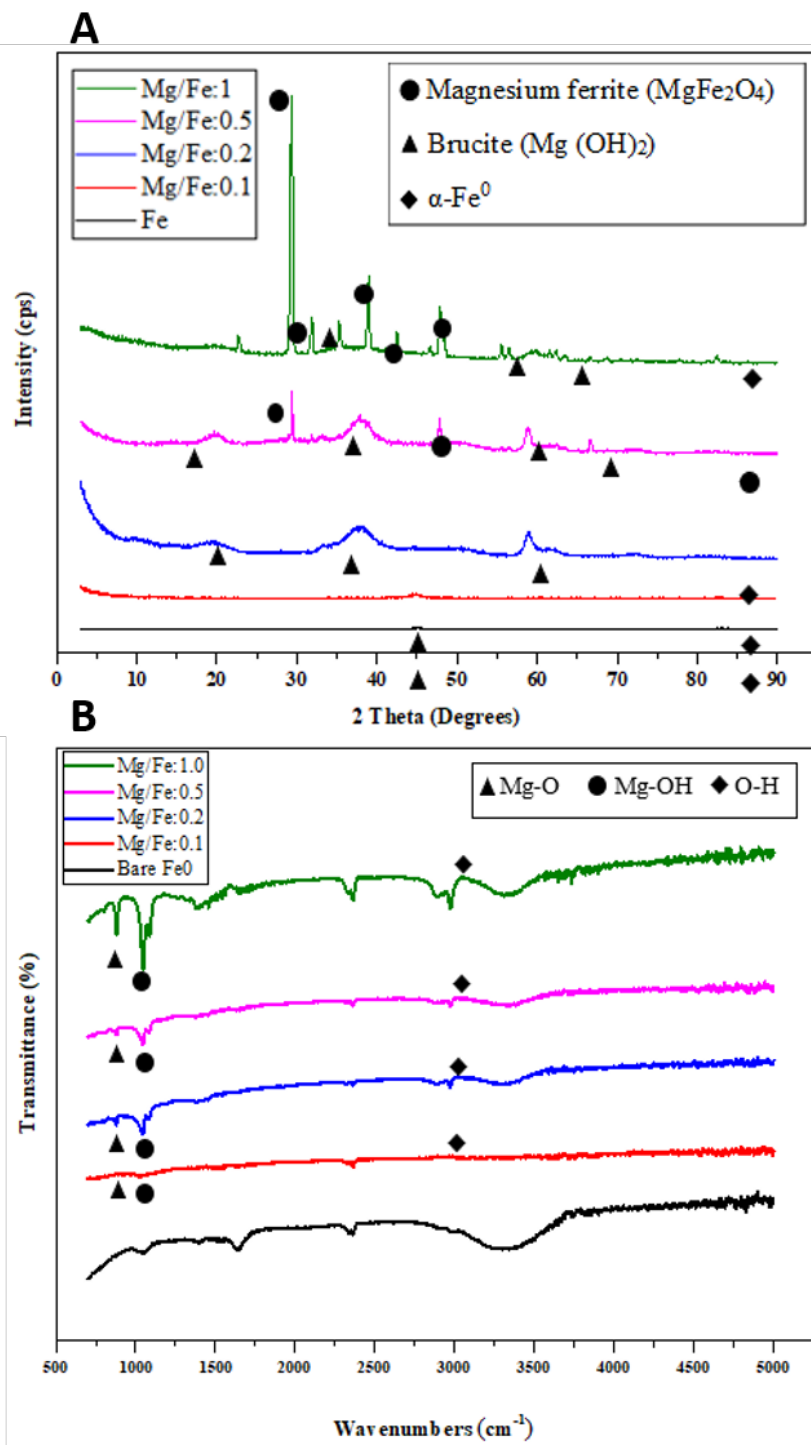


FIGURE 4.23: (A) XRD characterization of the synthesized bare and coated  $\text{Fe}^0$ , (B) FTIR characterization of the synthesized bare and coated  $\text{Fe}^0$

This latter confirms that the coating layer  $\text{Mg}(\text{OH})_2$  has been confirmed. Furthermore, the crystallinity increased with increasing the coating ratio owing to the strong crystalline characteristics of  $\text{MgFe}_2\text{O}_4$  detected in XRD analyses. Figure 4.23 (B) shows the peaks obtained at  $860\text{ cm}^{-1}$ , at  $1176\text{ cm}^{-1}$ , and at  $3378\text{ cm}^{-1}$ , which reflected the presence of Mg-O, Mg-OH, and O-H, respectively. This latter confirms the well coating of  $\text{Mg}(\text{OH})_2$  around the Fe core.

#### 4.5.2 Iron concentration analysis

The coated structure was adopted to protect the  $\text{Fe}^0$  nanoparticles from rapid corrosion. Therefore, it is expected that the slow decomposition of the  $\text{Mg}(\text{OH})_2$  coating layer would monitor the discharge of  $\text{Fe}^{2+}$  into the anode solution.  $\text{Fe}^{2+}$  concentrations are considered an indicator of  $\text{Fe}^0$  dissolution, where the higher  $\text{Fe}^{2+}$ , the more  $\text{Fe}^0$  dissolution (Maamoun et al., 2020). The coating shell performance evaluation was achieved through  $\text{Fe}^0$  measurements, and Figure 4.24 showed the obtained results. On the first day, the  $\text{Fe}^{2+}$  and total dissolved  $\text{Fe}^0$  concentrations were 36.45 and 41.94 mg/L, respectively. After 30 days of operation, the  $\text{Fe}^{2+}$  content decreased to be 27.12, 28.98, 21.80, 27.60, 27.42, and 26.45 mg/L for control, bare  $\text{Fe}^0$ , Mg/Fe:0.1, Mg/Fe:0.2, Mg/Fe:0.5, and Mg/Fe:1.0 MFCs, respectively. For the four coating ratios, the release of  $\text{Fe}^{2+}$  was lower compared to the bare  $\text{Fe}^0$ . These low values were mainly attributed to the  $\text{Mg}(\text{OH})_2$  layer around the  $\text{Fe}^0$  nanoparticles. However, the effect of increasing the coating ratio on the  $\text{Fe}^{2+}$  release was not clear owing to the natural oxidation/reduction reactions. The total dissolved  $\text{Fe}^0$  values were measured at the end of the experiments and values were 40.44, 43.72, 42.51, 26.02, 25.91, 25.71 mg/L for control, bare  $\text{Fe}^0$ , Mg/Fe:0.1, Mg/Fe:0.2, Mg/Fe:0.5, and Mg/Fe:1.0 MFCs, respectively. At the end of the experiments, the  $\text{Fe}^0$  dissolution was followed by a domination of  $\text{Fe}^{3+}$  concentration due to the biological  $\text{Fe}^{2+}$  oxidation rate. The continuous increase of  $\text{Fe}^{3+}$  concentration in the anode solution implied that the  $\text{Fe}^0$  core's continuous dissolution was kept up due to the presence and the extending effect of  $\text{Mg}(\text{OH})_2$  coating layer around the  $\text{Fe}^0$  particle, which was useful for preventing its rapid corrosion and consequently enhancing its reactivity over time. Also, the gradual release of  $\text{Fe}^{2+}$  into the anode solution could be favorable for biofilm formation and current generation. In fact, a high release of  $\text{Fe}^{2+}$  would have an inhibitory effect on bacterial growth (Bensaida et al., 2020). These results demonstrated that the  $\text{Mg}(\text{OH})_2$  shell lowered the corrosion process of  $\text{Fe}^0$  nanoparticles.

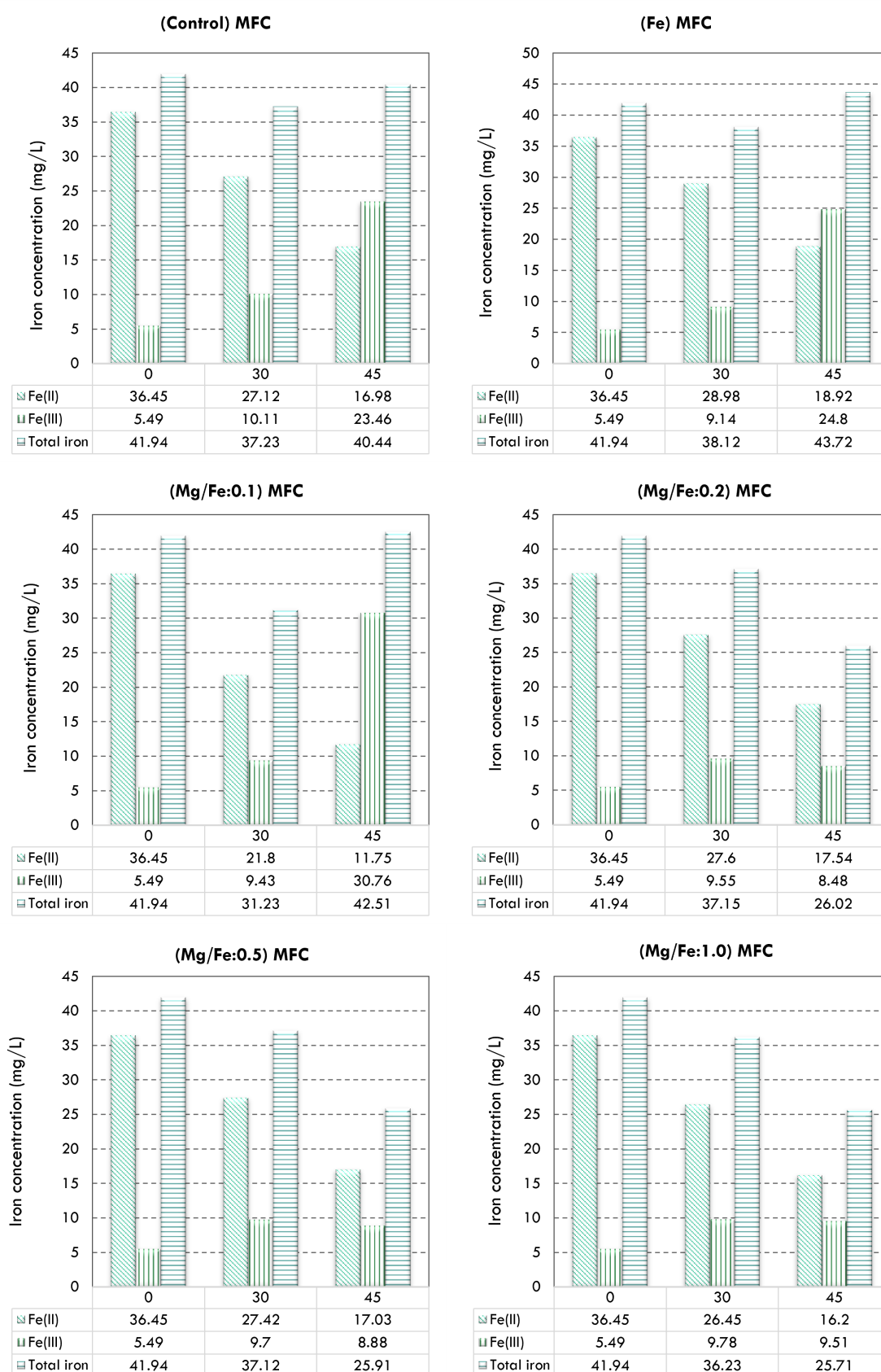


FIGURE 4.24:  $\text{Fe}^0$  analysis in the anolyte of: (a) control, (b) bare  $\text{Fe}^0$ , (c) Mg/Fe:0.1, (d) Mg/Fe:0.2, (e) Mg/Fe:0.5, and (f) Mg/Fe:1.0.

### 4.5.3 MFCs performance in time using bare and coated $\text{Fe}^0$ nanoparticles

The MFCs performances were illustrated through voltage measurements and power density calculations as detailed in Figure 4.25. Although the voltage was not stable all along with the experiments, it continuously increased in time. The accumulative cell voltage for the six studied MFCs is illustrated in Figure 4.25 (a), whereas Figure 4.25 (b) illustrates the corresponding power densities. During the first three days, the voltage recorded was initially negligible ( $< 0.1$  mV). However, a steep increase in electricity production was observed after day 5, which indicated a successful adaptation and colonization of the anode by electrochemically active bacteria. The accumulative voltage increased continuously to reach 118.4 mV (control), 559.90 mV (bare Fe), 286.5 mV (Mg/Fe:0.1), 640.80 mV (Mg/Fe:0.2), 131.7 mV (Mg/Fe:0.5), and 404.10 mV (Mg/Fe:1.0), after 45 days of operation under batch mode conditions. The voltage improvement was recorded to be 180 %, 43 %, 220 %, and 102 % for bare Fe, Mg/Fe:0.1, Mg/Fe:0.2, and Mg/Fe:1, respectively. Moreover, the power density and current values increased with respect to time to reach (135.54 W/g.VS ; 1.002 mA), (1059.08 W/g.VS ; 2.800 mA), (277.30 W/g.VS ; 1.433 mA), (1387.00 W/g.VS ; 3.204 mA), (38.97 W/g.VS ; 0.537 mA), and (551.68 W/g.VS ; 2.021 mA) for control, bare Fe, Mg/Fe:0.1, Mg/Fe:0.2, Mg/Fe:0.5, and Mg/Fe:1, respectively at day 45. Figure 4.27 presents the daily voltage values variations with respect to time. The maximum voltage values were 6.9 mV (control), 20.1 mV (bare Fe), 11.6 mV (Mg/Fe:0.1), 20.1 mV (Mg/Fe:0.2), 7 mV (Mg/Fe:0.5), and 33.8 mV (Mg/Fe:1.0).

The Mg/Fe:0.2 MFC showed the best performance in start-up time (less than five days). This improvement could result from the good bacterial adhesion to the anode surface with the moderate release of  $\text{Fe}^{2+}$  during the  $\text{Mg}(\text{OH})_2$  shell dissolution. However, the other three coating ratio (Mg/Fe:0.1, Mg/Fe:0.5, and Mg/Fe:1.0) showed a lower accumulative voltage than bare  $\text{Fe}^0$ . The coating ratio parameter was one of the factors restricting the MFC performance. The rapid and constant dissolution of the  $\text{Mg}(\text{OH})_2$  coating layer in Mg/Fe:0.1 would increase the concentration of  $\text{Fe}^{2+}$  in the anolyte. Therefore,  $\text{Fe}^{2+}$  will be oxidized and resulting in more available  $\text{Fe}^{3+}$ . These latter will be reduced in the form of  $\text{Fe}^{2+}$  owing to their high biological reduction rate, which could be enough to limit the produced current (Ter Heijne et al., 2011). As shown in Figure 4.27, the voltage generation was not stable, and the high release of  $\text{Fe}^{2+}$  led to a decrease in the voltage output. However, once  $\text{Fe}^{3+}$  had reduced, the voltage output started increasing. These results were in consistence with Ter Heijne et al., 2011's study where they highlighted the importance of the reduction reaction of  $\text{Fe}^{3+}$  to  $\text{Fe}^{2+}$  in electrical current generation using a lab-scale MFC.

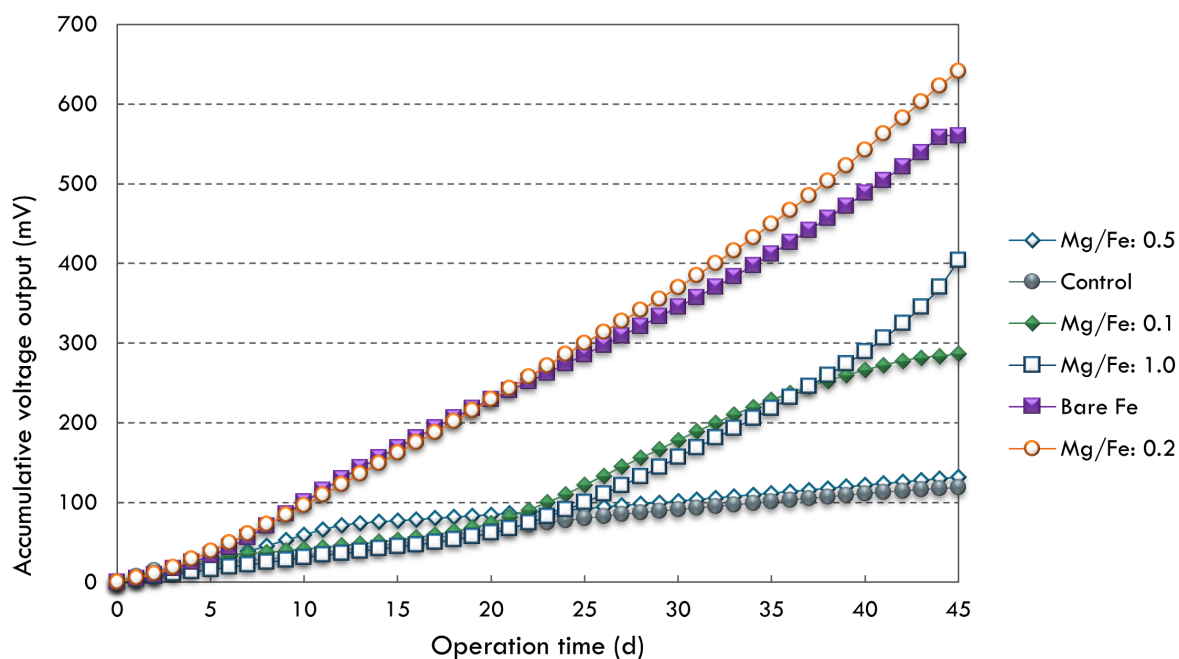


FIGURE 4.25: The representative accumulative cell voltage-time of MFCs equipped with bare and coated Fe nanoparticles.

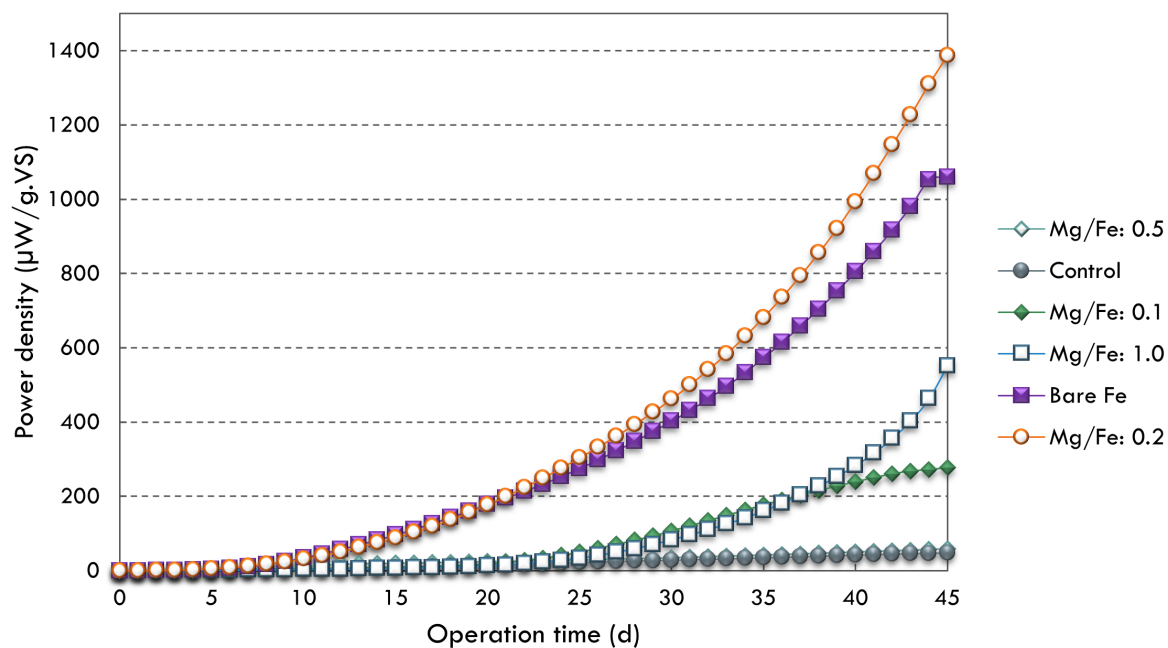


FIGURE 4.26: Power density-time curves plotted in Log scale of MFCs equipped with bare and coated Fe nanoparticles.

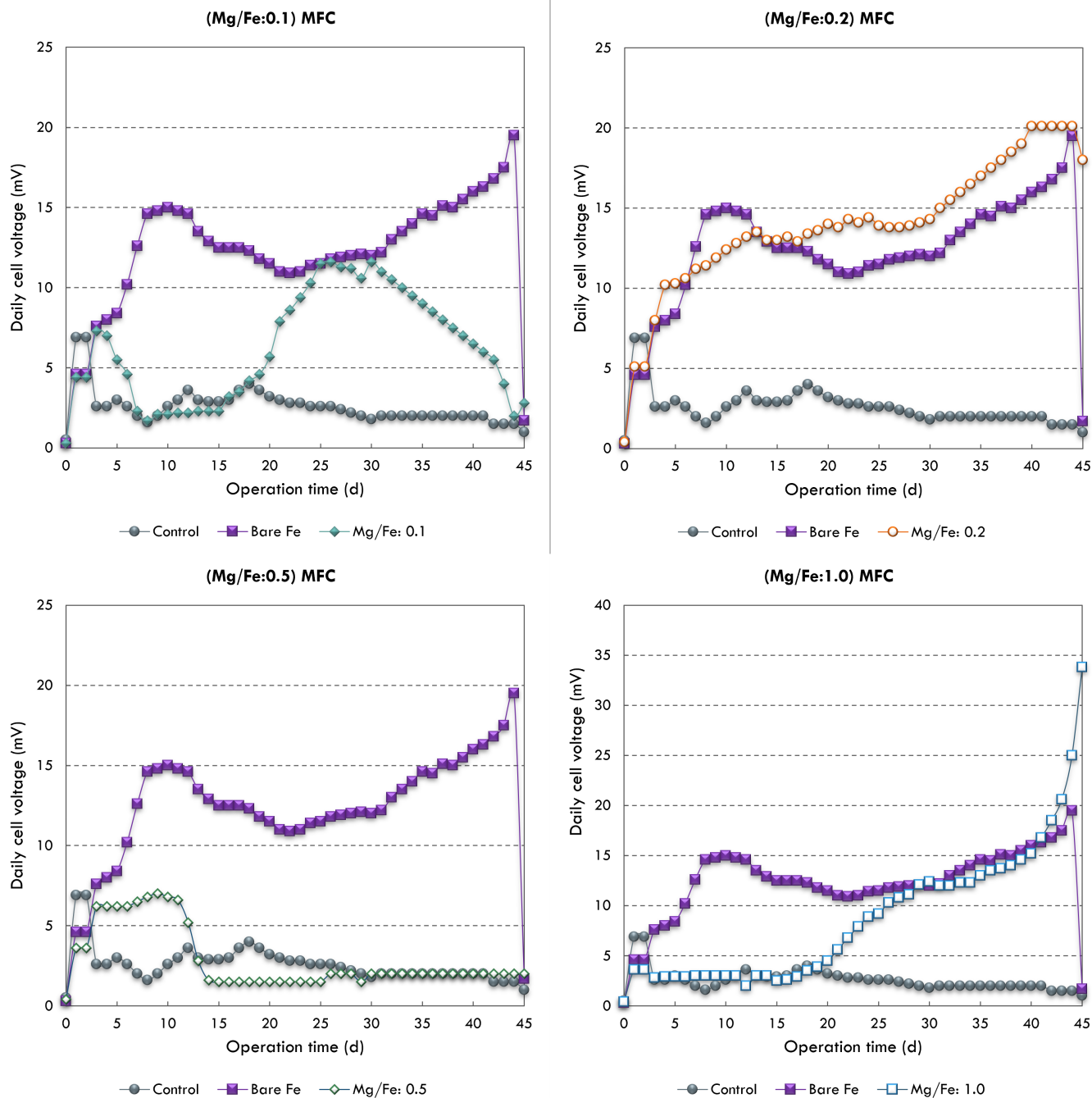
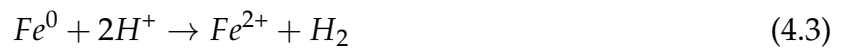
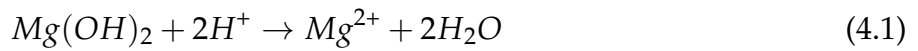


FIGURE 4.27: The daily cell voltage-time plots for MFCs equipped with bare  $\text{Fe}^0$  and coated  $\text{Fe}$  nanoparticles.

An increase in iron concentration resulted in higher power production. Moreover, Mg/Fe nanoparticles with a coating ratio of Mg/Fe:1.0 would possess a thick coating layer surrounding the iron nanoparticles, which would slow the electron transfer rate and reduce the Fe reactivity. The output voltage of Mg/Fe:1.0-supplemented MFC had a increasing trend, and the start-up time was more than 15 days of operation. These results correlate with TEM results, where the Mg(OH)<sub>2</sub> clouds varied to the coating ratio factor.

The internal resistance had a great significance in power output production by MFCs (Mathuriya and Yakhmi, 2016). Besides, the Mg(OH)<sub>2</sub> coating layer led to an increase in the anode solution conductivity. The mainly chemical reaction process in the anode chambers of supplemented MFCs was shown in the following equations (Li, Zhou, and Xu, 2017):



These chemical reactions would accelerate protons' transport to the cathode chamber, which could consequently enhance the current generation (Li, Zhou, and Xu, 2017). To further explore the performance of supplemented MFCs, the organic matter removal was carried out by total volatile solids (TVS) measurements. An MFC with a high TVS removal would consume more waste sludge substrate, promoting the exoelectrogens to produce more electrons and protons. As shown in Table 4.5, bare Fe MFC showed the highest TVS removal followed by Mg/Fe:0.2. Thus, finding an optimal coating layer would protect the Fe<sup>0</sup> nanoparticles from rapid corrosion and ensure a moderate release of Fe<sup>2+</sup>, which will be favorable for electron transfer and bacterial growth.

TABLE 4.5: Maximum power density, maximum current, TVS removal, conductivity, and coulombic efficiency (CE) from different MFCs using (S1) after 45 days. P<sub>max</sub>: maximal power. I at P<sub>max</sub>: current value obtained at P<sub>max</sub>. N: negative due to the increase of TVS.

MFC type	P <sub>max</sub> (μW/g.VS)	I at P <sub>max</sub> (mA)	TVS removal (%)	Conductivity (μS/cm)	CE (E-3 %)
Control	47.36	0.592	22.30	1245	0.0043
Fe <sup>0</sup>	1059.08	2.800	30.74	1157	0.0107
Mg/Fe:0.1	277.30	1.433	N	542	N
Mg/Fe:0.2	1387.25	3.204	25.00	1061	0.0140
Mg/Fe:0.5	58.60	0.659	N	1356	N
Mg/Fe:1.0	551.68	2.021	20.44	1396	0.0076

It is worth to note that the performance of MFCs is directly associated to the enrichment of exoelectrogens and electron transfer. Figure 4.28 illustrates the bacterial growth during the experiments period. At the beginning of experiments, the number of colonies was deficient due to bacterial cells' slow activity and biofilm slow formation, which generally depends on the adjustment and adaptation phase of exoelectrogens to the new system conditions. From day five on, the increase of bacterial cells started, and the maximum number of colonies was reached at day 14 for control MFC, at day 21 for Fe, Mg/Fe:0.1, Mg/Fe:0.2, and Mg/Fe:0.5 MFCs, whereas the number of bacterial cells in the Mg/Fe:1.0 MFC was the highest at day 35. The maximal number of colonies increased by 78 %, 122 %, 144 %, 156 %, and 44 % for Fe, Mg/Fe:0.1, Mg/Fe:0.2, Mg/Fe:0.5, and Mg/Fe:1.0, respectively, which will favor organic matter degradation and electron production and transport. Although the maximal number of colonies was improved by 156 %, Mg/Fe:0.5 did not improve the voltage output, and power generation was reduced by 71 % compared to control MFC. These findings suggest that bacterial growth is not the only factor deciding the MFC general output, and further investigations should be elaborated to understand the reasons behind the limited system output, such as waste sludge characteristics and operating system conditions.

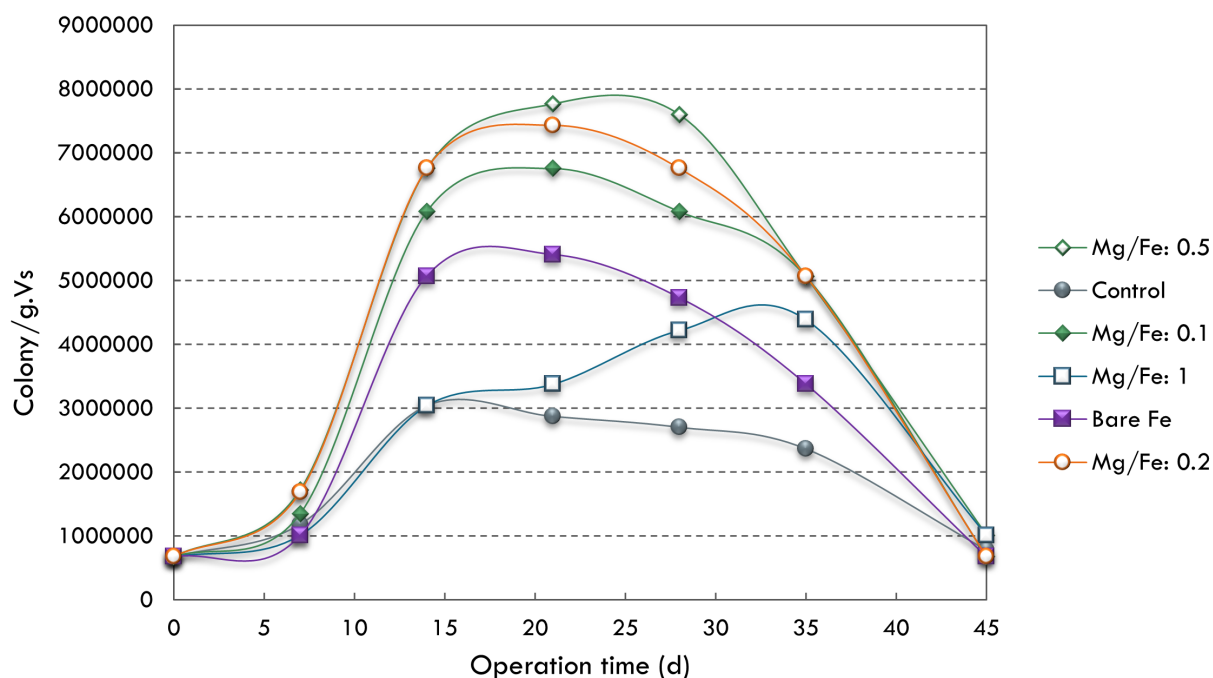


FIGURE 4.28: Bacterial growth response in the anode chamber of MFCs supplemented with bare and coated  $\text{Fe}^0$  nanoparticles (Mg/Fe:0.1, Mg/Fe:0.2, Mg/Fe:0.5, and Mg/Fe:1.0).

#### 4.5.4 Effect of system conditions variation on MFCs performance

In this section, we conducted a series of experiments to evaluate the response of MFCs to different biodegradable waste sludges. Four sludges (S1, S2, S3, and S4) were characterized in chapter 2, Table 2.1 and used as the primary fuel for MFCs operation. Figure 4.29 shows a considerable variation in the current generation. The lowest current output was obtained for the waste sludge S2 (conductivity= 499  $\mu\text{S}/\text{cm}$ ) having the lowest COD value as compared to S1 (conductivity= 497  $\mu\text{S}/\text{cm}$ ) and S3 (conductivity= 795  $\mu\text{S}/\text{cm}$ ). This result suggests that MFC output can be attributed to the COD level in the waste sludge. Nimje et al., 2012 mentioned that the used sludge characteristics are significant for the current generation; the organic matter content and wastewater components are prerequisites for microbial metabolic growth and reactions. However, the lowest current output was obtained for S4 (conductivity= 352.8  $\mu\text{S}/\text{cm}$ ), having the highest COD among the four waste sludges. This exciting result indicates that the tested waste sample's COD value is not the only crucial factor in the response of MFCs. Therefore, it becomes crucial to define the MFC's performance based on the organic matter content, the bacterial multiplication, and the waste sludge characteristics. For further investigation, S2 was used for the next experiments as the primary sludge.

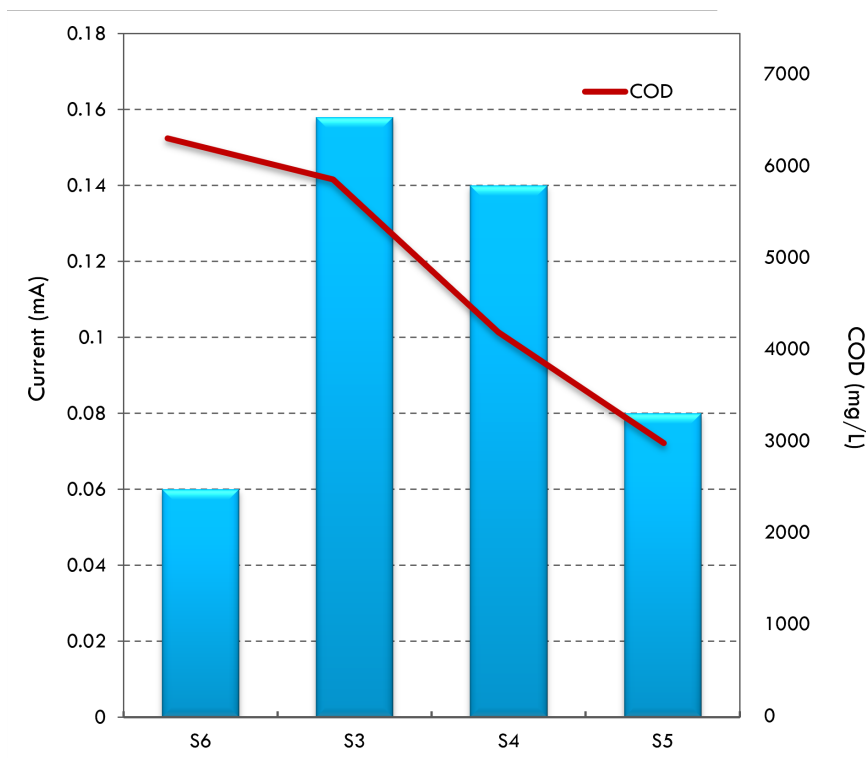


FIGURE 4.29: Current generated (red) by the MFCs when fed with different waste sludges whose COD is shown in red.

### MFC's response to pH variations

Mg/Fe:0.5 nanoparticles were added to the anode chamber of three operating MFCs under alkaline, neutral, and acidic conditions (pH= 12, 7, and 3) to study how pH variation affects the electron transfer and power output. pH values were adjusted only at the beginning of the experiments. We measured the open-circuit voltage (OCV). Recorded values were 0.576, 0.150, and 0.666 V for MFCs operated under pH 7, pH 3, and pH 12, respectively. The maximal daily voltage values were 15.2 mV (pH 7), 3.3 mV (pH 3), and 11.4 mV (pH 12). Figure 4.30 illustrates the accumulative cell voltage. Values were 186.30, 84.30, and 107.00 mV for MFCs operated under pH 7, pH 3, and pH 12, respectively. The accumulative voltage dropped by 54.75 % and 42.56 % under acidic and alkaline conditions. Figure 4.31 presents the power density output. The power density output decreased by 79.52 % and 67.01 % under acidic and alkaline conditions. The MFC response showed more stable output under neutral conditions.

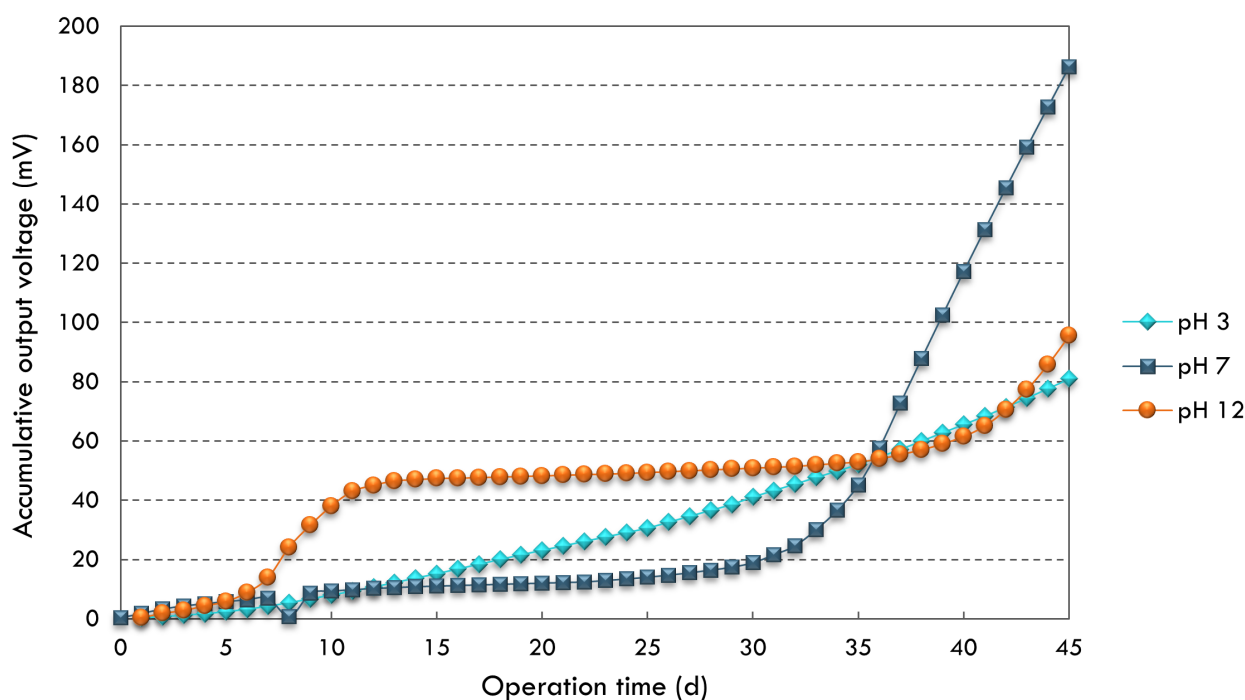


FIGURE 4.30: Variations of the cell voltage of MFCs when treated under acidic, neutral, and alkaline conditions. Curves are plotted in Log scale. MFCs were supplemented with Mg/Fe:0.5 for 45 days of operation.

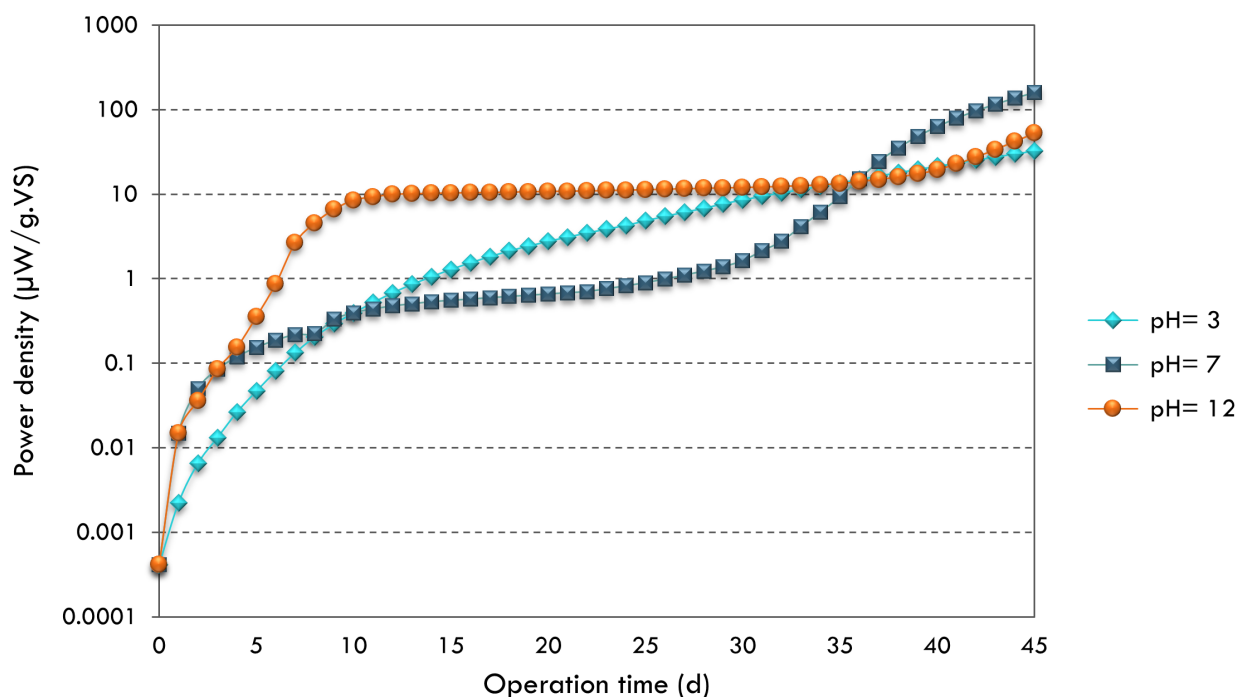


FIGURE 4.31: Power density of MFCs when treated under acidic, neutral, and alkaline conditions. Curves are plotted in Log scale. MFCs were supplemented with Mg/Fe:0.5 for 45 days of operation.

pH variation was recorded during the operation period and presented in Figure 4.32. For the MFC operating at neutral conditions, pH values were maintained between 6.95 and 7.68. The anolyte could sustain its neutral conditions, which was favorable for the anaerobic digestion and power generation. In contrast, pH values dropped from 12 to 7.91 during the first 7 days, and pH values remained between 7.83 and 8.03. The same behavior was observed for acidic conditions, where pH increased from 3.00 to 6.16. Table 4.7 illustrates the anolyte characteristics for the 3 studied MFCs. Although the resistivity was high under neutral conditions, the voltage output was the highest among the other MFCs. The iron ions concentration can justify these results.  $\text{Fe}^{2+}$  ions were comparatively high under acidic conditions (19.79 mg/L in pH 3 compared to 10.84 mg/L in pH 7), highlighting the opposite effect of high released ions on bacterial growth and organic matter degradation. Besides, most of the iron ions were in the form of  $\text{Fe}^{3+}$ . These latter have been proved to be essential for organic matter degradation in the presence of electroactive bacteria.

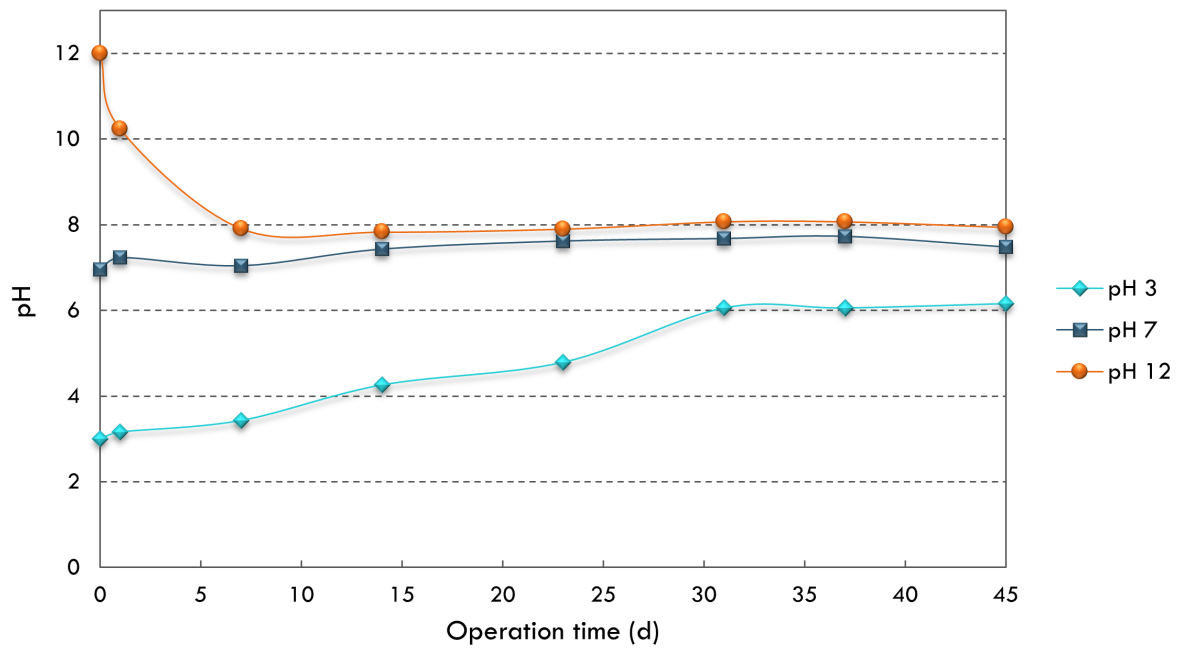


FIGURE 4.32: pH variations during the 45 days of operation. Curves are plotted in Log scale. MFCs were supplemented with Mg/Fe:0.5 for 45 days of operation.

TABLE 4.6: Waste sludge characteristics in the anode chambers fed with (S2) after 45 days. Initial waste sludge characteristics (S2) are described in chapter 2, Table 2.1.

Parameters	Units	MFC (pH 3)	MFC (pH 7)	MFC (pH 12)
Conductivity	$\mu\text{S}/\text{cm}$	1516	908	1389
Resistivity	$\Omega.\text{cm}$	656	1000	722
TDS	$\text{mg}/\text{L}$	757	448	699
Salinity	ppt	1.0	0.6	1.0
pH	-	6.16	7.48	7.94
ORP	mV	25	-53	-85
$\text{Fe}^{2+}$	$\text{mg}/\text{L}$	19.79	10.84	5.72
$\text{Fe}^{3+}$	$\text{mg}/\text{L}$	2.54	8.67	5.81
Total Fe	$\text{mg}/\text{L}$	22.33	19.51	11.53
TVS removal	%	N	48.40	64.84

### MFC's response to anoxic/aerobic conditions

This work explores the performance of MFCs regarding oxygen concentrations in cathodic chambers. Two MFCs were operated under anoxic conditions, whereas two pumps were used to inject air inside the cathode chambers and the experiments (aerobic). Figure 4.33 illustrates the impact of oxygen existence in the cathode chamber on the MFCs performance. The power density values were 45.75 and 24.80  $\mu\text{W/g.VS}$  controls MFCs under anoxic and aerobic conditions, whereas Mg/Fe-supplemented MFCs presented 767.21 and 131.96  $\mu\text{W/g.VS}$  under anoxic and aerobic conditions. It was clear that the oxygen injection in the anode chamber affected the overall MFC output. Mg/Fe improved the power density by 1577 % when operating under anoxic conditions. However, the improvement rate decreased under anoxic conditions, and MFC output was enhanced by 432.06 %.

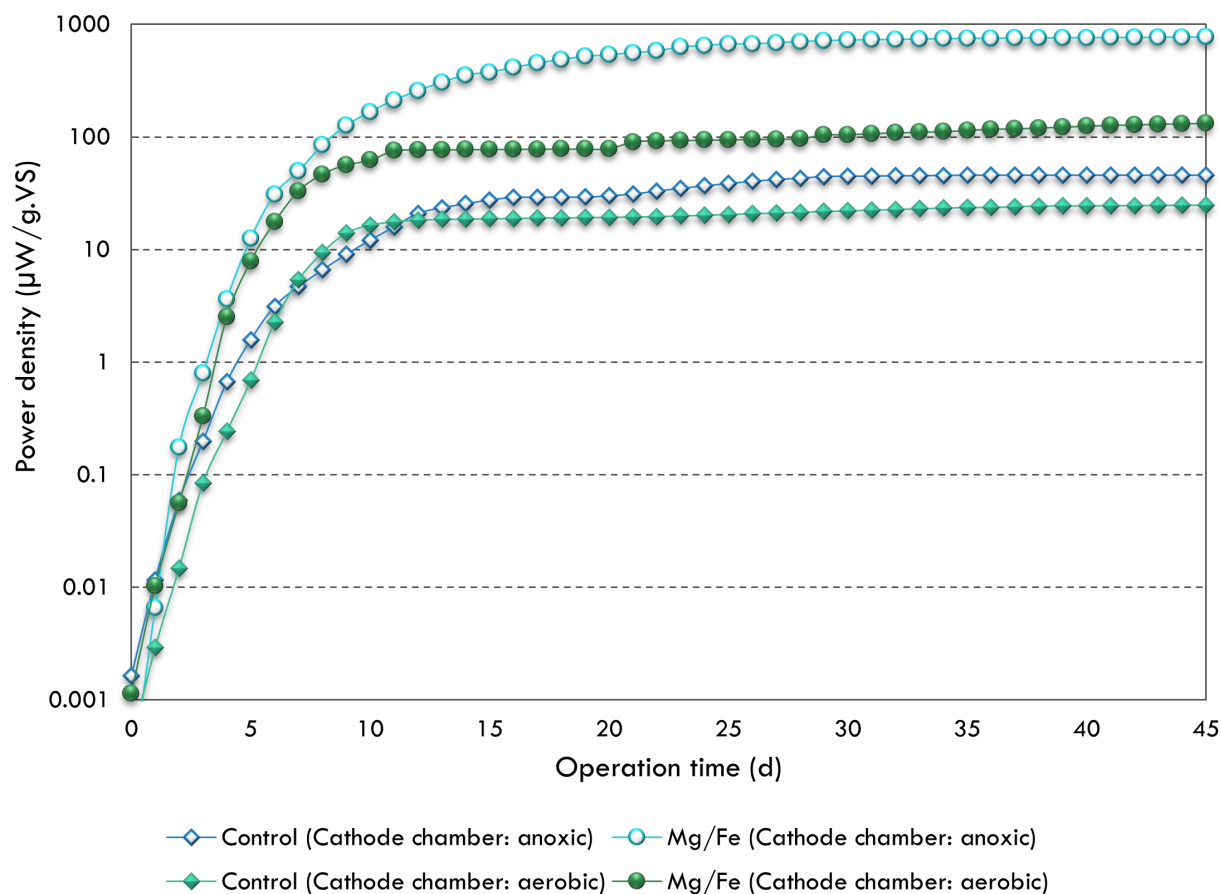


FIGURE 4.33: MFCs response to aerobic/anoxic conditions plotted in Log scale.

It was clear that pumping air inside the cathode chamber influenced the MFC response, mainly due to the oxygen transfer from the cathode to the anode side, which affected the anaerobic condition's performance. Moreover, oxygen affected the particle's performance and consequently decreased their efficiencies. Table 4.7 illustrates the anolyte characteristics in control and Mg/Fe-supplemented MFCs, after 45 days of operation. The oxygen diffusion from the cathode chamber to the anode chamber was apparent by increasing total iron concentrations in the examined MFCs. Iron concentrations values increased from 42.51 to 43.13 in control MFCs, and from 21.48 to 33.05 in Mg/Fe-supplemented MFCs. The inhibiting effect of oxygen diffusion can affect the activity of electroactive bacteria, and in contrast, activate non-exoelectrogenic bacteria, which are electrons acceptors. What is said can be proved by the TVS removal decrease by 10.23 % as detailed in Table 4.7. Moreover, the limited current output could be explained by the ORP values decrease under aerobic conditions due to the reduced reaction of the oxygen and electrons in the anode chamber.

TABLE 4.7: Waste sludge characteristics in the anode chambers fed with (S2) after 45 days. Initial waste sludge characteristics (S2) are described in chapter 2, Table 2.1.

Parameters	Units	Control (anoxic)	Control (aerobic)	Mg/Fe (anoxic)	Mg/Fe(aerobic)
Conductivity	$\mu S/cm$	238.1	210.4	202.4	239.4
Resistivity	$\Omega.cm$	4000	5000	5000	4000
TDS	mg/L	119	105	101	120
Salinity	ppt	0.1	0.1	0.1	0.1
pH	-	7.47	7.73	6.94	7.65
ORP	mV	-56	-69	-26	-64
$Fe^{2+}$	mg/L	36.63	30.62	14.08	22.91
$Fe^{3+}$	mg/L	5.88	12.51	7.40	10.14
Total Fe	mg/L	42.51	43.13	21.48	33.05
TVS removal	%	60.96	64.84	78.08	70.09

## 4.6 Conclusion

MFCs are a promising technology for power generation and wastewater treatment. However, many challenges are still limiting the technology to be applied in real scale applications. The high internal resistivity and low power generation are yet the main concerns of all researchers. This study came to evaluate the impact of  $\text{Fe}^0$  nanoparticles on MFC performance in terms of power generation and organic matter degradation. Two different samples of sludge were used and the maximum daily voltage obtained in the control MFC filled with S2 (COD= 37802 mg/L) increased by 182 % compared to the MFC filled with S1 (COD= 5561 mg/L). The addition of Fe nanoparticles reduced the daily voltage by 31 % and 9 % for the MFCs filled with S1 and S2, respectively. These results highlight the effect of organic matter content on the MFC response. In addition, the use of copper / $\text{Fe}^0$  bimetallic nanoparticles enhanced the maximum voltage value by 43.33 % and the power density by 65.57 %. However, the overall performance was not high as was expected. The ferric iron's reduction and the biomass growth can justify the increase of the anode chamber's internal resistivity. Moreover,  $\text{Fe}^0$  salts' addition exhibited a higher power output and a shorter start-up time.  $\text{Fe}^{3+}$  addition exhibited a higher power output by 295 % and a shorter start-up time. The microbial growth increased by 92.18 % and the anolyte's resistivity decreased with an increase in the organic matter digestion by 52.78 %. However, the amount of power generated in these MFCs was limited by the biological ferric iron reduction rate that was high enough to restrict the produced current.  $\text{Fe}^0$  coated nanoparticles with  $\text{Mg}(\text{OH})_2$  coating shell were introduced to the anode chamber of lab-scale microbial fuel cells (MFCs). Results proved that the iron-based nanoparticles effectively enhanced the MFCs voltage by more than 4 times and controlled the  $\text{Mg}(\text{OH})_2$  coating shell's dissolution and, therefore, the release of  $\text{Fe}^{2+}$ . This latter consequently increased the anolyte conductivity, enhanced the bacterial growth, and improved the organic matter degradation. However, the MFC response still low, and the use of real waste sludge is challenging.

## Chapter 5

# Conclusions and Future work

### 5.1 Conclusions

The energy demand is increasing, and waste management is considered the most critical research field in environmental biotechnology. MFCs create a genuinely sustainable way to produce energy and power or water infrastructure. In other words, if MFC delivers on its promise, wastewater would be waste no longer. To date, tremendous advances have been made, and further improvements are needed for MFCs to be economically practical.

In our study, MFC systems showed a potential for sustainable wastewater treatment and simultaneous power harvesting from domestic waste sludge. This study has focused on nanoparticle technology's effect on power generation. We developed a set of experimental studies to improve a lab-scale MFC performance. We started our research by collecting domestic waste sludge taken from the Mikasagawa wastewater treatment plant as a source to have a wide variety of the exoelectrogens bacteria needed for the MFC operation. The waste sludge analysis was a crucial step to identify the available nutrients and organic matter. The MFC performance investigation went through design and construction, voltage control, power density calculations, and organic matter degradation analysis. Besides, iron-based nanoparticle synthesis and preparation were an essential and delicate process, where any leakage of oxygen can affect the nanoparticles' reactivity and thus, affect the overall system performance. TEM characterizations showed that  $\text{Fe}^0$  morphology had crystalline and pure structure. The introduction of Cu particles led to a larger surface area and more ductile chain. Examining the consequences of adding  $\text{Fe}^0$  particles on bacterial communities was reflected through bacterial growth and biological wastewater treatment. Afterward, we discussed how bacteria use the anode as an electron acceptor and to what extent they generate electrical output. We evaluated the MFC technology relative to organic matter content.

This study demonstrated that it is possible to enhance bacterial growth and accomplish biological wastewater treatment using  $\text{Fe}^0$ -based nanoparticles.

- Bacterial growth increased to 84.61 % under  $\text{Cu}/\text{Fe}^0$  treatment added with an optimum concentration.
- The improvement was also reflected through chemical oxygen demand (COD) removal efficiency, which reached 33.21 %, 55.30 %, and 61.24 % for control,  $\text{Fe}^0$ , and  $\text{Cu}/\text{Fe}^0$  reactors, respectively.

We investigated the medium change effect on bacterial cell growth, and results showed that microbial colonies exhibited higher sensitivity to  $\text{Fe}^0$  treatment in a different studied medium. System conditions were varied, and the variation of oxygen concentration could alleviate the negative effect. The study proved that  $\text{Fe}^0$  and copper/ $\text{Fe}^0$  nanoparticles exhibited a positive effect on bacterial growth originated from a mixed culture inoculum as well as on the biological wastewater treatment. However, the medium showed high sensitivity with different wastewater. The effectiveness of the obtained results was examined for bioelectricity generation in the MFCs system. The use of bimetallic  $\text{Cu}/\text{Fe}^0$  nanoparticles enhanced the maximum voltage value by 43.33 % and the power density by 65.57 %. However, the overall performance was not high as was expected. The  $\text{Fe}^{3+}$  iron's reduction and the biomass growth could justify the increase of the anode chamber's internal resistivity.

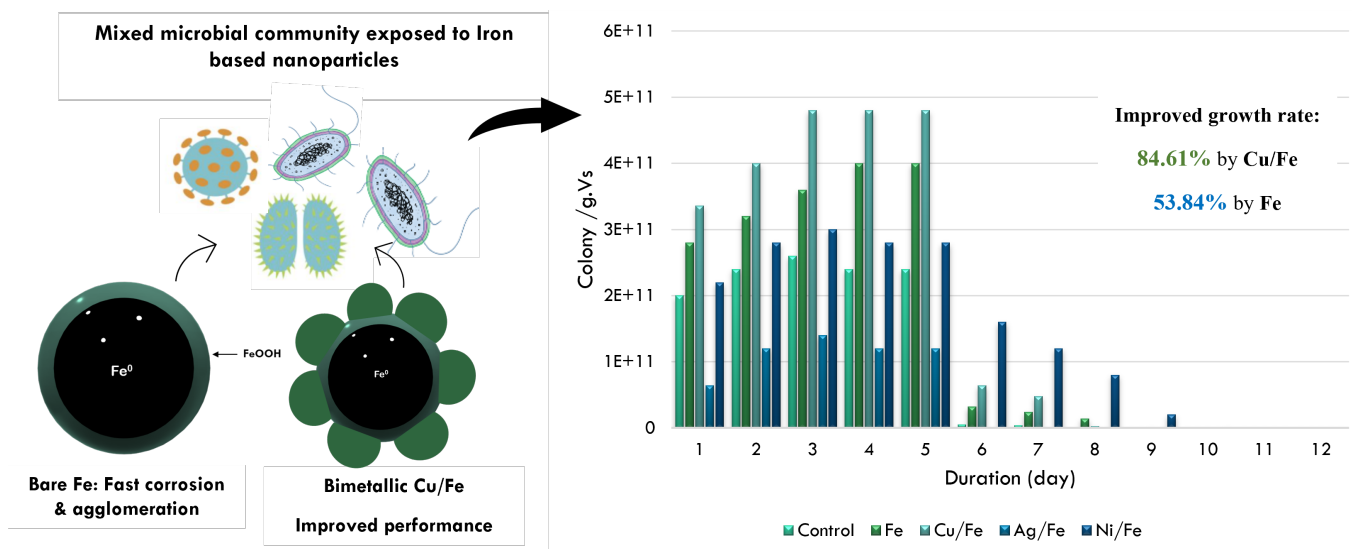


FIGURE 5.1: The response of mixed culture bacteria to  $\text{Fe}^0$ -based nanoparticles treatment.

Moreover,  $\text{Fe}^0$  salts' addition exhibited a higher power output and a shorter start-up time. The addition of  $\text{Fe}^0$  ions was favorable for microbial growth. The anolyte's resistivity decreased, and the organic matter digestion improved. However, the amount of power generated in these MFCs was limited by the biological  $\text{Fe}^{3+}$  iron reduction rate that was high enough to restrict the produced current. In a further step,  $\text{Fe}^0$  coated nanoparticles with  $\text{Mg}(\text{OH})_2$  coating shell come first to evaluate the response of a lab-scale MFCs to Mg/Fe nanoparticles treatment using real waste sludges.

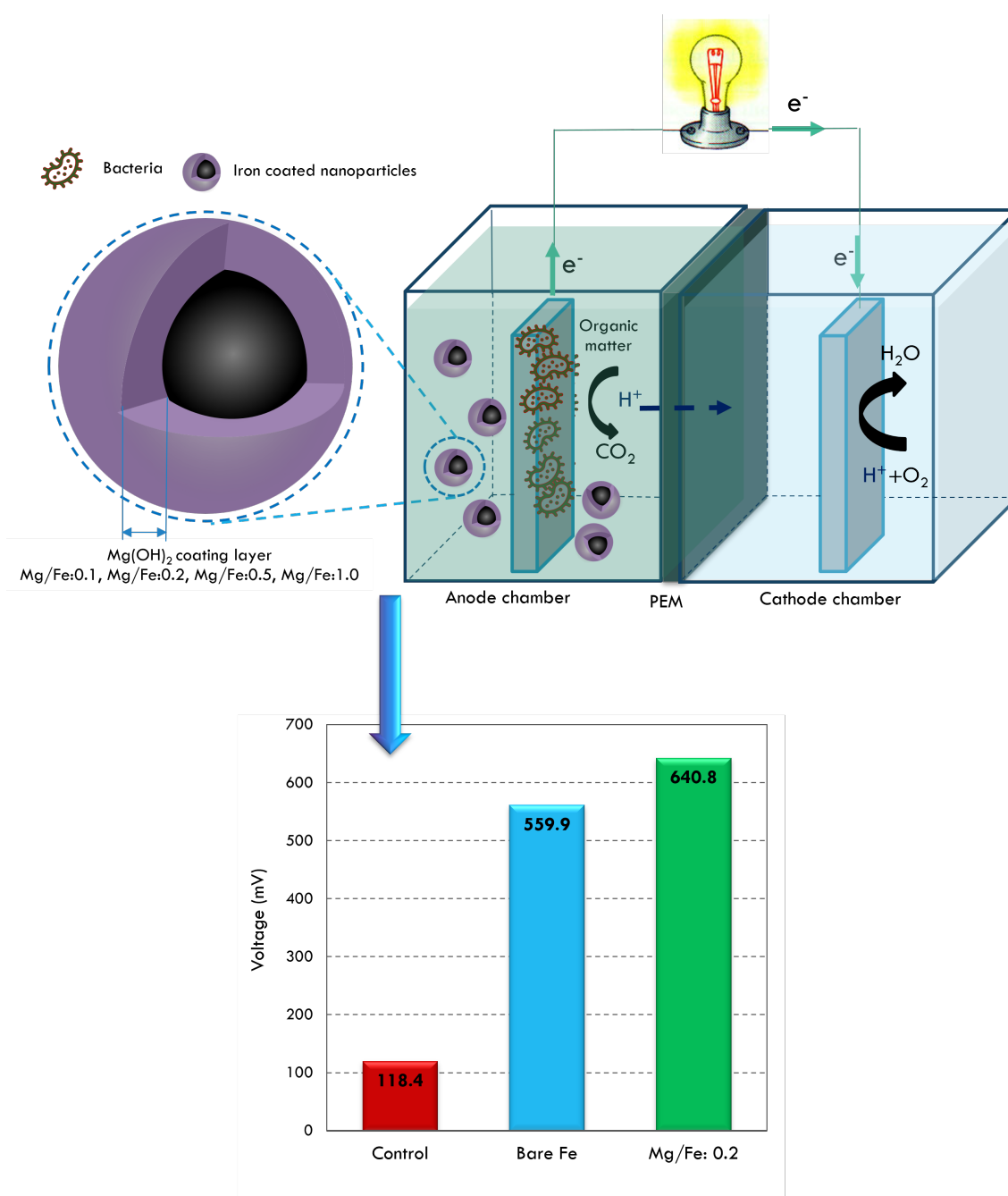


FIGURE 5.2: The response of microbial fuel cells to  $\text{Fe}^0$ -coated nanoparticles treatment.

To the best of our knowledge, only a few studies have focused on using  $\text{Mg}(\text{OH})_2$  for MFC technology, and none of them have investigated the effect of  $\text{Fe}^0$  nanoparticles coated with  $\text{Mg}(\text{OH})_2$  shell for bioelectricity generation. Results showed that:

- The voltage output increased by 441 % compared to the control and provide the maximal power density ( $1387.25 \mu\text{W/g.VS}$ ;  $3.204 \text{ mA}$ ).
- The current generation's stability was achieved under neutral pH and the power density output decreased by 82.80 % under aerobic conditions.

Results proved that the iron-based nanoparticles effectively enhanced the MFCs performance by controlling the  $\text{Mg}(\text{OH})_2$  coating shell's dissolution and, therefore, the release of  $\text{Fe}^{2+}$ . This latter consequently increased the anolyte conductivity, enhanced bacterial growth, and improved the organic matter degradation. However, the MFC response still low, and the use of real waste sludge is challenging. Results suggested that bacterial multiplication is not the only decisive parameter in MFC's output, and additional parameters should be considered.

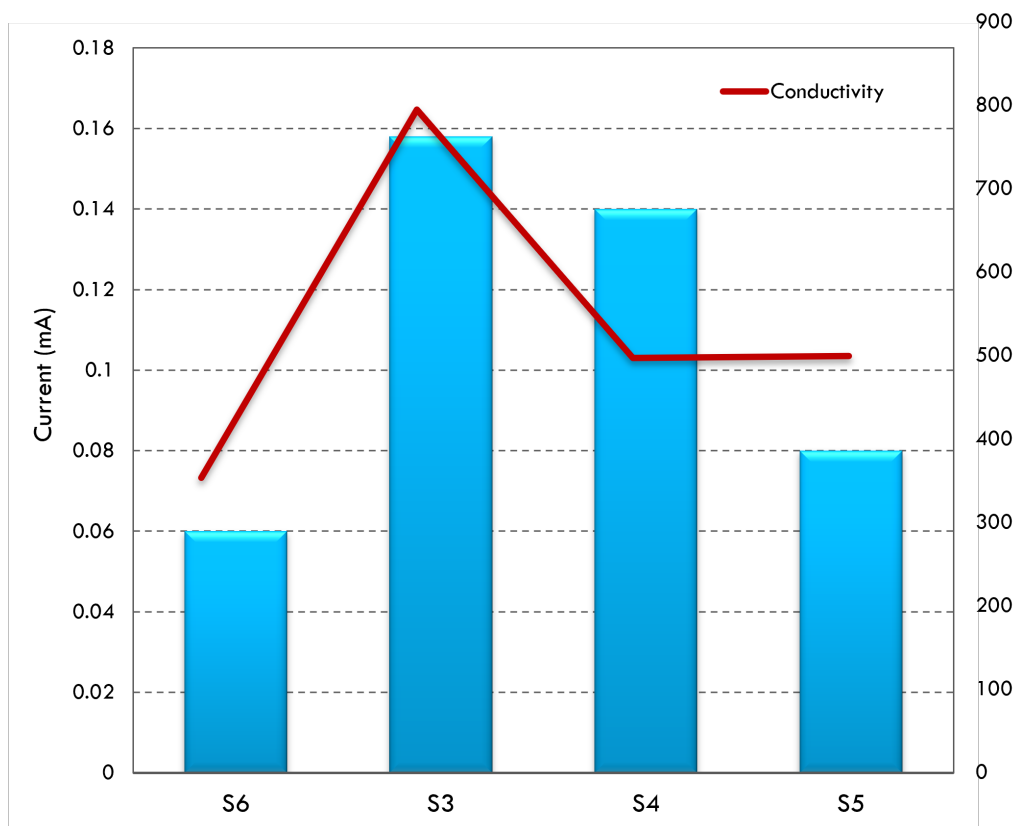


FIGURE 5.3: Current generated (red) by the MFCs when fed with different waste sludges whose conductivity is shown in red.

## 5.2 Future work

MFCs are a promising technology for power generation and wastewater treatment. However, many challenges are still limiting the technology to be applied in real-scale applications. The high internal resistivity and low power generation are yet the main concerns of all researchers. Besides, many challenges arise when using real wastewater as the substrate. Inoculum culture sources and substrate types, the MFC reactor configuration, operation conditions, electrode materials, external and internal resistances, and substrate types are essential parameters that affect microbial communities in MFCs. MFCs are a potential source of electrical energy from waste that is rich in organic matter. Many challenges have been facing the MFC technology:

- The electron transfer mechanisms,
- The low system performance,
- High resistivity, and
- Low Coulombic efficiency.

One primary reason behind the challenges mentioned above is that electrons given off during the organic matter digestion do not transfer well from the bacteria to the anode (the negative electrode). Laboratory investigation will be developed for wastewater treatment and bioelectricity generation using MFCs. The purpose of the future research is to improve the power performance of the MFC and the mechanisms by which microorganisms transfer electrons to electrodes.

MFCs in areas of energy conversion, production, and wastewater treatment have made the technology extremely attractive. In future studies, and to produce fuels and eventually eliminate our dependence on fossil fuels, the candidate will seek to:

- ★ Understand the mechanisms controlling the electron transfer rate,
- ★ Increase the efficiency of the organic matter degradation process, and
- ★ Enhance the electron transfer mechanisms.

Biofilm formation is a continuous and sequential process including transport, attachment, the formation of micro-colonies, and biofilm maturation in MFCs on the electrode surface. However, it is a very complex process and which is directly affected by:

- The type of substrate and their concentration,
- Operating conditions,
- Electrode materials,
- The type of bacterial strain (pure or mixed culture) and their metabolic pathways.

Fabricating artificial biofilms made of conducting polymers” would increase the anode performance and lead to high MFC performance. These synthesized biofilms could be supported with nanoparticles to improve their reactivity in a further step. Microbial fuel cell technology requires knowledge of different scientific and engineering fields, ranging from microbiology and electrochemistry to mechanical and environmental engineering. Many challenges will be addressed, including a more detailed analysis of energy production, consumption, and application. It is expected that fabricating artificial biofilms made of conducting polymers will improve the MFC performance mainly by:

- Increasing the rate of energy storage and conversion,
- Being a newly developed material for improving the energy conversion,
- Improve the electron transfer rate and the performance of the MFC system.

To sum up, the electricity production process in MFCs will help deal with waste. It may even help clean up contaminated soil and water. MFC technology could be used to generate power with biodegradable waste and sewage. At the same time, it could provide help with wastewater treatment and bioremediation. MFCs could also help monitor the amount of biodegradable material left in wastewater streams. They could also help with remote sensing, which is just one among several new alternative energy sources. Energy production in the future might be much cleaner and more sustainable than today.

# Bibliography

- Ahmad, Ayyaz et al. (2016). "Antibacterial activity of graphene supported FeAg bimetallic nanocomposites". In: *Colloids and Surfaces B: Biointerfaces* 143, pp. 490–498. ISSN: 18734367. DOI: [10.1016/j.colsurfb.2016.03.065](https://doi.org/10.1016/j.colsurfb.2016.03.065).
- Alan, Newman (1992). "Fuel Cells Come of Age". In: *Environmental Science and Technology* 26.11, pp. 2085–2086. ISSN: 15205851. DOI: [10.1021/es00035a602](https://doi.org/10.1021/es00035a602).
- Alatraktchi, Fatima Al Zahra a., Yifeng Zhang, and Irini Angelidaki (2014). "Nanomodification of the electrodes in microbial fuel cell: Impact of nanoparticle density on electricity production and microbial community". In: *Applied Energy* 116, pp. 216–222. ISSN: 03062619. DOI: [10.1016/j.apenergy.2013.11.058](https://doi.org/10.1016/j.apenergy.2013.11.058).
- Amen, Tareq W.M. et al. (2018). "Wastewater degradation by iron/copper nanoparticles and the microorganism growth rate". In: *Journal of Environmental Sciences (China)* 74, pp. 19–31. ISSN: 18787320. DOI: [10.1016/j.jes.2018.01.028](https://doi.org/10.1016/j.jes.2018.01.028). URL: <https://doi.org/10.1016/j.jes.2018.01.028>.
- Argueta-Figueroa, Liliana et al. (2014). "Synthesis, characterization and antibacterial activity of copper, nickel and bimetallic Cu-Ni nanoparticles for potential use in dental materials". In: *Progress in Natural Science: Materials International* 24.4, pp. 321–328. ISSN: 10020071. DOI: [10.1016/j.pnsc.2014.07.002](https://doi.org/10.1016/j.pnsc.2014.07.002). URL: <http://dx.doi.org/10.1016/j.pnsc.2014.07.002>.
- Bensaida, Khaoula et al. (2020). "Journal of Water Process Engineering The impact of iron bimetallic nanoparticles on bulk microbial growth in wastewater". In: *Journal of Water Process Engineering* August, p. 101825. ISSN: 2214-7144. DOI: [10.1016/j.jwpe.2020.101825](https://doi.org/10.1016/j.jwpe.2020.101825). URL: <https://doi.org/10.1016/j.jwpe.2020.101825>.
- Cai, Lu et al. (2018). "Sludge decrement and electricity generation of sludge microbial fuel cell enhanced by zero valent iron". In: *Journal of Cleaner Production* 174, pp. 35–41. ISSN: 09596526. DOI: [10.1016/j.jclepro.2017.10.300](https://doi.org/10.1016/j.jclepro.2017.10.300). URL: <https://doi.org/10.1016/j.jclepro.2017.10.300>.
- Cai, Lu et al. (2019). "Iron and carbon granules added to anode enhanced the sludge decrement and electrical performance of sludge microbial fuel cell". In: *Chemical Engineering Journal* 372. April, pp. 572–580. ISSN: 13858947. DOI: [10.1016/j.cej.2019.04.164](https://doi.org/10.1016/j.cej.2019.04.164). URL: <https://doi.org/10.1016/j.cej.2019.04.164>.

- Chaithawiwat, Krittanut et al. (2016). "Impact of nanoscale zero valent iron on bacteria is growth phase dependent". In: *Chemosphere* 144, pp. 352–359. ISSN: 18791298. DOI: [10.1016/j.chemosphere.2015.09.025](https://doi.org/10.1016/j.chemosphere.2015.09.025).
- Chen, Ruxia et al. (2020). "Removal of triphenyl phosphate by nanoscale zerovalent iron (nZVI) activated bisulfite: Performance, surface reaction mechanism and sulfate radical-mediated degradation pathway". In: *Environmental Pollution* 260, p. 113983. ISSN: 18736424. DOI: [10.1016/j.envpol.2020.113983](https://doi.org/10.1016/j.envpol.2020.113983). URL: <https://doi.org/10.1016/j.envpol.2020.113983>.
- Daraei, H. et al. (2019). "A comparative study on the toxicity of nano zero valent iron (nZVI) on aerobic granular sludge and flocculent activated sludge: Reactor performance, microbial behavior, and mechanism of toxicity". In: *Process Safety and Environmental Protection* 129, pp. 238–248. ISSN: 09575820. DOI: [10.1016/j.psep.2019.07.011](https://doi.org/10.1016/j.psep.2019.07.011). URL: <https://doi.org/10.1016/j.psep.2019.07.011>.
- Devasahayam, Mercy and Sam A. Masih (2012). "Microbial fuel cells demonstrate high coulombic efficiency applicable for water remediation". In: *Indian Journal of Experimental Biology* 50.6, pp. 430–438. ISSN: 00195189.
- Eljamal, Osama, Ahmed M E Khalil, and Nobuhiro Matsunaga (2017). "Experimental and Modeling Column Study of Phosphorus Removal by Permeable Reactive Materials". In: *International Journal of Environmental & Agriculture Research (IJOEAR)* ISSN 3.1, pp. 62–70.
- Eljamal, Osama, Junya Okawauchi, and Kazuaki Hiramatsu (2012). "Removal of Phosphorus from Water Using Marble Dust as Sorbent Material". In: *Journal of Environmental Protection* 03.08, pp. 709–714. ISSN: 2152-2197. DOI: [10.4236/jep.2012.38084](https://doi.org/10.4236/jep.2012.38084).
- Eljamal, Osama, Keiko Sasaki, and Tsuyoshi Hirajima (2013). "Sorption Kinetic of Arsenate as Water Contaminant on Zero Valent Iron". In: *Journal of Water Resource and Protection* 05.06, pp. 563–567. ISSN: 1945-3094. DOI: [10.4236/jwarp.2013.56057](https://doi.org/10.4236/jwarp.2013.56057).
- Eljamal, Osama et al. (2019). "Iron based nanoparticles-zeolite composites for the removal of cesium from aqueous solutions". In: *Journal of Molecular Liquids* 277, pp. 613–623. ISSN: 01677322. DOI: [10.1016/j.molliq.2018.12.115](https://doi.org/10.1016/j.molliq.2018.12.115). URL: <https://doi.org/10.1016/j.molliq.2018.12.115>.
- Eljamal, Ramadan et al. (2018). "Improvement of the chemical synthesis efficiency of nano-scale zero-valent iron particles". In: *Journal of Environmental Chemical Engineering* 6.4, pp. 4727–4735. ISSN: 22133437. DOI: [10.1016/j.jece.2018.06.069](https://doi.org/10.1016/j.jece.2018.06.069). URL: <https://doi.org/10.1016/j.jece.2018.06.069>.
- Fajardo, C. et al. (2012). "Assessing the impact of zero-valent iron (ZVI) nanotechnology on soil microbial structure and functionality: A molecular approach". In: *Chemosphere* 86.8, pp. 802–808. ISSN:

00456535. DOI: [10.1016/j.chemosphere.2011.11.041](https://doi.org/10.1016/j.chemosphere.2011.11.041). URL: <http://dx.doi.org/10.1016/j.chemosphere.2011.11.041>.
- Fajardo, C. et al. (2013). "Transcriptional and proteomic stress responses of a soil bacterium *Bacillus cereus* to nanosized zero-valent iron (nZVI) particles". In: *Chemosphere* 93.6, pp. 1077–1083. ISSN: 00456535. DOI: [10.1016/j.chemosphere.2013.05.082](https://doi.org/10.1016/j.chemosphere.2013.05.082). URL: <http://dx.doi.org/10.1016/j.chemosphere.2013.05.082>.
- Franks, Ashley E. and Kelly P. Nevin (2010). "Microbial fuel cells, a current review". In: *Energies* 3.5, pp. 899–919. ISSN: 19961073. DOI: [10.3390/en3050899](https://doi.org/10.3390/en3050899).
- Gajda, Iwona, John Greenman, and Ioannis A. Ieropoulos (2018). "Recent advancements in real-world microbial fuel cell applications". In: *Current Opinion in Electrochemistry* 11, pp. 78–83. ISSN: 24519111. DOI: [10.1016/j.coelec.2018.09.006](https://doi.org/10.1016/j.coelec.2018.09.006). URL: <https://doi.org/10.1016/j.coelec.2018.09.006>.
- Hamdan, Hamdan Z. and Darine A. Salam (2020). "Response of sediment microbial communities to crude oil contamination in marine sediment microbial fuel cells under ferric iron stimulation". In: *Environmental Pollution* 263, p. 114658. ISSN: 18736424. DOI: [10.1016/j.envpol.2020.114658](https://doi.org/10.1016/j.envpol.2020.114658). URL: <https://doi.org/10.1016/j.envpol.2020.114658>.
- He, Chuan Shu et al. (2017). "Impact of zero-valent iron nanoparticles on the activity of anaerobic granular sludge: From macroscopic to microcosmic investigation". In: *Water Research* 127, pp. 32–40. ISSN: 18792448. DOI: [10.1016/j.watres.2017.09.061](https://doi.org/10.1016/j.watres.2017.09.061). URL: <https://doi.org/10.1016/j.watres.2017.09.061>.
- Hu, Jianjun et al. (2018). "Feasible use of microbial fuel cells for pollution treatment". In: *Renewable Energy* 129, pp. 824–829. ISSN: 18790682. DOI: [10.1016/j.renene.2017.02.001](https://doi.org/10.1016/j.renene.2017.02.001). URL: <https://doi.org/10.1016/j.renene.2017.02.001>.
- Jia, Hui et al. (2017). "Enhancing simultaneous response and amplification of biosensor in microbial fuel cell-based upflow anaerobic sludge bed reactor supplemented with zero-valent iron". In: *Chemical Engineering Journal* 327, pp. 1117–1127. ISSN: 13858947. DOI: [10.1016/j.cej.2017.06.181](https://doi.org/10.1016/j.cej.2017.06.181). URL: <http://dx.doi.org/10.1016/j.cej.2017.06.181>.
- Kelly Orhorhoro, Ejiroghene (2017). "Experimental Determination of Effect of Total Solid (TS) and Volatile Solid (VS) on Biogas Yield". In: *American Journal of Modern Energy* 3.6, p. 131. ISSN: 2575-3908. DOI: [10.11648/j.ajme.20170306.13](https://doi.org/10.11648/j.ajme.20170306.13).
- Khalil, Ahmed M.E. et al. (2018). "Performance of nanoscale zero-valent iron in nitrate reduction from water using a laboratory-scale continuous-flow system". In: *Chemosphere* 197, pp. 502–512. ISSN: 18791298. DOI: [10.1016/j.chemosphere.2018.01.084](https://doi.org/10.1016/j.chemosphere.2018.01.084). URL: <https://doi.org/10.1016/j.chemosphere.2018.01.084>.

- Kim, Jung Hwan et al. (2018). "Electricity production and phosphorous recovery as struvite from synthetic wastewater using magnesium-air fuel cell electrocoagulation". In: *Water Research* 132, pp. 200–210. ISSN: 18792448. DOI: [10.1016/j.watres.2018.01.003](https://doi.org/10.1016/j.watres.2018.01.003). URL: <https://doi.org/10.1016/j.watres.2018.01.003>.
- Kong, Xiaoying et al. (2017). "Microbial fuel cells". In: *Bioenergy: Principles and Technologies* 2, pp. 387–427. DOI: [10.1515/9783110476217-007](https://doi.org/10.1515/9783110476217-007).
- Krasae, Nalinee and Kitirote Wantala (2016). "Enhanced nitrogen selectivity for nitrate reduction on Cu-nZVI by TiO<sub>2</sub> photocatalysts under UV irradiation". In: *Applied Surface Science* 380.3, pp. 309–317. ISSN: 01694332. DOI: [10.1016/j.apsusc.2015.12.023](https://doi.org/10.1016/j.apsusc.2015.12.023). URL: <http://dx.doi.org/10.1016/j.apsusc.2015.12.023>.
- Li, Meng, Shaoqi Zhou, and Mingyi Xu (2017). "Graphene oxide supported magnesium oxide as an efficient cathode catalyst for power generation and wastewater treatment in single chamber microbial fuel cells". In: *Chemical Engineering Journal* 328, pp. 106–116. ISSN: 13858947. DOI: [10.1016/j.cej.2017.07.031](https://doi.org/10.1016/j.cej.2017.07.031). URL: <http://dx.doi.org/10.1016/j.cej.2017.07.031>.
- Li, Ming et al. (2018). "Microbial fuel cell (MFC) power performance improvement through enhanced microbial electrogenicity". In: *Biotechnology Advances* 36.4, pp. 1316–1327. ISSN: 07349750. DOI: [10.1016/j.biotechadv.2018.04.010](https://doi.org/10.1016/j.biotechadv.2018.04.010). URL: <https://doi.org/10.1016/j.biotechadv.2018.04.010>.
- Liang, Bolong et al. (2020). "Hierarchically porous N-doped carbon encapsulating CoO/MgO as superior cathode catalyst for microbial fuel cell". In: *Chemical Engineering Journal* 385. December 2019, p. 123861. ISSN: 13858947. DOI: [10.1016/j.cej.2019.123861](https://doi.org/10.1016/j.cej.2019.123861). URL: <https://doi.org/10.1016/j.cej.2019.123861>.
- Liu, Da et al. (2020). "High performance of microbial fuel cell afforded by metallic tungsten carbide decorated carbon cloth anode". In: *Electrochimica Acta* 330, p. 135243. ISSN: 00134686. DOI: [10.1016/j.electacta.2019.135243](https://doi.org/10.1016/j.electacta.2019.135243). URL: <https://doi.org/10.1016/j.electacta.2019.135243>.
- Liu, Qian et al. (2018). "Response of the microbial community structure of biofilms to ferric iron in microbial fuel cells". In: *Science of the Total Environment* 631–632, pp. 695–701. ISSN: 18791026. DOI: [10.1016/j.scitotenv.2018.03.008](https://doi.org/10.1016/j.scitotenv.2018.03.008). URL: <https://doi.org/10.1016/j.scitotenv.2018.03.008>.
- Liu, Yiwen, Yaobin Zhang, and Bing Jie Ni (2015). "Zero valent iron simultaneously enhances methane production and sulfate reduction in anaerobic granular sludge reactors". In: *Water Research* 75, pp. 292–300. ISSN: 18792448. DOI: [10.1016/j.watres.2015.02.056](https://doi.org/10.1016/j.watres.2015.02.056). URL: <http://dx.doi.org/10.1016/j.watres.2015.02.056>.

- Logan, Bruce E. and John M. Regan (2006). "Electricity-producing bacterial communities in microbial fuel cells". In: *Trends in Microbiology* 14.12, pp. 512–518. ISSN: 0966842X. DOI: [10.1016/j.tim.2006.10.003](https://doi.org/10.1016/j.tim.2006.10.003).
- Luo, Jingyang et al. (2014). "Stimulating short-chain fatty acids production from waste activated sludge by nano zero-valent iron". In: *Journal of Biotechnology* 187, pp. 98–105. ISSN: 18734863. DOI: [10.1016/j.jbiotec.2014.07.444](https://doi.org/10.1016/j.jbiotec.2014.07.444). URL: <http://dx.doi.org/10.1016/j.jbiotec.2014.07.444>.
- Lv, Yuancai et al. (2017). "Bacterial effects and interfacial inactivation mechanism of nZVI/Pd on *Pseudomonas putida* strain". In: *Water Research* 115, pp. 297–308. ISSN: 18792448. DOI: [10.1016/j.watres.2017.03.012](https://doi.org/10.1016/j.watres.2017.03.012). URL: <http://dx.doi.org/10.1016/j.watres.2017.03.012>.
- Maamoun, Ibrahim et al. (2020). "Promoting aqueous and transport characteristics of highly reactive nanoscale zero valent iron via different layered hydroxide coatings". In: *Applied Surface Science* 506, December 2019, p. 145018. ISSN: 01694332. DOI: [10.1016/j.apsusc.2019.145018](https://doi.org/10.1016/j.apsusc.2019.145018). URL: <https://doi.org/10.1016/j.apsusc.2019.145018>.
- Marks, Stanislaw, Jacek Makinia, and Francisco Jesus Fernandez-Morales (2019). "Performance of microbial fuel cells operated under anoxic conditions". In: *Applied Energy* 250, April, pp. 1–6. ISSN: 03062619. DOI: [10.1016/j.apenergy.2019.05.043](https://doi.org/10.1016/j.apenergy.2019.05.043). URL: <https://doi.org/10.1016/j.apenergy.2019.05.043>.
- Mathuriya, Abhilasha Singh and J. V. Yakhmi (2016). "Microbial fuel cells - Applications for generation of electrical power and beyond". In: *Critical Reviews in Microbiology* 42.1, pp. 127–143. ISSN: 15497828. DOI: [10.3109/1040841X.2014.905513](https://doi.org/10.3109/1040841X.2014.905513).
- Munoz-Cupa, Carlos et al. (2021a). "An overview of microbial fuel cell usage in wastewater treatment, resource recovery and energy production". In: *Science of the Total Environment* 754, p. 142429. ISSN: 18791026. DOI: [10.1016/j.scitotenv.2020.142429](https://doi.org/10.1016/j.scitotenv.2020.142429). URL: <https://doi.org/10.1016/j.scitotenv.2020.142429>.
- (2021b). "An overview of microbial fuel cell usage in wastewater treatment, resource recovery and energy production". In: *Science of the Total Environment* 754, p. 142429. ISSN: 18791026. DOI: [10.1016/j.scitotenv.2020.142429](https://doi.org/10.1016/j.scitotenv.2020.142429). URL: <https://doi.org/10.1016/j.scitotenv.2020.142429>.
- Myung, Jaewook, Pascal E. Saikaly, and Bruce E. Logan (2018). "A two-staged system to generate electricity in microbial fuel cells using methane". In: *Chemical Engineering Journal* 352, July, pp. 262–267. ISSN: 13858947. DOI: [10.1016/j.cej.2018.07.017](https://doi.org/10.1016/j.cej.2018.07.017). URL: <https://doi.org/10.1016/j.cej.2018.07.017>.
- Najafpoor, Aliasghar et al. (2020). "Effect of magnetic nanoparticles and silver-loaded magnetic nanoparticles on advanced wastewater treatment and disinfection". In: *Journal of Molecular Liquids* 303,

- p. 112640. ISSN: 01677322. DOI: [10.1016/j.molliq.2020.112640](https://doi.org/10.1016/j.molliq.2020.112640). URL: <https://doi.org/10.1016/j.molliq.2020.112640>.
- Nimje, Vanita Roshan et al. (2012). "Comparative bioelectricity production from various wastewaters in microbial fuel cells using mixed cultures and a pure strain of *Shewanella oneidensis*". In: *Biore-source Technology* 104, pp. 315–323. ISSN: 09608524. DOI: [10.1016/j.biortech.2011.09.129](https://doi.org/10.1016/j.biortech.2011.09.129). URL: <http://dx.doi.org/10.1016/j.biortech.2011.09.129>.
- Obata, Oluwatosin et al. (2020). "Resilience and limitations of MFC anodic community when exposed to antibacterial agents". In: *Bioelectrochemistry* 134, p. 107500. ISSN: 1878562X. DOI: [10.1016/j.bioelechem.2020.107500](https://doi.org/10.1016/j.bioelechem.2020.107500). URL: <https://doi.org/10.1016/j.bioelechem.2020.107500>.
- Ozansoy, Cagil (2011). "Microbial Conversion of Biomass: a Review of Microbial Fuel Cells". In: *Progress in Biomass and Bioenergy Production*. DOI: [10.5772/19559](https://doi.org/10.5772/19559).
- Pan, Xiaofang et al. (2019). "Impact of nano zero valent iron on tetracycline degradation and microbial community succession during anaerobic digestion". In: *Chemical Engineering Journal* 359, September 2018, pp. 662–671. ISSN: 13858947. DOI: [10.1016/j.cej.2018.11.135](https://doi.org/10.1016/j.cej.2018.11.135). URL: <https://doi.org/10.1016/j.cej.2018.11.135>.
- Santoro, Carlo et al. (2017). "Microbial fuel cells: From fundamentals to applications. A review". In: *Journal of Power Sources* 356, pp. 225–244. ISSN: 03787753. DOI: [10.1016/j.jpowsour.2017.03.109](https://doi.org/10.1016/j.jpowsour.2017.03.109). URL: <http://dx.doi.org/10.1016/j.jpowsour.2017.03.109>.
- Ter Heijne, Annemiek et al. (2011). "Performance of a scaled-up Microbial Fuel Cell with iron reduction as the cathode reaction". In: *Journal of Power Sources* 196.18, pp. 7572–7577. ISSN: 03787753. DOI: [10.1016/j.jpowsour.2011.04.034](https://doi.org/10.1016/j.jpowsour.2011.04.034). URL: <http://dx.doi.org/10.1016/j.jpowsour.2011.04.034>.
- Vicari, Fabrizio et al. (2018). "Influence of the initial sludge characteristics and acclimation on the long-term performance of double-compartment acetate-fed microbial fuel cells". In: *Journal of Electroanalytical Chemistry* 825, May, pp. 1–7. ISSN: 15726657. DOI: [10.1016/j.jelechem.2018.08.003](https://doi.org/10.1016/j.jelechem.2018.08.003). URL: <https://doi.org/10.1016/j.jelechem.2018.08.003>.
- Wei, V., M. Elektorowicz, and J. A. Oleszkiewicz (2011). "Influence of electric current on bacterial viability in wastewater treatment". In: *Water Research* 45.16, pp. 5058–5062. ISSN: 18792448. DOI: [10.1016/j.watres.2011.07.011](https://doi.org/10.1016/j.watres.2011.07.011). URL: <http://dx.doi.org/10.1016/j.watres.2011.07.011>.
- Wu, Chao et al. (2013). "Electron acceptor dependence of electron shuttle secretion and extracellular electron transfer by *Shewanella oneidensis* MR-1". In: *Bioresource Technology* 136, pp. 711–714. ISSN: 18732976. DOI: [10.1016/j.biortech.2013.02.072](https://doi.org/10.1016/j.biortech.2013.02.072). URL: <http://dx.doi.org/10.1016/j.biortech.2013.02.072>.

- Wurzler, Nina et al. (2020). "Abundance of Fe(III) during cultivation affects the microbiologically influenced corrosion (MIC) behaviour of iron reducing bacteria *Shewanella putrefaciens*". In: *Corrosion Science* 174, February, p. 108855. ISSN: 0010938X. DOI: [10.1016/j.corsci.2020.108855](https://doi.org/10.1016/j.corsci.2020.108855). URL: <https://doi.org/10.1016/j.corsci.2020.108855>.
- Yi, Jing et al. (2014). "Effect of increasing total solids contents on anaerobic digestion of food waste under mesophilic conditions: Performance and microbial characteristics analysis". In: *PLoS ONE* 9.7. ISSN: 19326203. DOI: [10.1371/journal.pone.0102548](https://doi.org/10.1371/journal.pone.0102548).
- Yirsaw, Biruck D. et al. (2016). "Environmental application and ecological significance of nano-zero valent iron". In: *Journal of Environmental Sciences (China)* 44, pp. 88–98. ISSN: 18787320. DOI: [10.1016/j.jes.2015.07.016](https://doi.org/10.1016/j.jes.2015.07.016). URL: <http://dx.doi.org/10.1016/j.jes.2015.07.016>.
- Zhang, Jingxin et al. (2014). "A direct approach for enhancing the performance of a microbial electrolysis cell (MEC) combined anaerobic reactor by dosing ferric iron: ENRICHMENT and isolation of Fe(III) reducing bacteria". In: *Chemical Engineering Journal* 248, pp. 223–229. ISSN: 13858947. DOI: [10.1016/j.cej.2014.02.102](https://doi.org/10.1016/j.cej.2014.02.102). URL: <http://dx.doi.org/10.1016/j.cej.2014.02.102>.
- Zhao, Feng, Robert C T Slade, and John R Varcoe (2009). "Techniques for the study and development of microbial fuel". In: *Chemical Society Reviews* 39.7, pp. 1926–1939. URL: <https://core.ac.uk/download/pdf/102229.pdf>.
- Zhou, Jun et al. (2020). "Enhancement of methanogenic activity in anaerobic digestion of high solids sludge by nano zero-valent iron". In: *Science of the Total Environment* 703, p. 135532. ISSN: 18791026. DOI: [10.1016/j.scitotenv.2019.135532](https://doi.org/10.1016/j.scitotenv.2019.135532). URL: <https://doi.org/10.1016/j.scitotenv.2019.135532>.